Modification of Metallocene Alpha-Olefin Copolymer by UV-Irradiation

by

Muhammad Umar Farooq

A thesis
presented to the University of Waterloo
in fulfilment of the
thesis requirement for the degree of
Master of Applied Science
in
Chemical Engineering

Waterloo, Ontario, Canada, 2016

AUTHOR'S DECLARATION

I hereby declare that I am the sole author of this thesis. This is a true copy of the thesis, including any required final revisions, as accepted by my examiners.

I understand that my thesis may be made electronically available to the public.

Muhammad Umar Farooq

ABSTRACT

Linear low density polyethylene (LLDPE) is used widely in applications like lamination and agricultural films, as well as a modifier for low density (LDPE) and high density (HDPE) polyethylene. LLDPE is made by polymerizing ethylene with small amounts of alpha-olefins typically 1-butene, 1-hexene or 1-octene, to form a copolymer in a low pressure process. The LLDPE used in this thesis contained 93 – 100% ethylene by weight and 0 – 7% by weight 1-hexene as comonomer. The melt strength of LLDPE can be modified by introducing long chain branching (LCB) to its backbone and there are several techniques to accomplish that. In this work, free radicals are formed by adding benzophenone (BP) as a photo-initiator and by irradiating solid sheets of the LLDPE resin by using a UV lamp. As a result, LCB affects the rheological properties and this has been studied in this thesis.

UV irradiation via a mercury lamp was conducted using a design of experiments (DOE), implemented to elucidate the effects of three factors: BP concentration, time of irradiation and intensity of the UV lamp. The DOE stated 20 different sample runs to be done to better understand the changes in the rheology of the samples due to variation in the three factors.

The experiments began with addition of BP to the copolymer pellets in a batch mixer for homogenous mixing at 190 ^{o}C and 100 RPM for 5 – 7 minutes after which the LLDPE-initiator blend was pelletized and compression – molded in a hot press at 190 ^{o}C for 3 minutes at 20000 lb_f. The pressed sample sheets were then irradiated using the UV lamp for specific time period and lamp intensity according to the DOE. Pressurized air was used to cool down the area beneath the lamp which ranged from 31 – 37 ^{o}C before and after irradiation and 71 – 77 ^{o}C during batches.

Discs of 25 mm diameter and 1 mm thickness were subsequently cut from pressed irradiated sheets and were used for testing in the rotating parallel plate rheometer.

Different graphs and trends were prepared to analyze the rheology of each sample by strain and frequency sweep for 0.1 – 10 % strain and 0.1 – 100 Hz frequency, respectively. After determining the linear viscoelastic region, Storage, Loss and Crossover Moduli, Cole-Cole plot, Zero Shear and Complex Viscosity, Polydispersity Index, Modulus of Separation and ER, were studied for further understanding. All the results pointed to the fact that the MW was increased and LCBs/crosslinking was induced and hence, broadening effect of MWD in the samples was eventually seen, when BP, time and UV intensity were increased.

Differential Scanning Calorimetry (DSC) was later used to determine the melting and crystallization characteristics of all samples produced. Small chunks cut from the irradiated LLDPE sheets were inputted in the DSC apparatus and heat flow curves were extracted. The first heating cycle was neglected to omit any history the sample might have. The cooling cycle was used to analyze the onset crystallization temperature, crystallization enthalpy and the crystallization temperature. The second heating cycle was used to extract the melting temperature, enthalpy of melting and the onset melting temperature. The percentage crystallinity was also calculated to check which sample gave the highest amorphous content after UV treatment due to branching. Statistica was used to analyze the significance of factors studied and interactions between them.

In terms of rheological polydispersity, the effects of processing conditions on ER were evaluated at a 5% significance level, and it was found that:

(i) All three factors studied (BP concentration, irradiation time, lamp intensity) had a positive effect on ER, thus, increasing LCB and broadening MWD.

(ii) The two-factor interactions of BP concentration-irradiation time and BP concentration-lamp intensity had also a positive effect on ER, thus, increasing LCB and broadening MWD.

In terms of the melting and crystallization characteristics of the irradiated samples, the effects of all three processing conditions were evaluated and it was found that:

(i) Onset crystallization temperature and crystallization enthalpy were significantly affected by BP concentration and UV intensity.

(ii) Crystallization temperature was significantly affected by BP concentration.

(iii) Melting temperature was significantly affected by irradiation time.

(iv) Onset melting temperature was significantly affected by UV intensity.

In general, the results obtained in this research work show that UV irradiation can easily be used to modify LLDPE. Results from the statistical analysis can be used to form models for guiding further experiments in order to optimize the level of LCB in materials with controlled architecture. Future work can focus on developing direct correlations between processing conditions and LCB and MWD by using gel permeation chromatography measurements. Also, the effect of gel content on rheological behavior can be isolated from that of LCB.

ACKNOWLEDGEMENTS

I would like to express my deep and sincere gratitude to my supervisor, Professor Costas Tzoganakis, for his guidance, insight and encouragement throughout the course of my research. His supervision and feedback will go beyond my academic experience. During my stay in Canada, I benefited from his mentorship along with a solid bond of friendship, for which I am highly grateful and indebted for life. I would like to thank Professors Alexander Penlidis and Neil McManus for being on my committee and for the patient reading and critical and in-depth advice. Their valuable and useful comments made my thesis accurate and refined.

Special thanks to Prime Polymer Co. Ltd. Japan for providing me with their EVOLUE SP0510 material for my experiments and all the technical staff here at University of Waterloo for their extended help. I would like to thank my Polymer Processing Lab members Dr. Mo Meysami, Dr. Prashant Mutyala, Tadayoshi Matsumura, Shouliang Nie and Ankita Saikia for their continued help and assistance in and out of the lab. I would like to thank my ChemEng friends like Manoj Mathew, Ushnik Mukherjee, Sannan Toor, Siddharth Mehta, Yasaman Amintowlieh and Alison Scott for being so generous in sharing their vast knowledge.

Finally, I would like to thank my parents for their unconditional love and support throughout my life and my wife and soulmate Injla for staying by my side. Without my family it wouldn't have been possible for me to be who I am right now. I cannot thank them enough for what they have done for me and hope that they always stay by my side, helping me tackle and unravel all the challenges life has to throw at us.

Dedicated to my loving wife, Injla

For always being a critique and my sounding board

TABLE OF CONTENTS

LIST OF FIGURES

LIST OF TABLES

COMMON ABBREVIATIONS

PE – Polyethylene

HDPE – High Density Polyethylene

LDPE – Low Density Polyethylene

LLDPE – Linear Low Density Polyethylene

LCB – Long Chain Branching

NLCB – Number of Long Chain Branches

PP – Polypropylene

LCBPP – Long Chain Branched Polypropylene

T_g – Glass Transition Temperature

M_w – Weight Average Molecular Weight

MWD – Molecular Weight Distribution

CL – Crosslinking

XLPE – Crosslinked Polyethylene

LVE – Linear Viscoelastic

REX – Reactive Extrusion Process

DOE – Design of Experiments

EB – Electron Beam

BP – Benzophenone

UV – Ultraviolet

ZN – Ziegler Natta Catalyst

CCD – Central Composite Design

$-\alpha$ – Negative Extreme Star Point Limit

α – Positive Extreme Star Point Limit

n – Power Law Index

ω – Frequency of Oscillation

γ – Time Dependent Strain

γ_o – Time Dependent Strain at Zero Stress

$\dot{\gamma}$ – Strain Rate

σ – Time Dependent Stress

t – Time

δ – Phase Difference

η – Newtonian Viscosity

η* – Complex Viscosity

τ – Shear Stress

G´ – Storage Modulus

G" – Loss Modulus

G_c – Crossover Modulus

G* – Complex Modulus

G_{ref} – Reference Value Modulus

J* – Compliance Modulus

J´ – Storage Compliance

J˝ – Loss Compliance

tan δ – Loss Tangent

X_c – Percentage of Crystallinity

PDI – Polydispersity Index

ER – Rheological Polydispersity Index of High Molecular Weight Chains

PI – Rheological Polydispersity Index

MFI – Melt Flow Index

MFR – Melt Flow Rate

ModSep – Modulus of Separation

GPC – Gel Permeation Chromatography

ESR – Electron Spin Resonance

NMR – Nuclear Magnetic Resonance

DSC – Differential Scanning Calorimeter

MS – Mean Square

MSE – Mean Square Error or Mean Square Residual

SS – Sum of Squares

p – Error

R^2 – Variance

H_f – Enthalpy

CHAPTER 1

INTRODUCTION, OBJECTIVES AND THESIS OUTLINE

1.1 Introduction

Polyethylene is produced by free radical and coordination polymerization of ethylene. It is normally classified into three main categories based on density, i.e. low density (LDPE), linear low density (LLDPE) and high density (HDPE) polyethylene. The material of interest in this study is LLDPE. This LLDPE is the product of co-polymerization of ethylene with small amounts of 1-hexene (referred to as hexene from now on) which form short chain butyl branches of identical structure on the ethylene backbone. The catalyst used for this polymerization process is a metallocene catalyst. Advantages of using a metallocene catalyst compared to 3rd generation Ziegler-Natta catalysts include narrower molecular weight distribution, exceptional control over branching and sequence distribution of branches on the main chain and better tailoring of the final product. The purpose of this research is to study the effect of UV irradiation on LLDPE in the presence of a photo-initiator, treated for varying durations using a central composite design (CCD) of experiments. UV irradiation is expected to cause alteration in the chain microstructure and induce long chain branches. The samples used have a crystallinity content of approximately 40%. Based on previous research studies it is anticipated that an increase in the amorphous content of the material and a broadening effect on the molecular weight distribution will be obtained [1-4].

1.2 Objectives

The objective of this research work was to study the effect of UV irradiation on the rheological and thermal properties of a LLDPE. Expected changes in properties are the result of long chain branching and possibly crosslinking induced by the generation of free radicals by UV irradiation. UV irradiation treatment factors to be studied were irradiation intensity, photo-initiator concentration, and irradiation duration. Their effects on rheological and thermal properties were studied through oscillatory shear measurements using a parallel plate rheometer and differential scanning calorimetry (DSC).

1.3 Thesis Outline

Chapter 1:

In this introductory chapter, the objective of the research work is discussed and the thesis outline is presented.

Chapter 2:

In this chapter a literature review is presented summarizing previous similar work on polyethylene (PE) and polypropylene (PP). A comparison and discussion of various techniques used in the past to alter chain architecture and final properties to suit a range of practical uses is presented.

Chapter 3:

In this chapter we discuss the research methodology and experiments performed, and provide a brief overview of equipment used. The design of experiments is elaborated as it is the basis of what is hoped to be achieved in this thesis.

Chapter 4:

This chapter contains the analysis of the experimental results obtained through parallel plate rheometry and DSC. The results are discussed and statistically assessed to identify significant factors.

Chapter 5:

In this chapter final comments and deductions are made based on a review and comparison of all the results obtained. The possibility of future research furthering this study is also covered in the end.

CHAPTER 2

LITERATURE REVIEW

Ethylene or ethene ($CH_2 = CH_2$) is derived from either modification of natural gas (methane, ethane, propane mixture) or from catalytic cracking of crude oil into gasoline. For the polymerization of ethylene, it is piped directly from the refinery, in a highly purified form, to a separate polymerization plant. Here, under the right conditions of temperature, pressure and catalysis, the double bond of the ethylene monomer opens up and many monomer units link up to form long chains. In commercial polyethylene (PE), the number of monomer repeat units ranges on average from 1000 to 10,000 (molecular weight ranges from 28,000 to 280,000).

Polyethylene manufacturing processes are usually categorized into "high pressure" and "low pressure" operations. The former is generally recognized as producing conventional Low Density Polyethylene (LDPE) while the latter makes High Density Polyethylene (HDPE) and Linear Low Density Polyethylene (LLDPE).

ICI Britain first discovered in the 1930's that if ethylene gas was heated in the presence of less than 10 ppm of oxygen at high pressures of 1000 – 3000 bar and temperatures of 80 – 200˚C, it could polymerize to give a highly branched polyethylene with branches at every 20 – 50 carbons on the backbone chain [5]. They named it 'Polythene' which finds its single biggest application in the production of blown films today. It was found that the initial reaction was rather an unsystematic one producing a broad molecular size distribution and a density range of 0.915 – 0.930 g/cm^3. However, by controlling reaction factors it was possible to control the average molecular size (molecular weight).

Similar to the accidental discovery of LDPE in the 1930's, HDPE was discovered in 1952 unintentionally by researchers in Germany and Italy who were contemplating a more efficient polymerization technique for PE [5]. To be able to polymerize ethylene at lower pressures than the ICI process they developed a new aluminium based catalyst with which the process could be run at 10 – 80 bar and 70 – 300 ^{o}C. The resulting polymer was different; however it was much stiffer with higher density of 0.940 – 0.970 g/cm^3. Rheological analysis showed that the level of branching on the chains was significantly lower, so much so that the polymer could essentially be considered a linear one. The molecular weight distribution was narrower and the polymer had a rather high average chain length. HDPE is a hard semi-crystalline polymer (70% crystallinity) having no chain branching and with highest tensile strength in the order of 4600 psi.

The polymerization of ethylene to LLDPE is also a low pressure process first implemented by DuPont Canada in the 1950's. Unlike LDPE, HDPE and LLDPE do not have long chain branching, therefore they have better chain stacking and higher density and increased stiffness. The properties of the polymer that depend on molecular weight change significantly due to the difference in branching structure. A comparison of chain structures of HDPE and LDPE can be seen in Fig. 2.1. LLDPE has more branching than HDPE but less than that of LDPE and these are essentially formed due to the presence of small amount of another monomer like butene, hexene, or octene, as shown in Fig. 2.2 added during polymerization [5].

Fig. 2.1 shows how HDPE, LDPE and LLDPE are in terms of chain structure with HDPE as linear, LDPE as long chain branched and LLDPE as short chain branched. Fig. 2.2 shows the chemical structure of PE when butene, hexene or octene, is copolymerized with ethylene into LLDPE.

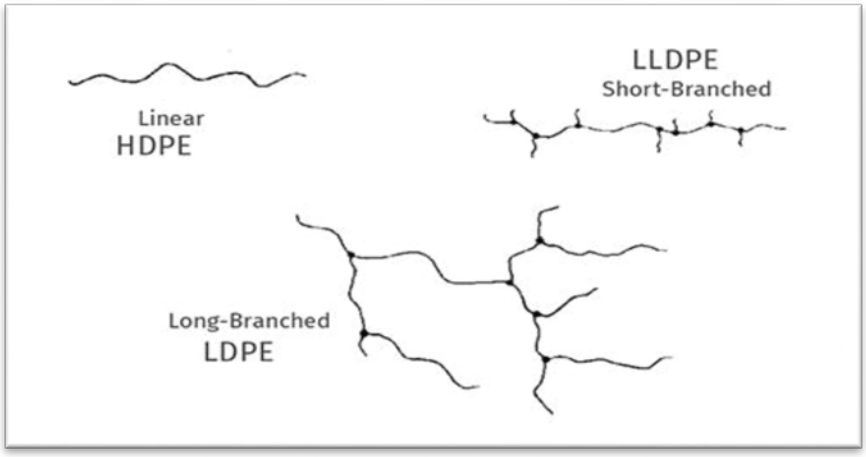

Figure 2.1 – Chain Structure for HDPE, LLDPE and LDPE [6]

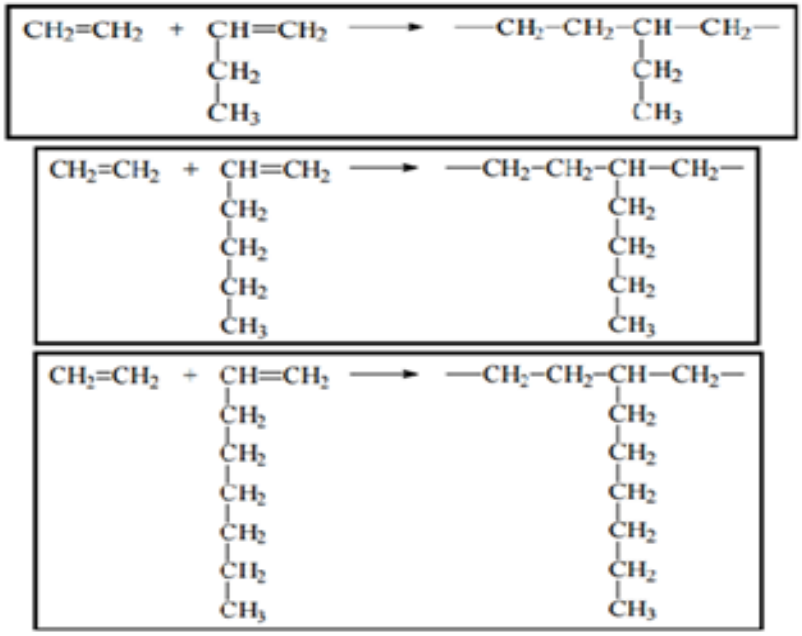

Figure 2.2 – Addition of Branches onto the PE backbone chain by Butene, Hexene and Octene [5]

As mentioned before, PE finds its most significant use in packaging as films. Its properties like toughness, extraordinary elongation and optical clarity of amorphous grade LDPE along with its resistance to most chemical solvents, low toxicity, high stability and extensive opportunity for recycling make it very suitable and effective for this application. Polymerized pellets of varying

shapes are converted into packaging materials by processes like sheet extrusion, calendering, blowing or extrusion coating on substrates like paperboard.

LLDPE has greater environmental stress crack resistance than LDPE. It also has better tensile and impact strength and puncture resistance given the difference of the long chain branching present in LDPE. LLDPE is a copolymer where longer alpha olefins are used as comonomers in small quantity which then add on to the main backbone forming short chain branches (Figure 2.2). The process of polymerization is essentially coordination polymerization and results in a narrow molecular weight distribution polymer with rather long chain molecules. It is semi-crystalline with up to 60% crystallinity and the density range is 0.915 – 0.925 g/cm^3. LLDPE melts between 122 – 127 ^{o}C and the glass transition temperature (T_g) is between -125 ^{o}C and -70 ^{o}C. LLDPE resins available in the market can have weight-average molecular weights (M_w) between 20,000 – 200,000. LLDPE due to shorter branches and higher crystallinity is more viscous and harder to process compared to LDPE. Therefore, the phenomenon of shear thinning is also lower in LLDPE than in LDPE.

Both LLDPE and HDPE are synthesized by coordination polymerization using either homogenous or heterogeneous catalysis using either 3rd Generation Ziegler-Natta using titanium tetrachloride-magnesium chloride catalyst systems, or using metallocene catalysts (aluminoxane on transition metal support like zirconium complexes), respectively. Metallocenes provide a higher molecular weight, narrower molecular weight distribution, better comonomer distribution and better stereo – regularity of the polymer. The polymer melt flow behavior is directly associated with its molecular weight distribution (MWD). This also means that careful manipulation of the MWD determines the melt processing conditions making it an important intrinsic property of the polymer.

Commercial polyethylene grades can be further modified to introduce branching or crosslinking through the use of peroxides, photo-initiation techniques, and electron beam (EB) or gamma ray irradiation. Free radicals generated by these techniques can remove hydrogen atoms from the backbone of the chains, thus, initiating sites for branching with another radical centre. However, there are several problems associated with these methods such as the high cost of EB or gamma radiation and the toxicity of peroxide initiators which render the plastic unsafe in applications in the food packaging industry [7].

A method of crosslinking for polyethylene was discovered by Oster in the 1950's [8, 9]. They found that using UV irradiation of 200 – 300 nm wavelength range induced crosslinks in the PE films, which were enhanced a 1000 times if a photo – initiator like benzophenone was added. The process was not used industrially until after the 1990's. There still remain some limitations to photo-crosslinking of PE, mainly the inability to be used for samples any thicker than 3mm as UV light does not penetrate easily in thicker samples and the rate of the photo-crosslinking reaction is very slow giving a rather non-homogenously crosslinked PE. Thus, this process finds use only in applications like photocuring and other surface modifications. It was recently shown that the photo-crosslinking process can be successfully utilized for wire insulation as well where Ranby et al. developed a continuous laboratory method using enhanced photoinitiating systems for crosslinking PE in bulk [10].

Despite these limitations, photocrosslinking does have several advantages over the other two commercial processes. These include cost efficiency associated with the simplicity of the required apparatus and the reduced polymer oxidation and degradation. Also, UV light is easy and safe to

handle unlike chemical reagents. As a result, photo-initiated reactions have been of much interest to researchers and industry alike.

In order to overcome the limitations associated with photocrosslinking of PE, two main advances have been made: (i) use of enhanced photoinitiating systems comprising of a photoinitiator and a multifunctional crosslinker, and (ii) manipulation of process variables such as reaction conditions, concentrations of initiator and crosslinker, intensity of light etc.

Photocrosslinking means that the crosslinks in PE chains are brought about by UV light. However, because there are no light absorbing groups in the PE, a photoinitiator is added. The emission spectrum of the light source, anywhere between 200 – 400 nm, is carefully selected to align with the absorption spectrum of the initiator. There are two types of radical initiator used in PE photocrosslinking: cleavable photoinitiators or alpha cleavage type and uncleavable, that functions by hydrogen extraction or electron transfer. It was shown by Chen et al. (2003), who studied 18 types of initiators used for HDPE, that the cleavable initiators like benzophenone and xanthone were much more efficient [11].

In order to implement this process at an industrial scale, enhanced photoinitiating systems are used where a multifunctional crosslinker is used in combination with a photoinitiator. It has been shown that using a combination of 4-chlorobenzophenone (BP) and triallyl – cyanurate (TAC) in comparison to using just BP increases the number of free radicals formed and the same amount of gel content is formed in less than half the irradiation time. It has also been shown that in addition to increasing the number of crosslinks formed, TAC also considerably increases the homogeneity of the crosslinking in thick polymer samples.

In addition to these, there are a few other factors that influence the photocrosslinking of PE. For example, higher irradiation temperatures result in more efficient crosslinking of the polymer melt due to a greater extent of segmental motion and easier movement of the active radicals through the sliding chains. The rate of gel formation rises with the intensity of UV irradiation as well. The presence of oxygen in the photocrosslinking process environment, on the contrary, has an impeding effect on photocrosslinking as oxygen molecules compete with the chains to join with active radicals, thereby reducing the amount of gel formed.

The changes observed in polymer morphology, chain structure, thermal behavior, crystallinity, thermal and photo – oxidative stability after photocrosslinking of a sample give proof of the process being effective and useful. Results of a DSC thermogram of LDPE at increasing irradiation times at 100 ^{o}C (a temperature lower than the melting point) show two melting peaks instead of one [12]. The first peak can be interpreted to be caused by the endothermic formation of gel in the amorphous region and interfacial region of the polymer material while the second and more common peak is due to formation of crystals in the polymer as the crosslinked sample is cooled from 100 ^{o}C to room temperature. There is a significant drop in crystallinity of a polymer sample before and after it is photocrosslinked, as LDPE crystallinity drops from 53.2% to 43.2%, while for HDPE it drops from 77% to 58.6% at a gel content of 91.3%. This is because the crosslinks formed at a temperature higher than the crystallization temperature in the amorphous region restrict those chains to fold properly into lamellae and lattice. As a consequence of reduced crystallinity the density of an LDPE sample also drops from 0.924 gm/cm^3 to 0.920 gm/cm^3 at 83.5% crosslinking. The melting point also drops from 380 K to 378.5 K.

Gel formation in PE enhances the physical performance of the polymer giving more opportunities for PE with tailor made properties. In general, crosslinking improves toughness and gives superior

stress cracking, stiffness and better chemical resistance and excellent electrical insulation. All of these factors can be manipulated to achieve best combination of properties for any use. Irradiation apparatus for photocrosslinking of PE have been recently developed and have found application in the manufacture of crosslinked polyethylene (XLPE) TV wires, power cables, coating, lamination, etc. The manufacturing process essentially consists of the resins being homogenously blended with additives like the photocrosslinker, multifunctional crosslinker, antioxidant, stabilizer, etc., after which they are extruded and crosslinked in the melt state in an extruder for a specific time [12].

The UV photocrosslinking process has some preferential advantages over the conventional ones like chemical crosslinking (using peroxides), EB and gamma irradiation. The most important of these is the very feasible cost associated with the whole process, investment, apparatus etc. The apparatus is easy to maintain, operations are simple and UV light is easily available. It also allows rapid crosslinking in a one-step process so that a continuous manufacturing line is possible. Photocrosslinking can be done at room temperature for thin samples and in the melt for thicker samples. It is an environmentally safe process eliminating any release of harmful waste. A block diagram (Figure 2.3) shows an example of a process where PE wire insulation is being photocrosslinked from start to end [12].

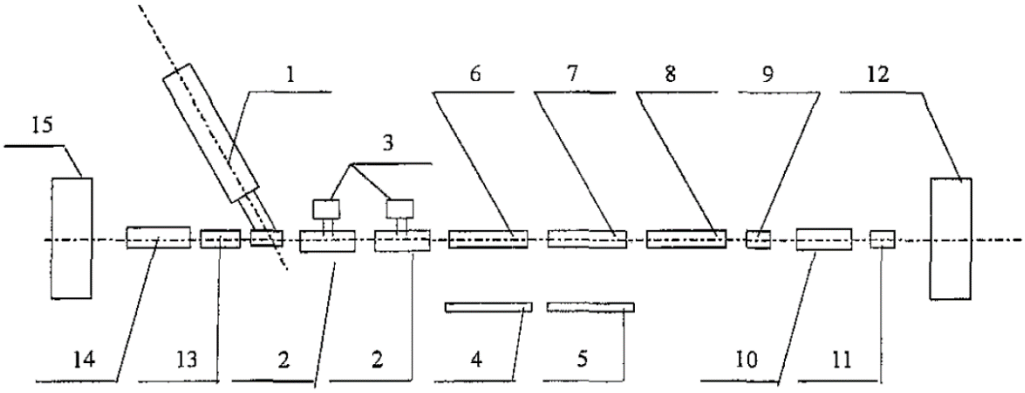

1) Extruder; 2) UV irradiation unit; 3) exhaust fan; 4) cabinet of electric controller; 5) cabinet of electrical system; 6) hot water tank; 7) warm water tank; 8) cool water tank 9) length counter; 10) down-drawing; 11) test machine of breakdown; 12) take up; 13) preheater; 14) up-drawing; 15) pay-off

Figure 2.3 – Production Line Block Diagram for Photocrosslinked PE (XLPE) Wire and Cables [12]

Another example of a continuous process is a Reactive Extrusion Process (REX), in which the polymer sample is photodegraded or crosslinked in the extrusion barrel (see Figure 2.4) [13].

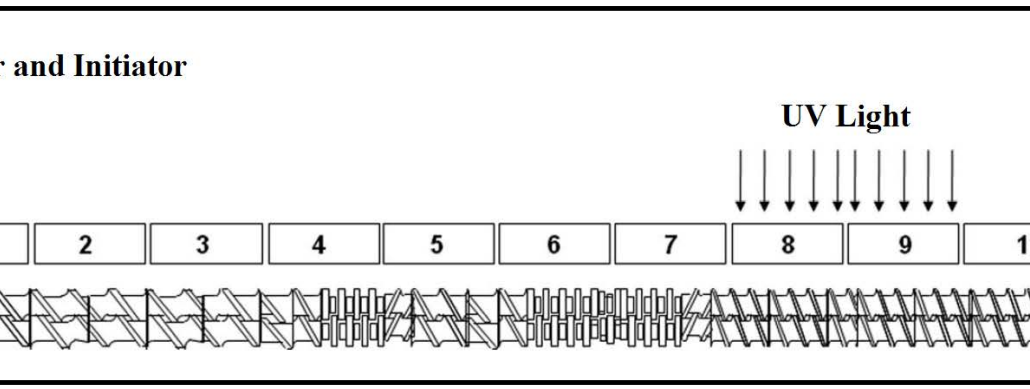

Figure 2.4 – Screw Configuration and Experimental Setup [13]

Long chain branches increase the melt strength of a polymer which is a desirable property especially in production of films, sheets and continuous die forming applications. This effect has

been observed in polypropylene in which long chain branches have been introduced. There are two main methods used for the introduction of LCB in a polymer: (i) thermo – chemical methods, using peroxides in conjunction with multifunctional monomers like styrene, allylic acid and acrylic, and (ii) methods using high energy radiation like electron beam and gamma radiation [7, 13].

Methods employing chemical reagents, like peroxides, have a few disadvantages. Firstly, they are toxic chemicals making them unsafe for handling and for health and safety purposes. Moreover, the processing temperatures are well above the initiator activation temperature and therefore some unwanted and inconsistent degradation occurs in the polymer compromising its final physical properties. Various techniques such as gel permeation chromatography (GPC) and rheometry can be used to study the difference between samples in which LCB is introduced. GPC results for EB irradiated samples have shown that the number of long chain branches (NLCB) introduced increases with respect to molar mass of the sample to a certain limit after which the NLCB becomes constant. The radiation intensity (20 – 150 kGy) also does not have any effect on increasing the branching and degradation is more evident in longer chains. Rheological tests and elongation for EB samples also have shown that zero shear viscosity increases with radiation dosage, and elongational viscosity and strain hardening are also reported to increase. Both EB and gamma rays have certain safety concerns and are also rather expensive to be employed in industries readily. UV irradiation in the presence of photoinitiator like benzophenone (BP) has been successful in introducing LCB in this regard. The BP absorbs energy from UV irradiation wavelength of 215, 254 and 300 nm, and then in its excited state abstracts hydrogen from the PP backbone thereby forming a macroradical inducing subsequent hydrogen abstraction. This method of using a photo-initiator with UV is also called photo-modification and can be used in both the melt and solid

states. It is also favorable over the other methods because of the good controllability of branch formation and thus reduced degradation and absence of high temperatures [14-16].

Photomodification can be used as a means of changing the rheology of a polymer to achieve tailored-made properties. In order to study the change in molecular structure, viscosity, degradation, branches and crosslinking, different molecular characterization techniques are used such as gel permeation chromatography (GPC) to identify changes in structure and MWD, shear rheometry, nuclear magnetic resonance (NMR), electron spin resonance (ESR), differential scanning calorimeter (DSC) to obtain heat of fusion and melting points, and extensional rheometry [17-19].

Polyethylene is the highest volume produced commodity plastic today. Its extensive usage and market share make it an important topic of study and improvement. Its degradation during processing and recycling and other such phenomena are few of the areas of improvement and can be studied by looking at thermal-oxidation in the polymer. Changes in the molecular structure of polymer like introduction of long chain branches, chain scission, and crosslinking are all caused by thermal degradation. Experimental work on low-density polyethylene (LDPE) under thermal oxidative conditions has shown that strain hardening can be increased due to excessive LCB formation during degradation [20-22].

LCBs were introduced in high density polyethylene (HDPE) by photo-modification during a reactive extrusion process [23]. A central composite response surface design was used to study the effects of processing variables such as photo-initiator concentration, flow rates of HDPE, UV light intensity, and extruder screw speed. A set of standardized tests were performed to study the changes induced by the specific levels of processing factors in each modified sample. Soxhlet

extraction experiments showed very small amounts of gel formation while GPC measurements showed that the PDI of the samples remained the same with a slight increase in molecular weight (MW). The presence of long chain branches was evident by the linear viscoelastic (LVE) behavior at low frequencies in oscillatory shear tests. An increase in zero shear viscosity and relaxation time further confirmed the presence of LCBs [23].

Melt rheological behavior of a polymer is directly related to the polymer's molecular structure, extent and nature of branching, molecular weight, polydispersity and MWD. It is possible to obtain some level of polydispersity measure using rheological data The measure of polydispersity index (PI) can be calculated from the cross-over modulus (G_c) in linear viscoelastic rheological data [24].

Polyethylene is widely used in extrusion coating applications. The two factors that must be controlled in extrusion coating processes are the neck-in and draw-down speed. Neck-in is the difference in the width of the die and the width of the coating on the substrate, while draw-down speed is the speed at which the coated substrate can be pulled without breaking. A high draw-down speed increases the neck-in which compromises the quality and strength of the coating. Rheological modification of the PE can improve performance associated with neck-in at high draw-down speeds. It has been shown that shear modification of highly branched polymers reduces the melt strength of the material. MWD modality and comonomer types also affect the melt strength of the polymer. This means that lower branching, shorter branches and narrower MWD polymer will have lower melt strength. High melt strength means better performance at high draw-down speeds and reduced neck-in [25-27].

UV irradiation is a kind of high-energy irradiation that has been implemented as a modification method in polymer research for quite some time. Reference [28] explored the role of morphology

and physical structure in the photo-degradation behavior of PP, concluding that the initial physical structure of PP, which included the crystal size, molecular orientation and the degree of crystallinity, influence the photo-oxidation by modifying the permeability of oxygen and absorption characteristics of UV [13].

A technique developed to change the melt properties of PP involves the use of photo-initiators along with UV irradiation, to induce long chain branching (LCB) and/or crosslinking (CL). Statistical design of experiments was used to study the effect of processing conditions, such as type and concentration of photo-initiator, duration of irradiation, UV lamp intensity and cooling air pressure etc., on rheological and molecular weight characteristics and level of branching. Samples were evaluated through linear viscoelastic (LVE) measurements, extensional rheometry, gel content measurements, differential scanning calorimetry (DSC) and gel permeation chromatography (GPC). Results showed successful modification of PP and enhanced strain hardening behavior without significant gel formation [29, 30].

Another technique for modification in the rheology and increasing the melt strength of PP is by the use of gamma radiation, where Cobalt 60 is used as a gamma ray source to produce excited states and energetic ions. However, the intensity of gamma radiation causes beta-scission, losing good control on the modification. Since polydispersity (PDI) and molecular weight also affect the melt flow behavior and processing characteristics, adjusting these parameters can also contribute to changes in rheology and hence, many applications of tailored properties of PP can be made [31-33].

In another study [15], it was seen that UV irradiation was a safe and cheap process, in order to generate free radicals and modify the molecular structure in PP. When using a twin-screw extruder,

a controlled rheology PP of decreased polydispersity (PDI) was achieved, using UV energy and photo-initiators for effective degradation.

A similar study was conducted by Huang et al. [34], where the control of PP degradation in the melt state was demonstrated to form long chain branched PP (LCBPP) for foaming applications. According to that experiment, acrylic co-agents were used and the radiation was carried out in the last two zones of the twin screw extruder. Amintowlieh et al. [47], modified PP to increase its melt strength. Samples were irradiated in the solid state and effects (LCB extent and degradation) were measured by manipulating variables such as concentration of photo-initiator (benzophenone), duration of exposure to radiation, intensity of UV lamp and pressure of cooling air which result in the formation of long chain branching on PP backbone.

CHAPTER 3

EXPERIMENTAL

3.1 Materials

The LLDPE polymer resin used in this work was an alpha-olefin copolymer with hexene being the comonomer. Its composition was 93 – 100 % by weight ethylene and 0 – 7 % by weight hexene. This resin was acquired from Prime Polymers Co. Ltd., Tokyo, Japan, and its commercial name is Evolue^{TM} and grade number is SP0510 (properties are listed in Table 3.1). Benzophenone (BP) used in the study as the UV initiator (also known as diphenyl ketone) was supplied by Sigma – Aldrich Canada, product number W213403, having a formula of $C_{13}H_{10}O$ and a molecular weight of 182.22 g/mol. Both materials were used as received.

Table 3.1 Properties data sheet according to EVOLUE^{TM} Prime Polymer Co. Ltd.

Physical	**Nominal Value Unit**	**Test Method**
Density	0.903 g/cm³	ISO 1183
Melt Mass-Flow Rate (MFR) (190°C/2.16 kg)	1.2 g/10 min	ISO 1133
Environmental Stress-Cracking Resistance	> 1000 hr	ASTM D1693
Hardness	**Nominal Value Unit**	**Test Method**
Shore Hardness (Shore D, Injection Molded)	49	ISO 868
Mechanical	**Nominal Value Unit**	**Test Method**
Tensile Stress (Break, Injection Molded)	2610 psi	ISO 527-2
Tensile Strain (Break, Injection Molded)	> 500 %	ISO 527-2
Flexural Modulus (Injection Molded)	16000 psi	ISO 178
Impact	**Nominal Value Unit**	**Test Method**
Charpy Unnotched Impact Strength	No Break	ISO 179
Thermal	**Nominal Value Unit**	**Test Method**
Vicat Softening Temperature	85 °C	ISO 306
Melting Temperature	98 °C	ISO 11357-3

3.2 Equipment and Procedures

3.2.1 Batch Mixer

Predetermined amounts of the polymer and BP were blended in a batch mixer. A Haake Rheocord 90 batch mixer system equipped with a Rheomix 3000 chamber and roller – blade rotors was used connected to RC 9000 software to monitor the mixing of the samples and set the conditions required for mixing accordingly. Melt mixing of the LLDPE polymer and BP was carried out at 190 ^{o}C and 100 rpm rotor speed for 7 – 8 minutes after which the sample was allowed to be air – cooled. The process of blend preparation in a batch mixer was divided into two steps. First, the LLDPE resin was loaded into the mixer and melted under heat and shear from the rotors. Second, BP was gradually added into the polymer melt. Stabilization of torque over time indicated achievement of steady state and completion of the mixing cycle. The maximum mixing temperature went up to 220 ^{o}C and torque varying from sample to sample as every sample had a different quantity of BP added to it according to the Design of Experiments (DOE), later discussed in the thesis. Figure 3.1 shows the front and top view of the batch mixer where screws are visible as the mixer is partially opened for understanding.

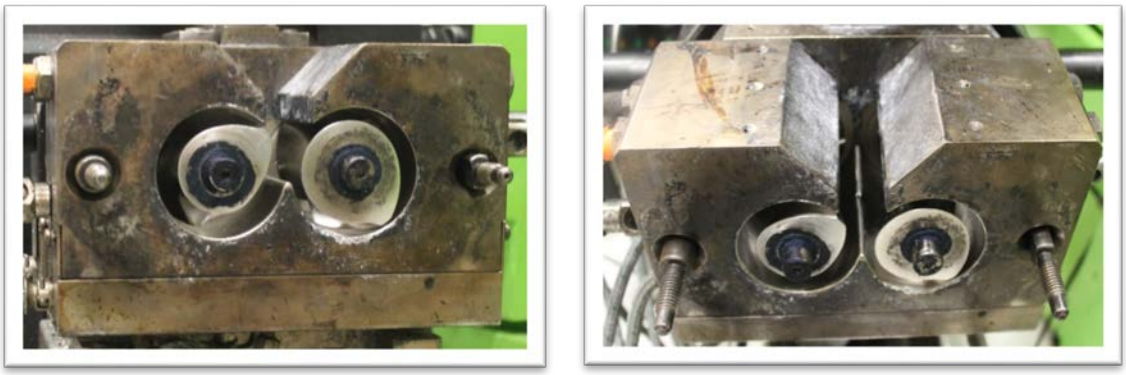

Figure 3.1 – Haake Rheocord 90 Batch Mixer
(Left – Front View, Right – Top View)

3.2.2 Grinder

The cooled samples from the batch mixer were subsequently ground into small chunks using a Wiley Will grinder (Fig. 3.2) where left image shows the whole grinder and the inner mechanism along with the cutters is visible in the image on the right.

Figure 3.2 – Wiley Will Grinder and Rotational Blades

3.2.3 Hot Press

The ground plastic blend sample was then melted and compression–molded in a thermo – controlled hot press of 13x13x2 mm square steel mold at 190 ^{o}C for 3 minutes at 20000 lb_f. A PHI Press (Fig. 3.3) was used for pressing the square sheets of the samples. The sheets were later cooled by quenching them in a water bath to avoid thermal – oxidation degradation at room temperature [36].

Figure 3.3 – PHI Compression Molding Press

3.2.4 UV Lamp

The pressed plastic sheets were then irradiated using a CON-TROL-CURE® VersaCure Modular UV Systems from UV Process Supply (Fig. 3.4) for specific time periods and lamp intensities according to the DOE. Pressurized air was used to cool down the area beneath the lamp which ranged from 31 – 37 °C before and after irradiation and 71 – 77 °C during different batches of samples [7]. The left image in Fig. 3.4 shows the UV lamp while the right image is its intensity controller.

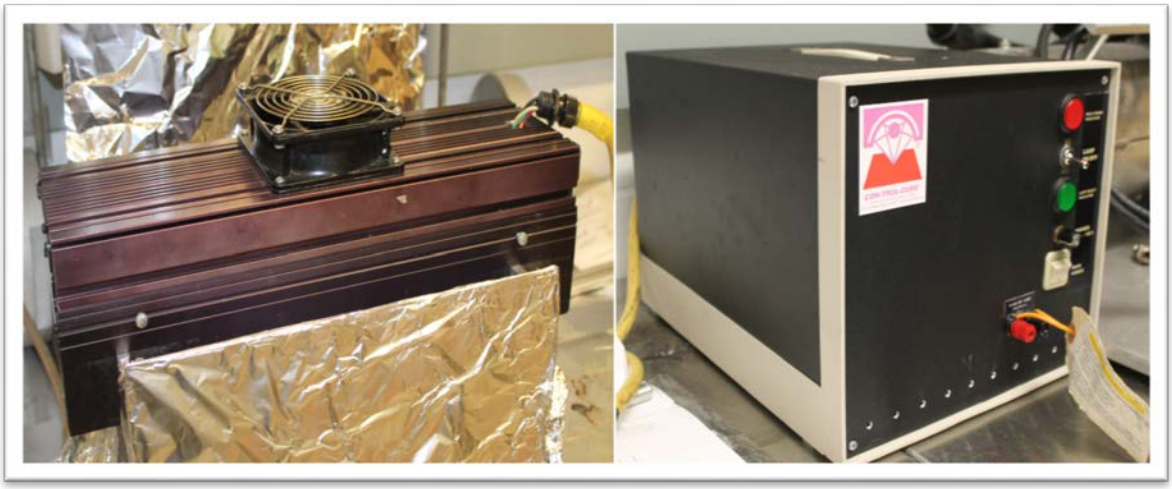

Figure 3.4 – UV Lamp and its Controller with Intensity Set Points

According to the DOE, samples were irradiated at specific set points on the UV lamp in order to expose the samples to the required intensity. The UV lamp had twelve set points as shown in Table 3.2.

Table 3.2 – UV Lamp Set Points and its Intensities

Intensity Set Points	Intensity Percentage
1	47.0
2	51.8
3	56.6
4	61.4
5	66.2
6	71.0
7	75.8
8	80.6
9	85.4
10	90.2
11	95.0
12	99.8

If the DOE called for a value of intensity lying in between two set points in Table 3.2, two samples were irradiated, one on the higher intensity and the other on the lower one. Both samples were then analyzed and every result was averaged for the sample which had to be exposed to the UV intensity for a value lying in between those two set points. It was assumed that a similar result would have been obtained if that intensity set point value was available to be used [16].

3.2.5 Parallel Plate Rheometer

Discs of 25 mm diameter and 1 mm thickness were cut from the irradiated plaques using a round sharp – edged cutting die (ODC Tooling and Molds Inc.). These were used for testing in the parallel plate rheometer.

Linear viscoelastic properties were measured through strain and frequency sweep for 0.1 – 10 % strain and 0.1 – 100 Hz frequency, respectively, and the results were used to calculate different rheological polydispersity measures (i.e. Polydispersity Index, Modulus of Separation, ER, etc.) in order to assess the effect of processing conditions on polymer structure [23].

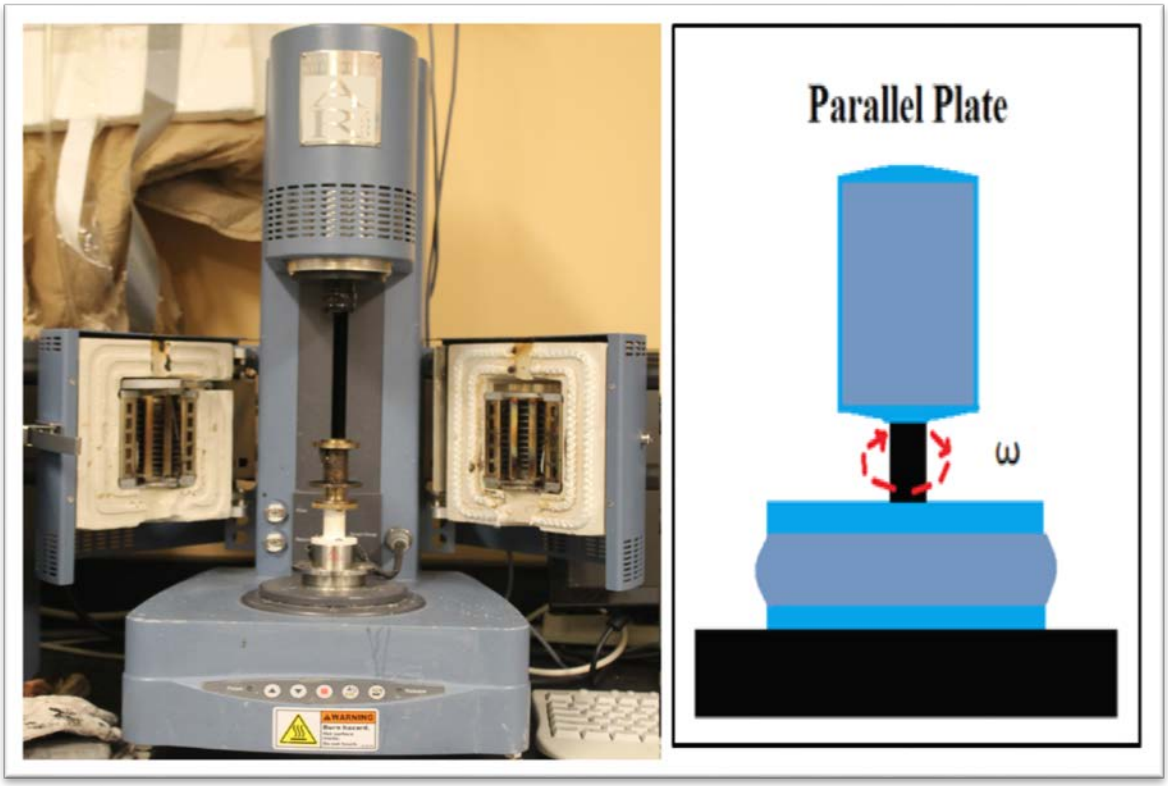

Figure 3.5 – Parallel Plate Rheometer (AR2000 TA Instrument) and Illustration of Oscillating Parallel – Plates Geometry

Oscillatory shear tests were performed using a TAI AR2000, a controlled – stress rotational rheometer (see Fig. 3.5). To avoid thermo-oxidative degradation during testing, pure nitrogen gas was pumped into the rheometer oven to provide an inert atmosphere. The image on the left in Fig. 3.5 shows the rheometer while the image on the right shows the mechanism of oscillation at different frequencies.

The sample disks were loaded on the lower plate in the test chamber which was preheated at 190 °C. The disks were melted for 3 minutes in the chamber and the upper plate was then lowered down to the target gap of around 1 mm until it came in contact with the sample disk. The normal force being applied on the sample when the sample and the plates come in contact was then relaxed to zero before starting to conduct the experiment and record the measurements.

All the samples underwent strain sweep test at 100 Hz frequency first in order to determine the linear viscoelastic region and ensure that the subsequent frequency sweep tests have been performed at strains within the linear viscoelastic (LVE) region [7].

3.2.6 Differential Scanning Calorimetry (DSC)

Differential Scanning Calorimetry (DSC) experiments were carried out using a Universal Analysis 2000 (TA Instruments) calorimeter (see Fig. 3.6) to determine the melting and crystallization characteristics of the irradiated samples.

Figure 3.6 – TAI Differential Scanning Calorimetry (DSC)

A small chunk of sample was cut from the irradiated sheet and put in a Tzero – aluminium pan and covered with a lid. The pan with the lid was put in the mold to be pressed. Left image of Fig. 3.7 shows the press, and the right image shows different molds where the blue colored one was used for Tzero – Aluminium pan and lid as there has to be no reaction happening inside the heating/cooling chambers of the DSC. Other molds are used for different purposes, e.g., if there is a reaction happening during any experimental cycle.

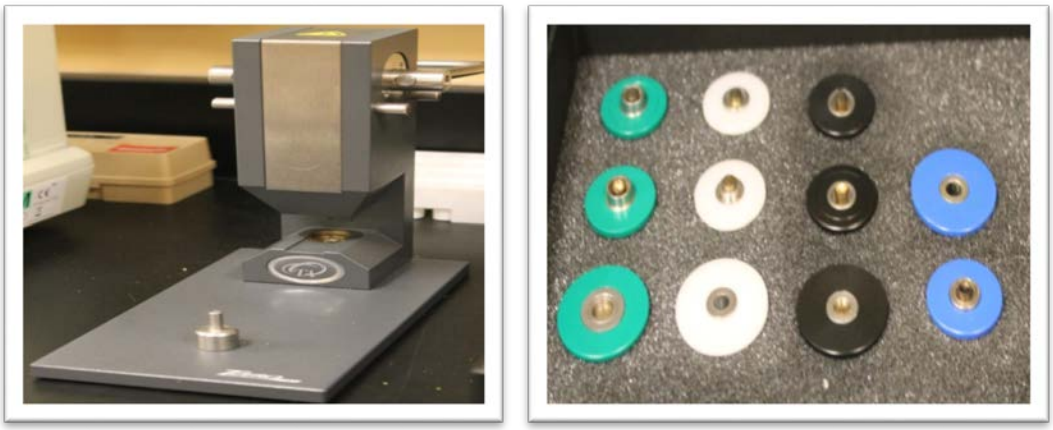

Figure 3.7 – Press on Left, Molds for Different Pans and Lids on Right

Initially, a Tzero aluminium pan was weighed for zero error and referencing, after which small chunks of sample between 9.5 mg to 12 mg were cut and put in the pans to be closed in a press. The closed pans were put in the DSC chamber and were exposed to heating/cooling/heating cycles at a rate of 10 ^{o}C/min. Nitrogen and air were supplied to the chamber at 50 ml/min to keep the system inert and to cool the system, respectively. Heat flow versus temperature graphs were obtained from the experimental heating and cooling cycles. These graphs were then analyzed to determine the crystallization and melting points as well as the heats of melting and crystallization. Percentage of crystallinity (X_c) was also calculated for every sample run and compared with the virgin material for analysis [15].

3.3 Design of Experiments

In order to study the effect of different processing factors on the rheological properties of the samples, a statistical design of experiments (DOE) was used. In this study, three independent variables were taken into consideration. These were BP (photo-initiator) concentration, time of exposure to UV irradiation and intensity of the UV lamp. BP concentration was calculated in weight percent, irradiation time in seconds and lamp intensity in percentage.

A regular central composite design (CCD) was employed, where centre points are denoted by the level 0. The quantity of the centre point runs is a factor of the independent variables used for the experiment. End points are denoted by level -1 or 1, which is the distance between the centre of the design and the factorial point. These end points are limits of the independent variable used. The star points are denoted by level $-\alpha$ or α, which are an estimation of curvature augmenting the centre points. This CCD is an orthogonal and rotatable design. For a model of three factors, the design is described as a sphere around a cube, which is the case in this study.

A Box–Wilson Central Composite Design (CCD) (see Fig.3.8) was implemented to calculate the set of values to be used for the three independent variables. In this design, the three variables are indicated along the x_1, x_2, and x_3 axes, fenced by the end points and star points marking the extreme condition points of the curvature.

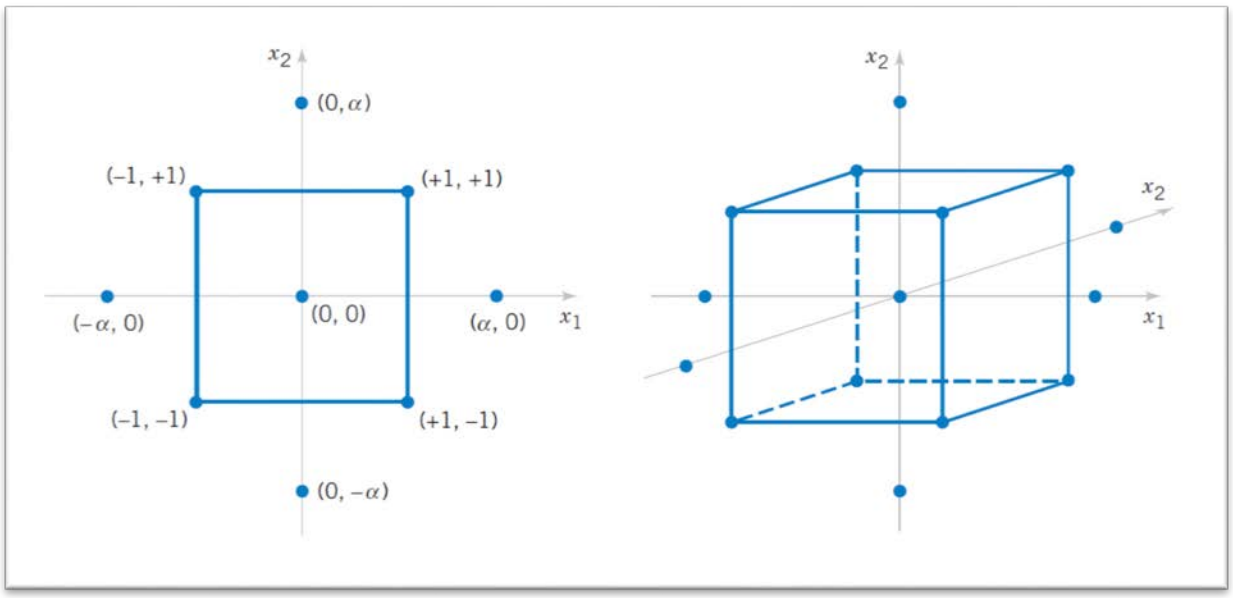

Figure 3.8 – Circumscribed CCD with Coordinates [37]

The value of alpha depends on the orthogonal blocking, that is whether the design is divided into blocks or not. Blocking affects the estimation of coefficients in the model. Note that alpha is calculated based on no blocking in this study.

With k being the number of factors, the value F of the factorial runs is equal to 2^k, therefore, F is 8 for this study. For star and centre points, the number of samples to be prepared was 6 each, as the formula is 2 x k. Thus, 20 samples were to be prepared according to the DOE shown in Table 3.3.

Table 3.3 – DOE Experimental Conditions

Run	**BP**	**Time**	**Intensity**
1	1	1	1
2	1	1	-1
3	1	-1	1
4	1	-1	-1
5	-1	1	1
6	-1	1	-1
7	-1	-1	1
8	-1	-1	-1
9	α	0	0
10	0	α	0
11	0	0	α
12	-α	0	0
13	0	-α	0
14	0	0	-α
15	0	0	0
16	0	0	0
17	0	0	0
18	0	0	0
19	0	0	0
20	0	0	0

The value of α was calculated as follows:

$$alpha = (2^k)^{1/4} = (2^3)^{1/4} = 1.682 \quad [3.1]$$

$$-\alpha = X - \left[alpha * (\frac{R}{2})\right] \quad [3.2]$$

$$\alpha = X + \left[alpha * (\frac{R}{2})\right] \quad [3.3]$$

$$X = \frac{x+y}{2} \quad [3.4]$$

$$R = y - x \quad [3.5]$$

Note that 'alpha' is the constant, depending on the number of factors used, while α is the star point.

In Equations 3.1 – 3.5, -α and α are the star point limits, x and y are the end point limits (-1 and 1, respectively), X is the average of the end points and R is the difference between the end point limits.

The independent variable values for this design are shown in Table 3.4:

Table 3.4 – Independent Variables and their Values for DOE

Variables	-α level	-1 level	+1 level	+α level	0 level
BP (wt %)	0.00	0.13	0.50	0.63	0.32
Time (s)	19.80	30.00	60.00	70.20	45.00
Intensity (%)	47.00	56.60	80.60	90.20	68.60

As mentioned earlier, the UV lamp had specific set points which limited us to select the exact set points. Table 3.5 indicates which set point values were to be used according to the required lamp intensity. Run 1 was the sample to be tested at maximum BP, time, and intensity, therefore it was done twice (as sample runs Test 1 and 1) to minimize any human errors and achieve a realistic set of results. Sample runs 9, 10, 12, 13 and 15 to 20 had to be done on two different set points as the required intensity according to our DOE was lying exactly in between two set points. Thus, these runs were carried out on a set point above and below the required value and averaged, assuming that the value will be more or less similar.

Table 3.5 – Experimental conditions according to feasible lamp Set Points

Run	BP	Time	Intensity	Set Points
1	0.50	60.00	80.60	8
2	0.50	60.00	56.60	3
3	0.50	30.00	80.60	8
4	0.50	30.00	56.60	3
5	0.13	60.00	80.60	8
6	0.13	60.00	56.60	3
7	0.13	30.00	80.60	8
8	0.13	30.00	56.60	3
9	0.63	45.00	68.60	5\6
10	0.32	70.20	68.60	5\6
11	0.32	45.00	90.20	10
12	0.00	45.00	68.60	5\6
13	0.32	19.80	68.60	5\6
14	0.32	45.00	47.00	1
15	0.32	45.00	68.60	5\6
16	0.32	45.00	68.60	5\6
17	0.32	45.00	68.60	5\6
18	0.32	45.00	68.60	5\6
19	0.32	45.00	68.60	5\6
20	0.32	45.00	68.60	5\6

Table 3.6 shows the exact experimental conditions used for every sample run along with the virgin material (not mixed with BP or exposed to UV). The virgin material will be used for comparison and analysis.

Table 3.6 – Actual conditions used in DOE

S. No.	Sample	BP	Time	Intensity	Set Points
1	Test 1	0.50	60.00	80.60	8
2	1	0.50	60.00	80.60	8
3	2	0.50	60.00	56.60	3
4	3	0.50	30.00	80.60	8
5	4	0.50	30.00	56.60	3
6	5	0.13	60.00	80.60	8
7	6	0.13	60.00	56.60	3
8	7	0.13	30.00	80.60	8
9	8	0.13	30.00	56.60	3
10	9 (05)	0.63	45.00	66.20	5
11	9 (06)	0.63	45.00	71.00	6
12	10 (05)	0.32	70.20	66.20	5
13	10 (06)	0.32	70.20	71.00	6
14	11	0.32	45.00	90.20	10
15	Virgin Material	-	-	-	-
16	12 (05)	0.00	45.00	66.20	5
17	12 (06)	0.00	45.00	71.00	6
18	13 (05)	0.32	19.80	66.20	5
19	13 (06)	0.32	19.80	71.00	6
20	14	0.32	45.00	47.00	1
21	15	0.32	45.00	66.20	5
22	16	0.32	45.00	66.20	5
23	17	0.32	45.00	66.20	5
24	18	0.32	45.00	71.00	6
25	19	0.32	45.00	71.00	6
26	20	0.32	45.00	71.00	6

CHAPTER 4

RESULTS AND DISCUSSION

4.1 Rheological Analysis

Linear viscoelastic properties of all samples were measured using oscillatory shear measurements. Oscillatory shear techniques are well developed [7, 15] and can provide information on the elastic and viscous properties of polymeric materials resulting from varying structural characteristics [38].

As previously described, the disks used in testing were cut from the irradiated plaques and used in a parallel plate rheometer at 190 ^{0}C in the presence of a nitrogen atmosphere to avoid thermo – oxidative degradation and/or crosslinking during testing. An oscillatory rheometer's basic principle is to induce a sinusoidal shear deformation in the sample and measure the resultant stress response, the time scale probe being determined by ω of the shear deformation. The sample is put between the plates and normal force and gap is zeroed. The required temperature, that is 190 ^{o}C for this experiment, is inputted in the TAI AR2000 software. The preheated sample was softened first by keeping the chamber at the required temperature for 3 minutes before the strain sweep and frequency sweep tests were performed. For the strain sweep, the rotating plate's frequency of oscillation (ω) was kept constant at 99.5 Hz or 625.2 rad/s (highest frequency) and the linear viscoelastic region (LVE) was determined [38].

Subsequently, frequency sweep tests were performed to determine the storage modulus (G´), the loss modulus (G˝) and the complex viscosity η^* of each sample. The loss factor or the loss tangent (tan δ) was determined as the ratio of G" to G´.

Figure 4.1 shows an example of a strain sweep test for sample run 9(05) indicating that the LVE region extends until about 4% deformation. In this figure, storage modulus (G'), loss modulus (G") and complex viscosity (η*) is shown against strain (γ). The range of strains in which these three properties remain almost constant defines the linear viscoelastic region (LVE) region in which the material response is independent of the strain magnitude.

Figure 4.2 shows data from a frequency sweep test for sample run 9(05) for storage and loss moduli as well as complex viscosity against angular frequency (ω). When frequency sweep is performed by using a strain magnitude in the LVE [39], such a figure shows the effect of frequency on material properties.

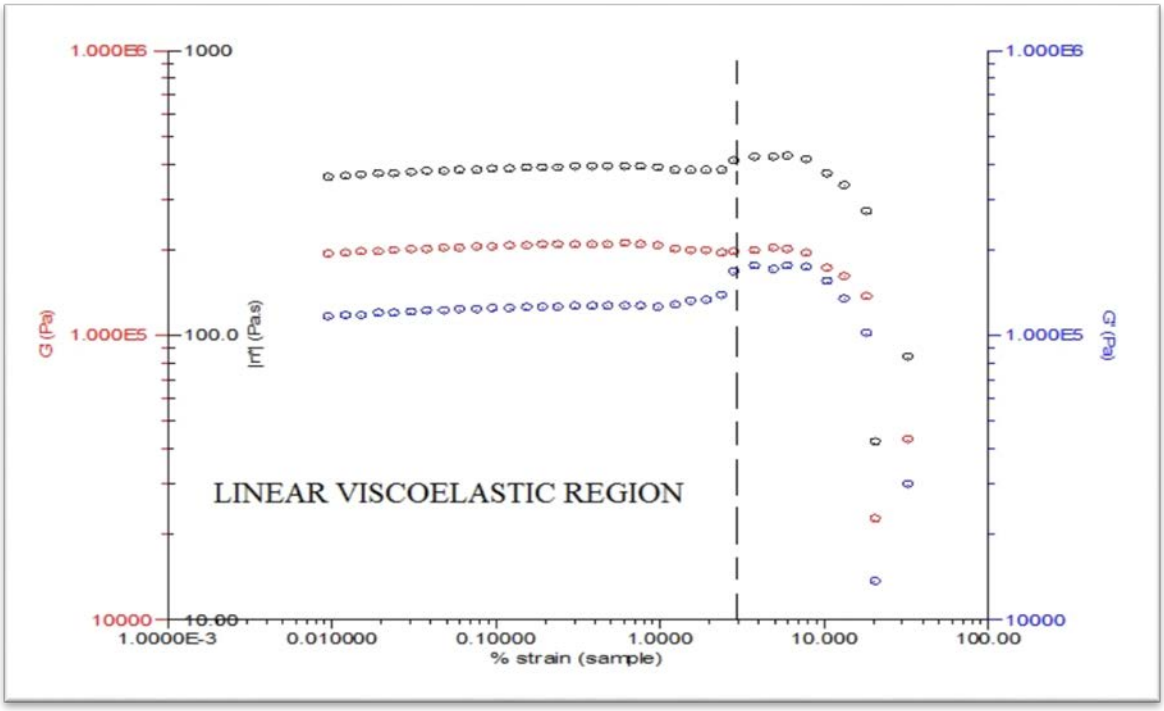

Figure 4.1 – Strain Sweep result of sample run 9(05) showing the LVE region till 4% deformation

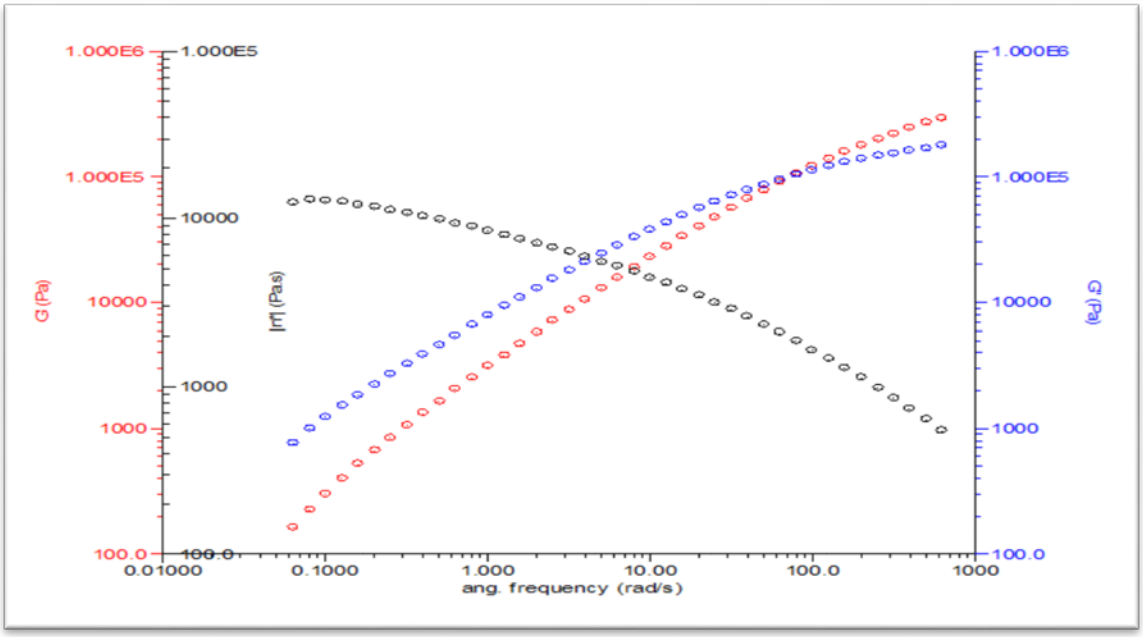

Figure 4.2 – Frequency Sweep results of sample run 9(05) showing G´, G˝ and η* vs ω

A Cole – Cole plot of the same sample run 9(05) is shown in Figure 4.3 in comparison to the virgin material. This type of a plot can be used to determine changes in sample polydispersity based on its slope at low moduli values. Another typical plot used for all the runs to determine the crossover modulus (G_c) (the common modulus value for G' and G") is shown in Figure 4.4. This crossover modulus is later on correlated to the rheological polydispersity index (PI).

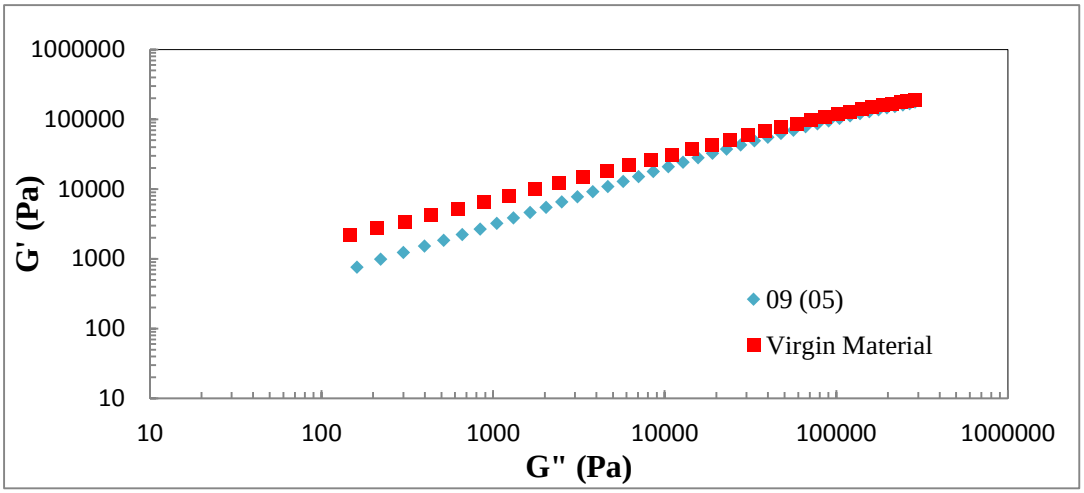

Figure 4.3 – Cole-Cole Plot for sample run 9(05) and Virgin Material

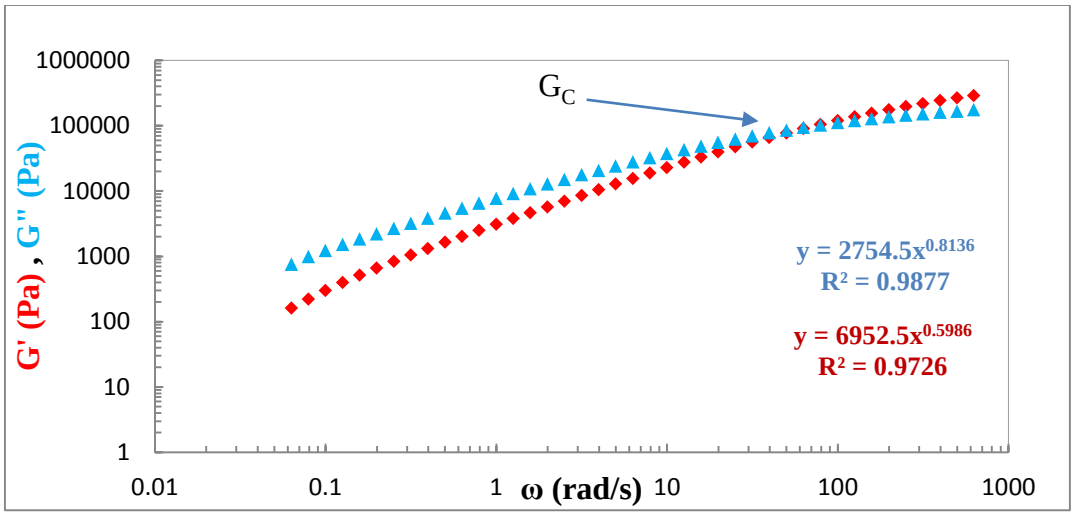

Figure 4.4 – Crossover Modulus G_C for sample run 9(05) calculated at the intersection of G´ and G˝

4.2 Comparison of Results in terms of Storage Modulus (G´)

All the sample runs were compared with the virgin material in terms of the storage modulus. It was observed that storage modulus increased for all of them at low frequencies. This is an indication of increased long chain branching and possibly crosslinking [15]. Figure 4.5 shows the comparison of some of the sample runs to highlight the trend of increasing values of G' as a function of frequency (ω).

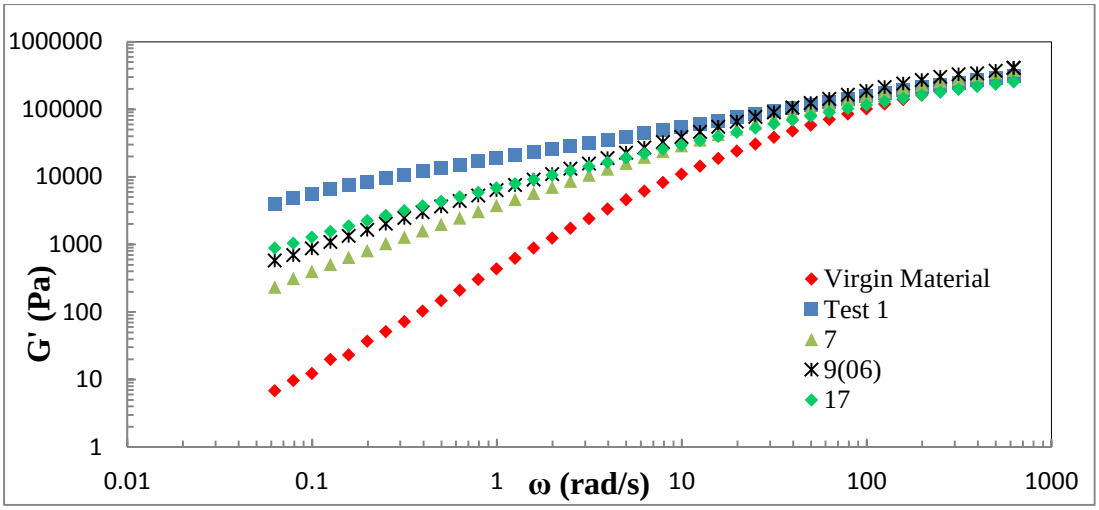

Figure 4.5 – G´ vs ω for sample runs, Test 1, 7, 9(06) and 17 with the Virgin Material

4.3 Comparison of Results in terms of Complex Viscosity (η^*)

In the following set of graphs, selective comparison of samples is presented in terms of complex viscosity data. In general, increasing zero-shear viscosity indicates the presence of branching and/or crosslinking in the samples. Samples are compared to the virgin material to determine if UV – irradiation induced any branching, or even crosslinking, in the material. Figure 4.6 shows a comparison between sample runs 16 and 19 and the virgin material. These sample runs have the same BP concentration and times of exposure while the intensity of the UV – irradiation is different. According to Table 3.6, sample run 16 was done at set point 5 on the UV lamp with 66.2% intensity of irradiation and sample run 19 on set point 6 with 71% intensity.

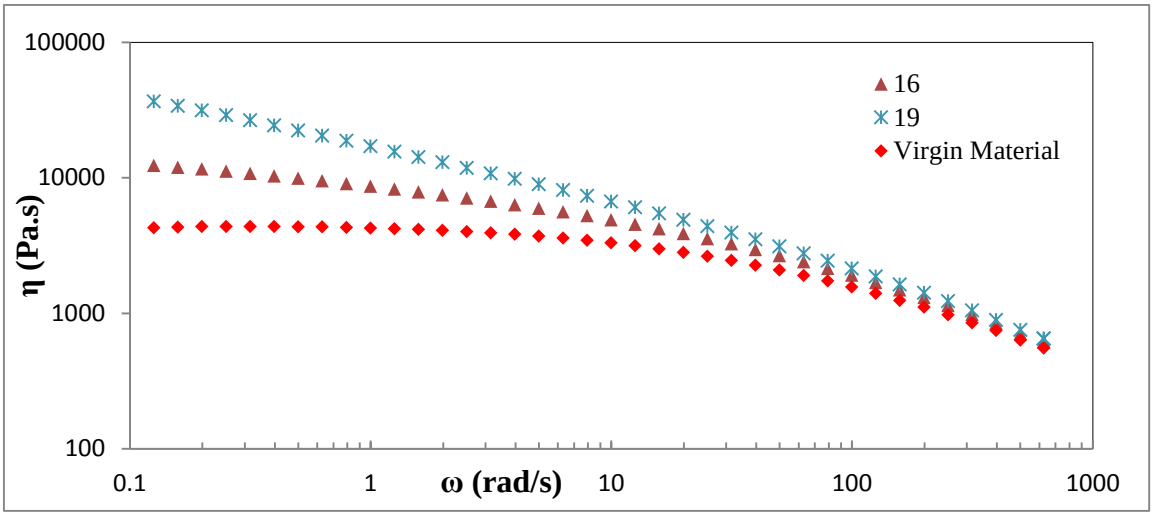

Figure 4.6 – Viscosity Comparison of sample runs 16 and 19 with the Virgin Material

As can be seen in Figure 4.6, increasing the UV intensity increases significantly the zero-shear viscosity while it is not affecting the shear thinning region. This indicates the presence of branching. Comparing sample runs 16 and 19 shows that a Newtonian plateau is almost observed in sample run 16. This indicates that branching is present. The absence of a plateau for sample run 19 indicates the presence of crosslinking [7, 15-16, 23].

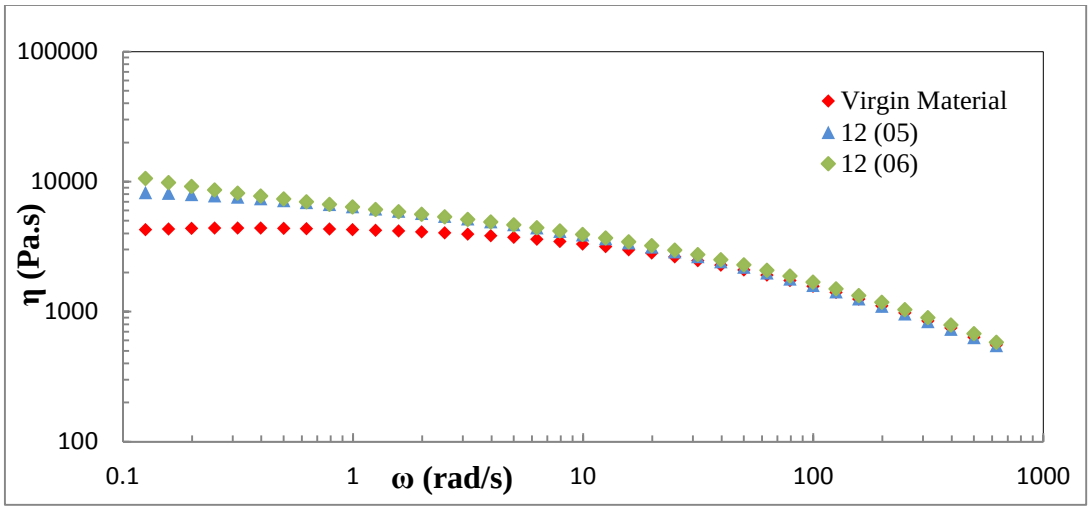

Figure 4.7 – Viscosity Comparison of sample runs 12(05) and 12(06) with the Virgin Material

Figure 4.7 compares sample runs 12(05) and 12(06) (at zero BP concentration) with the virgin material. The difference between the samples is the change in the intensity of the UV lamp from set point 5 to 6 and intensity from 66.2% to 71% in sample runs 12(05) and 12(06), respectively. It can be seen that increasing UV intensity increases the zero-shear viscosity. However, this effect is not so pronounced in the absence of BP.

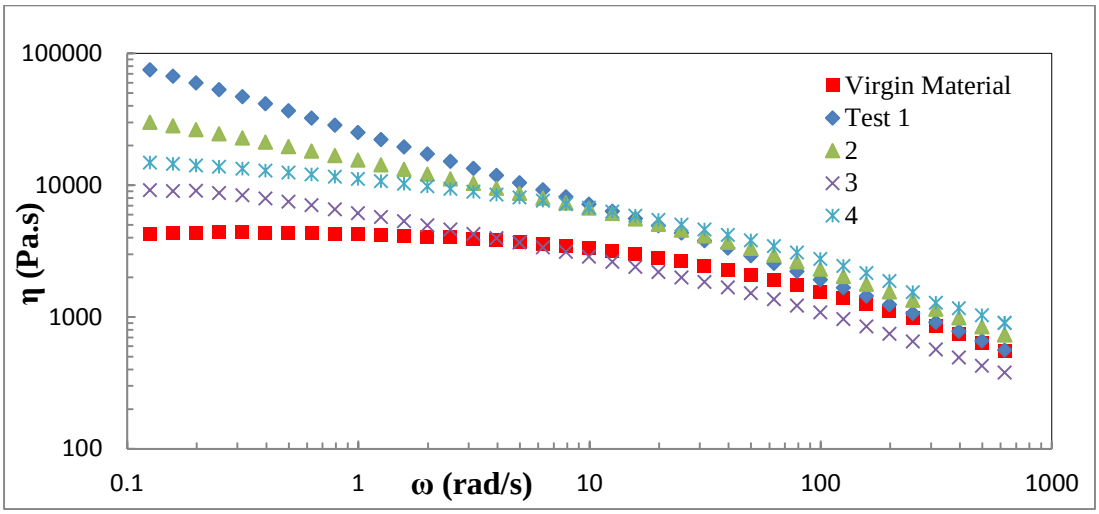

Figure 4.8 – Viscosity Comparison of sample runs, Test 1, 2, 3 and 4 with the Virgin Material

Figure 4.8 compares sample runs Test 1, 2, 3 and 4 with the virgin material. All four sample runs were done at the same BP concentration of 0.5 wt%. The differences in the four samples are that sample runs Test 1 and 2 had the same exposure time (60 sec) but different lamp intensities, 80.6% intensity for sample run Test 1 and 56.6% intensity for sample run 2. Sample runs 3 and 4 had the same exposure time (30 sec) but different lamp intensities, 80.6% intensity for sample run 3 and 56.6% intensity for sample run 4. It can be seen that higher exposure time (sample runs Test 1, 2 versus 3, 4) lead to increased viscosity at low frequencies. The absence of a Newtonian plateau for sample runs Test 1, 2 indicates the presence of crosslinking. Sample runs 3, 4 both show a Newtonian plateau indicating the presence of branching in comparison with the virgin material. Comparing sample runs Test 1, 3 and 2, 4 shows that the effect of exposure time is more pronounced at higher UV intensities.

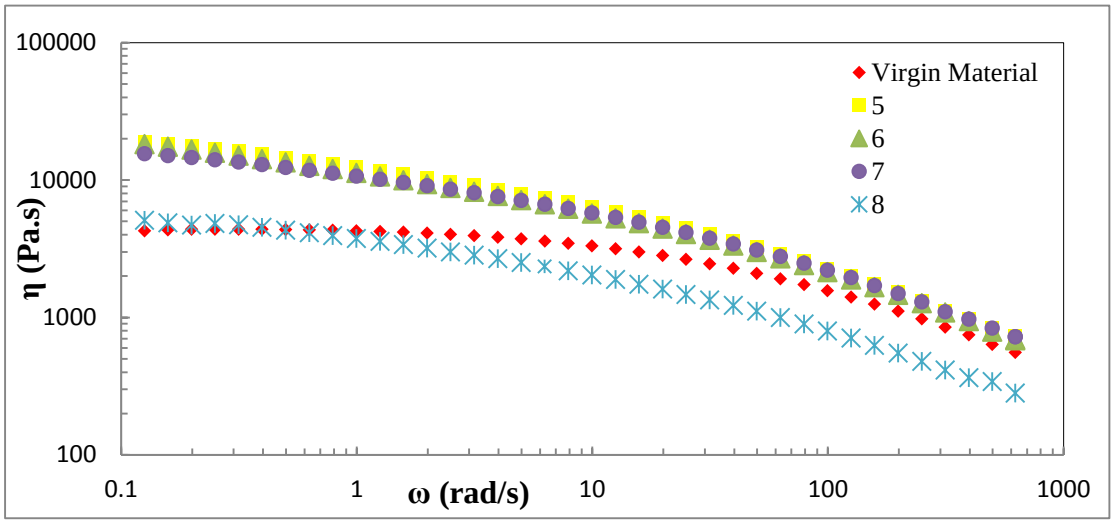

Figure 4.9 – Viscosity Comparison of sample runs 5, 6, 7 and 8 with the Virgin Material

Figure 4.9 compares sample runs 5, 6, 7 and 8 with the virgin material. All four sample runs were done at the same BP concentration of 0.13 wt%. Sample runs 5 and 6 had the same time of exposure (60 sec) but different lamp intensities of 80.6% and 56.6%, respectively. Sample runs 7 and 8 had

the same time of exposure (30 sec) but different lamp intensities of 80.6% and 56.6%, respectively. In comparison to the virgin material, sample runs 5, 6 and 7 have higher viscosity at low frequencies and do not exhibit a Newtonian plateau. Sample run 8 has a similar zero-shear viscosity to that of the virgin material but it is more shear thinning, indicating increased branching without crosslinking. From the comparison of these samples it appears that at low BP concentration and long exposure times, change in UV intensity has no effect (as seen in terms of η_0 for sample runs 5 and 6) but at low BP concentration and small exposure times, change in UV intensities has a pronounced effect (as seen in terms of shear thinning for sample runs 7 and 8).

4.4 Comparison of Results in terms of Loss Tangent

One test on any sample gives an idea of what property that sample might possess but a series of experiments gives a certainty of that property of any sample to be there for a fact. Likewise, the loss tangent plot gave an extra explanation of the fact that branching did get induced due to UV – irradiation. All the sample runs showed that branching was present in the samples after exposure to UV. Figure 4.10 shows comparison of some of the sample runs with the virgin material. All sample runs have their trend lines way below the virgin material trend line, which demonstrates the presence of branching or crosslinking.

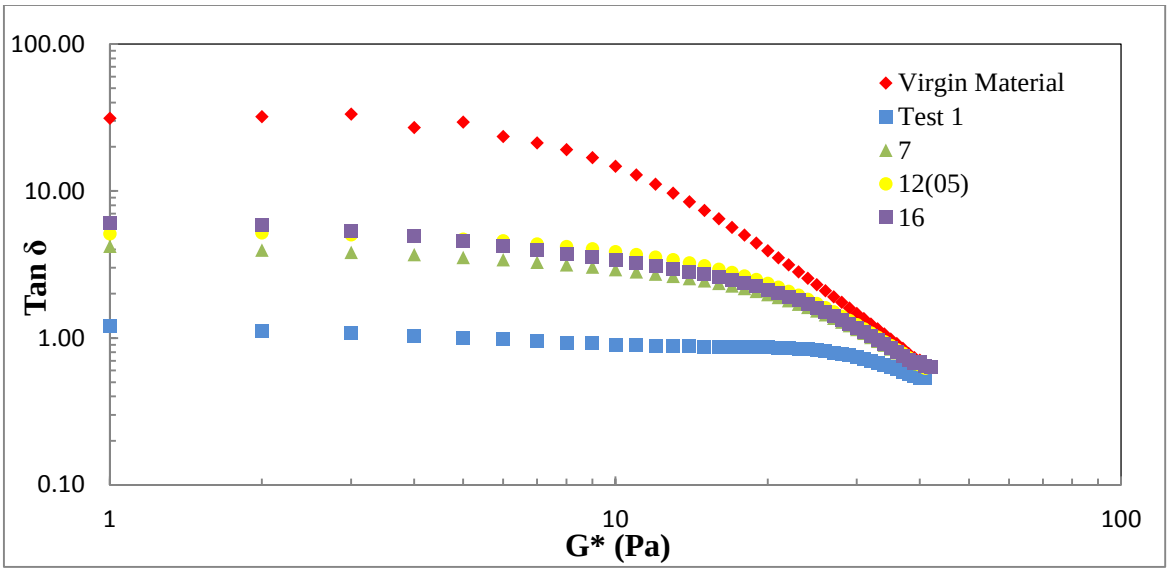

Figure 4.10 – Loss Tangent of sample runs, Test 1, 7, 12(05) and 16 with the Virgin Material

The virgin material has higher values of tan δ at lower values of G* (G* is the complex modulus) compared to other sample runs. Sample run Test 1 appears to have the highest percentage of branching as it has the lowest values of loss tangent in the overall comparison amongst other runs. Sample runs 7, 12(05) and 16 have trend lines in between the trend lines of the virgin material and sample run Test 1; this indicates that although they do have some percent branching in them after exposure to UV, a greater amount is seen only in run Test 1. Sample run 7 has a 0.13% BP by weight with 30 second time of irradiation and UV lamp intensity of 80.6% (same intensity of sample run 1) while the BP and exposure time for sample run Test 1 is 50% and 60 seconds, respectively. The difference in these two sample runs is seen clearly as the sample run Test 1 curve is way lower than the curve of sample run 7. The time of exposure and lamp intensity is the same in sample runs 12(05) and 16, which is 68.6% lamp intensity and 45 seconds irradiation time, the only difference being the intensity of the UV lamp. Sample run 12(05) had no BP added to it, while sample run 16 had 0.32% BP by weight and the difference is clearly visible in Figure 4.10, where the tan δ – G^* curve for sample run 12(05) is lower than sample run 16. This is because sample run

12(05) is going through the process of photo – oxidation and is degrading, broadening the MWD and hence a lower curve is obtained in comparison to sample run 16. The tan δ – G^* curves for the compared sample runs are lowest compared to the virgin material, which points towards the fact that LCB is present in these samples and the MWD is hence broadened. Thus, it can be said that the reduction of the tan δ value at the lower G^* represents more elastic behavior due to LCB and broadening of MWD.

4.5 Modulus of Separation

Modulus of separation (ModSep) is one measure of rheological polydispersity [26], which can be calculated from linear viscoelastic properties. The equations of G' and G" against ω are shown in Table 4.1. These were derived by fitting the G' and G" data and are used to calculate the values of ω corresponding to the same reference modulus value for G' or G".

Table 4.1 – Equation of G' and G" vs ω per sample run

	Equation for G' vs ω	Equation for G" vs ω
Test 1	G'=(18122*(ω´^0.4668))	G"=(16644*(ω˝^0.397))
1	G'=(4630.2*(ω´^0.3285))	G"=(3109.6*(ω˝^0.3086))
2	G'=(7321.1*(ω´^0.6712))	G"=(12626*(ω˝^0.5287))
3	G'=(2449.8*(ω´^0.752))	G"=(4778*(ω˝^0.5889))
4	G'=(2671.5*(ω´^0.9018))	G"=(9682.5*(ω˝^0.6403))
5	G'=(4195*(ω´^0.7862))	G"=(10272*(ω˝^0.5731))
6	G'=(4210.4*(ω´^0.765))	G"=(9427.2*(ω˝^0.5806))
7	G'=(3497.6*(ω´^0.8095))	G"=(8926.3*(ω˝^0.6007))
8	G'=(1605*(ω´^0.7581))	G"=(2944.3*(ω˝^0.6364))
9 (05)	G'=(2754.5*(ω´^0.8136))	G"=(6952.5*(ω˝^0.5986))
9 (06)	G'=(6018.4*(ω´^0.7274))	G"=(12167*(ω˝^0.5577))
10 (05)	G'=(7980.9*(ω´^0.6912))	G"=(14613*(ω˝^0.5251))
10 (06)	G'=(7390.8*(ω´^0.7025))	G"=(14244*(ω˝^0.5332))
11	G'=(2416*(ω´^0.8125))	G"=(5942.4*(ω˝^0.6071))
Virgin Material	G'=(376.78*(ω´^1.209))	G"=(3655.4*(ω˝^0.7471))
12 (05)	G'=(1695.6*(ω´^0.8978))	G"=(5414.3*(ω˝^0.6545))
12 (06)	G'=(1897.4*(ω´^0.8617))	G"=(6081.9*(ω˝^0.6378))
13 (05)	G'=(1381.8*(ω´^0.9833))	G"=(6309.8*(ω˝^0.6782))
13 (06)	G'=(1606.1*(ω´^0.9674))	G"=(7010.8*(ω˝^0.679))
14	G'=(2521.6*(ω´^0.7684))	G"=(5857.5*(ω˝^0.5896))
15	G'=(2472.7*(ω´^0.6282))	G"=(3901.6*(ω˝^0.501))
16	G'=(2478.1*(ω´^0.8524))	G"=(7431.5*(ω˝^0.6106))
17	G'=(6454.7*(ω´^0.6164))	G"=(9498.7*(ω˝^0.4857))
18	G'=(2725.2*(ω´^0.8488))	G"=(8147.3*(ω˝^0.6102))
19	G'=(9198.5*(ω´^0.6151))	G"=(13381*(ω˝^0.4888))
20	G'=(3691.1*(ω´^0.8045))	G"=(9418.4*(ω˝^0.5833))

In this study, the reference modulus value G_{ref} is 500 Pa and ModSep is calculated from Equation 4.1. The calculated ModSep values are listed in Table 4.2, which shows that the ModSep for the virgin material is 18.116 (no units since it is a ratio of frequencies) and all the other sample runs have ModSep values between 15.958 and 0.106, which are lower than that of the virgin materials.

This shows that the sample runs that have ModSep values between 16 and 9 have slight branching induced while other sample runs have a higher level of LCB induced in them.

$$ModSep = {\omega'}/_{\omega''} \quad [4.1]$$

Table 4.2 – Values of ω at G_{ref} = 500 Pa and ModSep per sample run

	ω'	ω"	ModSep
Test 1	0.00046	0.00015	3.120
1	0.00114	0.00268	0.426
2	0.01834	0.17357	0.106
3	0.12085	0.02165	5.582
4	0.15594	0.00977	15.958
5	0.06684	0.28480	0.235
6	0.06171	0.00636	9.707
7	0.09045	0.00825	10.968
8	0.21472	0.06167	3.482
9 (05)	0.12278	0.01231	9.974
9 (06)	0.03270	0.00327	10.003
10 (05)	0.01817	0.00162	11.242
10 (06)	0.02162	0.00187	11.564
11	0.14388	0.01696	8.486
Virgin Material	1.26369	0.06975	18.116
12 (05)	0.25661	0.02626	9.772
12 (06)	0.21274	0.01989	10.694
13 (05)	0.35565	0.02380	14.945
13 (06)	0.29931	0.02047	14.624
14	0.12176	0.01539	7.910
15	0.07851	0.01656	4.742
16	0.15293	0.01203	12.708
17	0.01577	0.00233	6.768
18	0.13564	0.01032	13.143
19	0.00879	0.00120	7.316
20	0.08334	0.00652	12.785

4.6 Rheological Polydispersity Index

Polydispersity index (PI) is calculated by using the same equations in Table 4.1 to calculate the cross-over modulus G_C [26], which is the intersecting point of both equations for G' and G". G_C is used in Equation 4.2 to calculate PI values shown in Table 4.3.

$$PI = {10^5}/{G_c} \qquad [4.2]$$

Table 4.3 – Values of G_c and PI

	G_c	PI
Test 1	1.03E+04	9.7
1	6.48E+00	15401.3
2	9.53E+04	1.0
3	5.33E+04	1.9
4	2.27E+05	0.4
5	1.14E+05	0.9
6	1.19E+05	0.8
7	1.32E+05	0.8
8	7.03E+04	1.4
9 (05)	9.15E+04	1.1
9 (06)	1.23E+05	0.8
10 (05)	9.89E+04	1.0
10 (06)	1.12E+05	0.9
11	8.50E+04	1.2
Virgin Material	1.44E+05	0.7
12 (05)	1.23E+05	0.8
12 (06)	1.68E+05	0.6
13 (05)	1.85E+05	0.5
13 (06)	2.25E+05	0.4
14	9.43E+04	1.1
15	2.35E+04	4.3
16	1.19E+05	0.8
17	3.99E+04	2.5
18	1.34E+05	0.7
19	5.71E+04	1.8
20	1.11E+05	0.9

The values of PI mentioned in Table 4.3 have a sample run 1 value that is not correct, which shows that the curves of G' and G" against ω are not intersecting and the trend lines are interpolated to achieve an estimated value. This estimate is not correct as it is not an exact crossover modulus, which leads to an incorrect PI for that sample run. PI is inversely correlated with G_C and is expected to reflect changes in the breadth of MWD of sample runs, similar to ModSep, while ER (discussed in the next section) is only sensitive to the high MW part of the MWD [16]. Looking at the values of PI, the virgin material has a value of 0.7 and most of the sample runs have PI higher than that. This means that the MWD is broadening. Only a few sample runs have PI around 0.4 to 0.6, which shows that the MWD is narrow in these runs. These runs include sample runs 4, 12(06), 13(05) and 13(06). If we see the DOE for the specific changes between these sample runs, it can be seen that although sample run 4 had 0.5% by weight BP, low UV lamp intensity and also the time of exposure restricted the MWD broadening. Similarly 12(06) had no BP in it, but it was irradiated by UV for a certain time which means it was slightly degraded. Sample runs 13(05) and 13(06) had a moderate amount of BP and UV irradiation intensity of the lamp but the time of exposure was very little, therefore, LCB was not achieved, in fact, the sample started to slightly degrade.

4.7 Calculation of ER

ER is another rheological polydispersity index reflecting changes of the high molecular weight end of the MWD [26]. It is basically the PI of high molecular weight chains. In order to calculate the ER, Cole – Cole plots were used but in a shortened way. The plots of G' vs G" had too many points and the trend line was a curve, so the points on lower values of the modulus (both storage and loss) were used that gave straight lines with the same slope.

$$ER = Slope \times G' \quad [4.3]$$

Equation 4.3 was used to calculate the ER. The storage modulus in the equation is calculated by inputting 500 Pa as G''_{ref} in the equation of the line shown in Table 4.4. R^2 of these straight lines was 1 for all the sample runs on the average. Figure 4.11 shows an example of the Cole – Cole plot for sample run 1 with the first ten points from the data that have the same slope, also showing that the R^2 is almost 1 and the trend line is indeed straight [16].

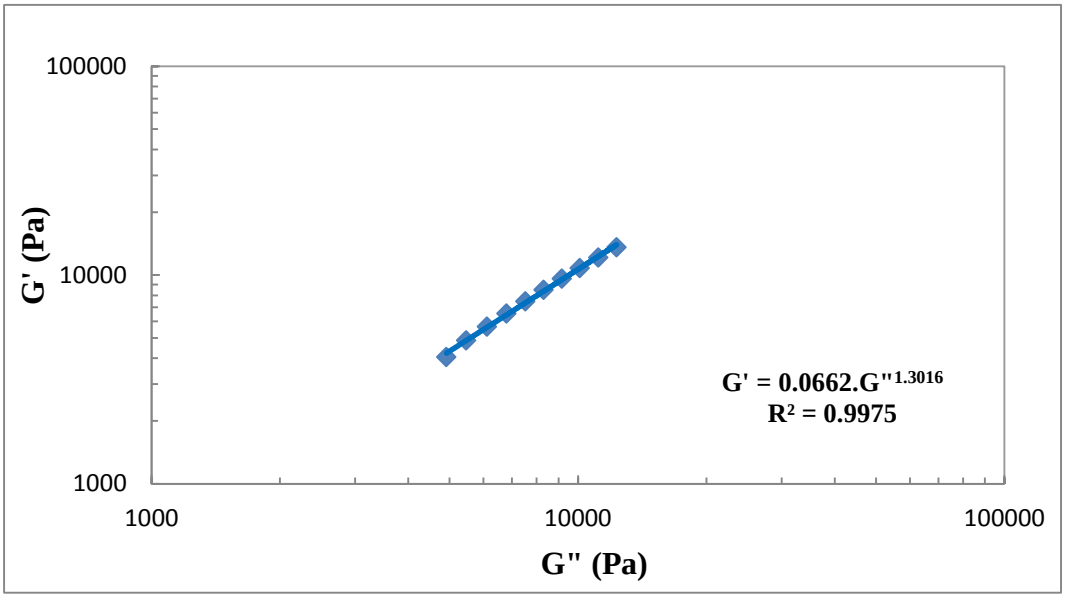

Figure 4.11 – Cole-Cole plot used to calculate ER for sample run, Test 1

$$y = k \ . \ x^n \quad [4.4]$$

$$G' = C_2 \ . \ G''^{C_1} \quad [4.5]$$

Table 4.4 – Equation of G' and G" vs ω per sample run

	Slope	Equation	G' (at G''_{ref})	ER
Test 1	1.3016	$G' = 0.0662.G''^{1.3016}$	215.6936	0.281
1	1.4144	$G' = 0.0591.G''^{1.4144}$	388.1599	0.549
2	1.3388	$G' = 0.0277.G''^{1.3388}$	113.7263	0.152
3	1.3087	$G' = 0.0422.G''^{1.3087}$	143.6992	0.188
4	1.4381	$G' = 0.0057.G''^{1.4381}$	43.3774	0.062
5	1.4320	$G' = 0.0094.G''^{1.432}$	68.8736	0.099
6	1.3964	$G' = 0.0153.G''^{1.3964}$	89.8531	0.125
7	1.1986	$G' = 0.0608.G''^{1.1986}$	104.4453	0.125
8	0.5600	$G' = 8.6421.G''^{0.56}$	280.5708	0.157
9 (05)	1.3281	$G' = 0.0236.G''^{1.3281}$	90.6597	0.120
9 (06)	1.1971	$G' = 0.0767.G''^{1.1971}$	130.5366	0.156
10 (05)	1.2883	$G' = 0.0373.G''^{1.2883}$	111.8902	0.144
10 (06)	1.4049	$G' = 0.0135.G''^{1.4049}$	83.5828	0.117
11	1.1496	$G' = 0.0981.G''^{1.1496}$	124.2811	0.143
Virgin Material	1.3543	$G' = 0.004.G''^{1.3543}$	18.0832	0.024
12 (05)	1.1543	$G' = 0.0718.G''^{1.1543}$	93.6581	0.108
12 (06)	0.6535	$G' = 2.9963.G''^{0.6535}$	173.9251	0.114
13 (05)	1.2111	$G' = 0.0281.G''^{1.2111}$	52.1710	0.063
13 (06)	0.6675	$G' = 1.4963.G''^{0.6675}$	94.7504	0.063
14	0.9383	$G' = 0.5738G''^{0.9383}$	195.5258	0.183
15	0.6439	$G' = 6.8237.G''^{0.6439}$	373.1528	0.240
16	1.3807	$G' = 0.0125.G''^{1.3807}$	66.5852	0.092
17	1.3115	$G' = 0.0446.G''^{1.3115}$	154.5375	0.203
18	1.3160	$G' = 0.0196.G''^{1.316}$	69.8394	0.092
19	1.3165	$G' = 0.0396.G''^{1.3165}$	141.5433	0.186
20	1.2163	$G' = 0.0477.G''^{1.2163}$	91.4694	0.111

Equation 4.4 is the power law for ER calculation and is modified to better understand how values of the unknowns were found in Equation 4.5. The obtained values of ER were divided by the

normalized slope of 0.001 or 10^{-3}. These values were put in the software Statistica for significance check and the following combinations gave the most significant results.

Table 4.5 – Significance check from Statistica for ER values

	BP	Time	Intensity	ER
Av. 1	1	1	1	0.410
2	1	1	-1	0.152
3	1	-1	1	0.188
4	1	-1	-1	0.062
5	-1	1	1	0.098
6	-1	1	-1	0.125
7	-1	-1	1	0.125
8	-1	-1	-1	0.157
Av. 9	α	0	0	0.139
Av. 10	0	α	0	0.131
11	0	0	α	0.142
Av. 12	-α	0	0	0.120
Av. 13	0	-α	0	0.069
14	0	0	-α	0.183
Av. 15-20	0	0	0	0.179

Different combinations of sample runs were put in Statistica to check for significance because sample runs 1, 9, 10, 12, 13 and 15 to 20 were conducted at slightly different settings of exposure intensity of UV due to the limitations of having fixed set points. As discussed earlier in Chapter 3, these sample runs had values which lied between two set points, so sample run 1 was done twice to get a more reliable value; sample runs 9, 10, 12 and 13 were done at higher (66.2% intensity) and lower (71% intensity) set points to the required value (68.6% intensity), and later averaged on the assumption that the same values would have been achieved if set points could have been set to the required intensities. Table 4.6, shows how this was done.

Table 4.6 – Sample runs at different Set Points

	BP	Time	Intensity	Set Point	Actual Intensity
Test 1	1	1	1	8	80.6
1	1	1	1	8	80.6
9 (05)	α	0	0	5	66.2
9 (06)	α	0	0	6	71.0
10 (05)	0	α	0	5	66.2
10 (06)	0	α	0	6	71.0
12 (05)	-α	0	0	5	66.2
12 (06)	-α	0	0	6	71.0
13 (05)	0	-α	0	5	66.2
13 (06)	0	-α	0	6	71.0
15	0	0	0	5	66.2
16	0	0	0	5	66.2
17	0	0	0	5	66.2
18	0	0	0	6	71.0
19	0	0	0	6	71.0
20	0	0	0	6	71.0

Table 4.7 – Statistica results for the ER values

ANOVA; Var.:Var4; R-sqr=.93489; Adj:.8177 (Spreadsheet2) 3 factors, 1 Blocks, 15 Runs; MS Residual=.0011807					
	SS	**df**	**MS**	**F**	**p**
(1) BP (L)	0.041409	1	0.041409	35.07312	0.001957
BP (Q)	0.011994	1	0.011994	10.15888	0.024338
(2) Time (L)	0.016124	1	0.016124	13.65684	0.014065
Time (Q)	0.009826	1	0.009826	8.32250	0.034392
(3) Intensity (L)	0.021027	1	0.021027	17.80922	0.008327
Intensity (Q)	0.010933	1	0.010933	9.25993	0.028652
1L by 2L	0.017205	1	0.017205	14.57251	0.012406
1L by 3L	0.024531	1	0.024531	20.77754	0.006067
2L by 3L	0.002346	1	0.002346	1.98714	0.217701
Error	0.005903	5	0.001181		
Total SS	0.090672	14			

Table 4.7 shows the significance results obtained from Statistica. It is evident that the linear and quadratic BP, time and intensity were significant along with the interaction of BP by time and BP by intensity, at a significance level of 5%. Based on this analysis, model in Eq. 4.6 can be used to describe the significant effects of process conditions on ER:

$$Y = 0.1671 + 0.0372(BP) - 0.0004(BP)^2 + 0.0333(T) - 0.0003(T)^2 + 0.0358(I) - 0.0004(I)^2 + 0.0464(BP.T) + 0.0554(BP.I) \quad [4.6]$$

4.8 Differential Scanning Calorimetry (DSC) Analysis

The melting and crystallization characteristics of all samples were analyzed by differential scanning calorimetry (DSC) using a Universal Analysis 2000 (TA Instruments) instrument. Initially, the equipment was equilibrated at 35 °C and heated to 200 °C, where it was equilibrated again and allowed to stabilize for 5 minutes isothermally. The second cycle of the experiment was to cool the system from 200 °C to -20 °C, where it was equilibrated and stabilized isothermally for 5 minutes again. The last cycle of the experiment was to heat the system again from -20 °C to 200 °C after which the system was brought to room temperature to clear the chamber and start a new sample run with the same procedure. Four variables were recorded for evaluation and further analysis. These were time (min), temperature (°C), heat flow (mW) and heat capacity (mJ/°C) [15, 23].

An example of the first heating cycle is shown for sample run Test 1 in Figures 4.12/4.13 illustrating the determination of melting peaks and enthalpy.

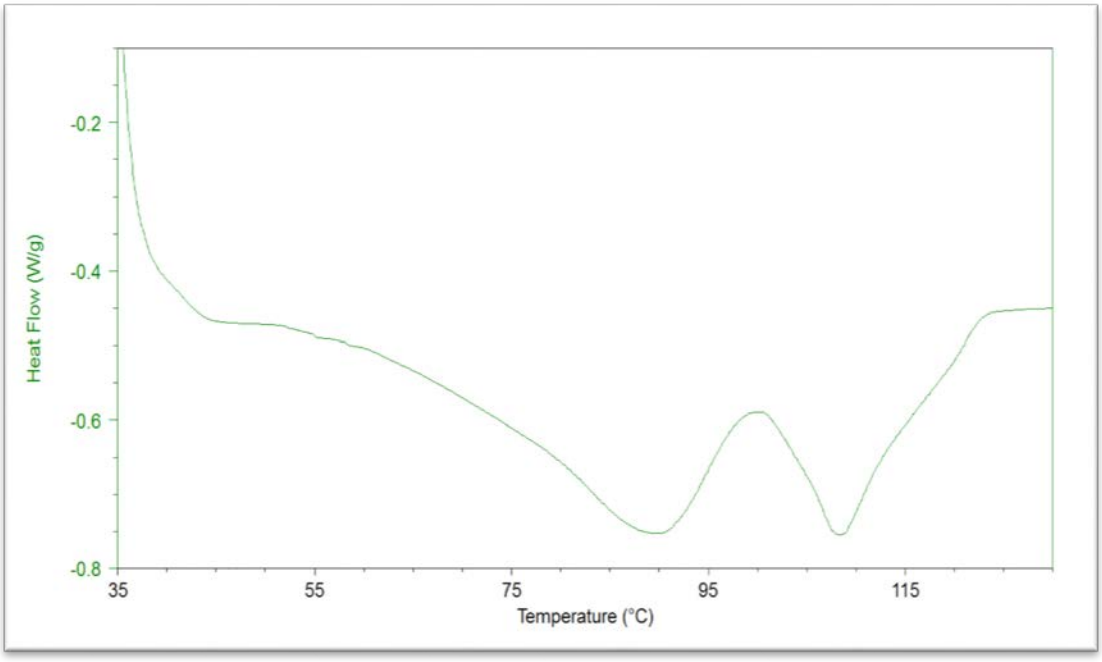

Figure 4.12 – DSC plot for First Heating Cycle of sample run, Test 1 in terms of Temperature

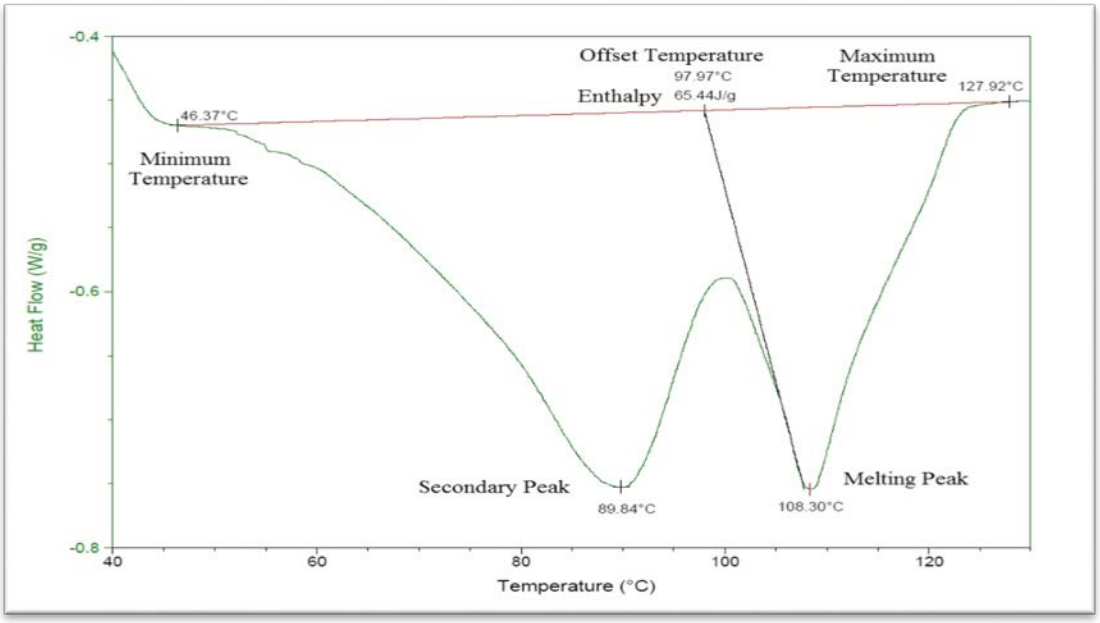

Figure 4.13 – DSC plot for First Heating Cycle of sample run, Test 1 with Extracted Values

Table 4.8 shows all the extracted values of the first heating cycle for all sample runs.

Table 4.8 – Extracted results for First Heating Cycle for all sample runs

	Min. Temp. (°C)	Max. Temp. (°C)	Offset Temp. (°C)	Enthalpy (J/g)	Peak (°C)	Secondary Peak (°C)
Test 01	46.37	127.92	97.97	65.44	108.30	89.84
01	47.79	127.65	88.38	57.24	103.12	84.73
02	47.74	128.32	62.20	54.76	104.37	-
03	50.36	130.32	70.57	52.73	103.50	-
04	47.39	127.33	66.92	54.74	104.29	-
05	57.22	126.95	82.49	48.45	103.99	87.82
06	54.16	127.11	72.74	54.25	104.00	81.67
07	48.33	128.20	75.66	54.18	104.18	81.89
08	62.55	128.51	75.32	42.20	104.50	-
09 (05)	55.23	129.01	69.61	53.58	103.70	77.54
09 (06)	50.92	127.55	71.36	55.09	104.18	-
10 (05)	53.72	127.25	81.47	51.69	103.77	87.84
10 (06)	53.08	127.69	74.58	54.44	103.86	81.96
11	55.97	129.25	73.66	47.73	105.45	-
Virgin Material	48.27	131.66	54.62	69.63	104.70	-
12 (05)	48.50	127.34	62.69	54.85	103.43	-
12 (06)	45.60	131.17	54.26	56.80	103.51	-
13 (05)	49.06	128.80	69.49	61.53	103.97	-
13 (06)	46.38	127.74	69.99	59.44	103.11	-
14	48.01	128.66	68.48	53.81	103.94	-
15	50.55	129.39	69.96	59.82	103.82	-
16	51.25	128.66	65.80	52.75	104.22	-
17	50.75	127.86	75.31	57.19	103.52	-
18	51.00	129.16	62.74	55.92	104.60	-
19	49.54	128.83	62.03	52.22	103.89	-
20	44.51	131.36	71.14	73.94	93.19	112.19

Examples of the cooling and second heating cycles are shown in Figures 4.14/4.15 for sample run Test 1. The extracted results for these cycles are listed in Tables 4.9/4.10. A tangent is drawn (denoted by the red line) between the minimum and maximum temperatures, which defines the range of the cycle under review. The enthalpy is calculated within these limits using the exothermic heat flow curves extracted and values tabulated for further analysis.

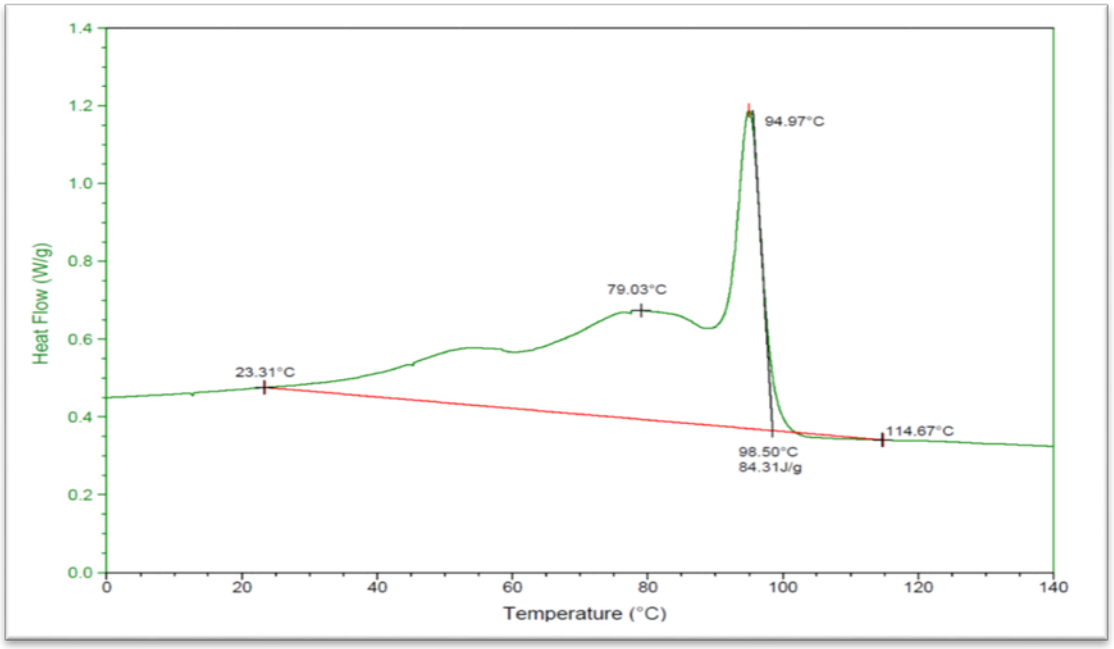

Figure 4.14 – DSC plot for Cooling Cycle of sample run, Test 1 with Extracted Values

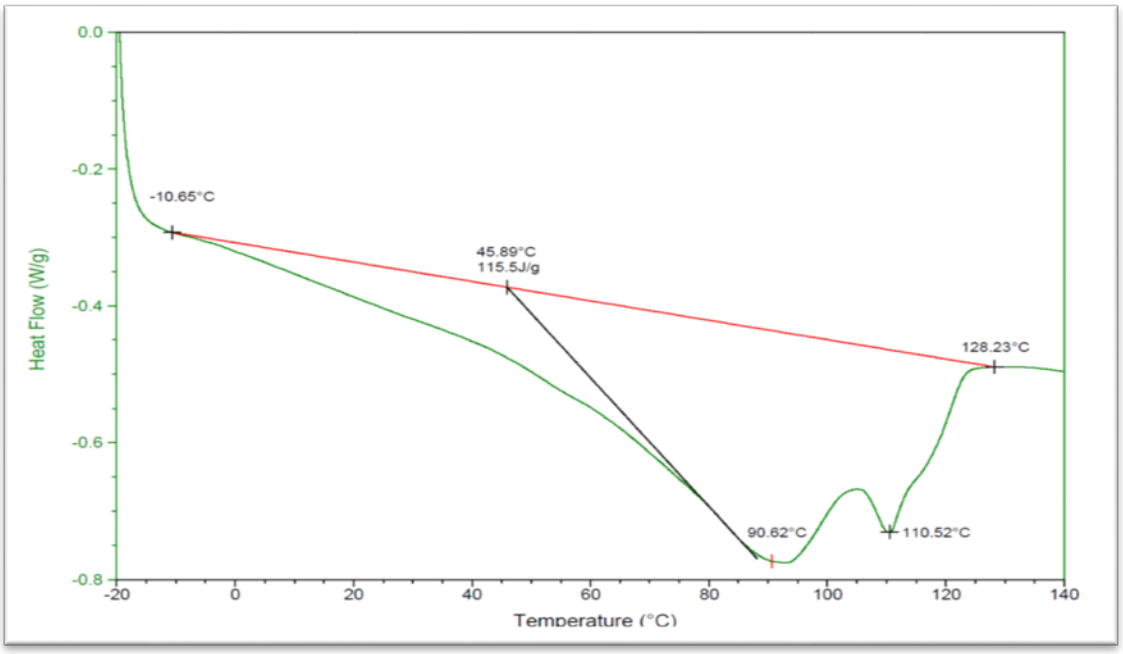

Figure 4.15 – DSC plot for Second Heating Cycle of sample run, Test 1 with Extracted Values

Table 4.9 – Extracted results for Cooling Cycle for all sample runs

	Min. Temp. (°C)	Max. Temp. (°C)	Offset Temp. (°C)	Enthalpy (J/g)	Peak (°C)	Secondary Peak (°C)
Test 01	23.31	114.67	98.50	84.31	94.97	79.03
01	33.69	106.83	98.45	72.04	94.99	78.04
02	-12.67	111.61	101.23	94.07	97.27	79.13
03	-10.22	111.61	102.20	98.59	94.91	77.22
04	29.21	107.54	100.64	79.37	96.92	78.54
05	31.74	107.01	99.65	74.13	96.18	78.11
06	29.78	106.97	99.76	78.84	96.24	78.36
07	34.16	103.06	98.01	76.26	94.37	77.54
08	34.31	104.84	98.00	72.72	94.12	76.95
09 (05)	34.68	106.30	99.30	75.88	95.79	77.85
09 (06)	9.85	106.74	99.37	92.45	95.83	78.56
10 (05)	-9.14	108.02	97.75	105.40	94.16	77.54
10 (06)	-12.56	113.73	97.92	103.70	94.19	77.22
11	32.98	107.39	99.55	71.03	95.91	78.04
Virgin Material	-28.35	108.77	96.67	121.60	91.85	75.63
12 (05)	-11.61	108.32	97.32	105.10	93.20	76.16
12 (06)	-11.81	105.46	96.25	103.70	92.43	76.39
13 (05)	-13.29	106.84	97.82	118.10	94.46	77.57
13 (06)	-14.11	107.41	97.87	111.80	94.34	77.82
14	-13.58	107.14	99.07	103.30	95.48	77.74
15	-11.29	109.38	97.73	105.80	94.12	77.44
16	-11.39	110.70	99.72	104.00	96.18	78.66
17	-10.64	113.45	98.76	107.50	95.08	78.83
18	-10.22	111.18	98.62	107.10	95.00	78.39
19	-11.09	109.26	99.87	101.70	96.17	78.56
20	-12.94	116.19	100.23	99.91	96.48	78.36

Table 4.10 – Extracted results for Second Heating Cycle for all sample runs

	Min. Temp. (°C)	Max. Temp. (°C)	Offset Temp. (°C)	Enthalpy (J/g)	Peak (°C)	Secondary Peak (°C)
Test 01	-10.65	128.23	45.89	115.50	90.62	110.52
01	-11.37	126.89	43.72	107.20	91.14	110.16
02	-10.83	132.69	42.20	112.30	91.11	111.87
03	-2.83	132.88	48.76	92.27	91.91	110.46
04	-11.83	127.88	46.72	105.90	91.33	111.78
05	-9.73	134.49	43.81	114.50	92.08	111.47
06	-11.23	127.26	42.61	115.90	92.13	111.34
07	-9.87	128.29	41.73	112.80	90.84	110.21
08	-10.89	127.95	43.57	103.40	90.81	110.21
09 (05)	-12.23	130.06	44.96	113.90	91.52	111.26
09 (06)	-10.23	129.62	43.57	109.50	91.54	111.06
10 (05)	-10.23	129.94	45.04	115.80	91.35	109.97
10 (06)	53.58	127.95	74.59	54.33	103.86	81.77
11	-10.40	133.32	44.11	104.80	92.30	112.22
Virgin Material	-25.52	133.58	43.65	121.40	92.41	111.20
12 (05)	-6.26	131.72	47.15	93.68	92.07	109.43
12 (06)	-11.23	128.63	38.26	114.50	90.27	108.96
13 (05)	-10.89	128.51	39.44	131.70	90.95	109.87
13 (06)	-12.35	130.41	37.08	132.00	91.16	109.97
14	-10.09	127.95	40.66	109.70	91.25	111.12
15	-10.00	131.00	41.82	124.30	91.16	110.20
16	-8.94	131.00	42.19	115.50	91.65	111.61
17	-8.59	130.06	45.61	102.60	90.72	110.44
18	-9.76	128.53	44.70	110.00	91.47	110.91
19	-9.65	130.65	44.09	107.30	91.48	111.49
20	-9.41	132.41	41.71	115.40	92.30	112.20

The crystallization onset temperature (max temperature from cooling cycle) was first analyzed to determine the effect of processing conditions. Data in Table 4.11 were used in Statistica. Results of maximum temperature or the onset temperature of crystallization from the cooling cycle were used first, to check for significance in Statistica. The ANOVA results are shown in Table 4.12. It can be seen that BP concentration (linear and quadratic terms) and intensity (quadratic term) had significant effects on the onset of crystallization at a significance level of 5%.

Table 4.11 – Significance check for the Max. Temp. from the Cooling Cycle

	BP	Time	Intensity	Max. Temp. (ºC)
Av. 1	0.50	60.00	80.60	110.75
2	0.50	60.00	56.60	111.61
3	0.50	30.00	80.60	111.61
4	0.50	30.00	56.60	107.54
5	0.13	60.00	80.60	107.01
6	0.13	60.00	56.60	106.97
7	0.13	30.00	80.60	103.06
8	0.13	30.00	56.60	104.84
Av. 9	0.63	45.00	68.60	106.52
Av. 10	0.32	70.20	68.60	110.88
11	0.32	45.00	90.20	107.39
Av. 12	0.00	45.00	68.60	106.89
Av. 13	0.32	19.80	68.60	107.13
14	0.32	45.00	47.00	107.14
Av. 15 & 20 (1)	0.32	45.00	68.60	112.79
Av. 16 & 18	0.32	45.00	68.60	110.94
Av. 17 & 19	0.32	45.00	68.60	111.36

Virgin material and sample run 20 were tested twice. As discussed earlier, some sample runs were done twice due to limitations of the UV lamp set points; two of virgin material and sample run 20's data were an addition to the experimentation set. As it is seen in Table 4.11, an average is taken between sample run 15 and 20(1) which means that the first run done for sample 20 is used as 20(1) for the averaging.

Table 4.12 – Statistica results for the Max. Temp. from the Cooling Cycle

ANOVA; Var.:Max. Temp.; R-sqr=.75501; Adj:.44002 (Spreadsheet3) 3 factors, 1 Blocks, 17 Runs; MS Residual=4.286298					
	SS	**df**	**MS**	**F**	**p**
(1) BP (L)	26.1156	1	26.11561	6.092812	0.042936
BP (Q)	31.2596	1	31.25963	7.292920	0.030615
(2) Time (L)	17.9341	1	17.93411	4.184056	0.080061
Time (Q)	8.7262	1	8.72622	2.035841	0.196673
(3) Intensity (L)	0.2267	1	0.22667	0.052882	0.824697
Intensity (Q)	24.3271	1	24.32712	5.675554	0.048714
1L by 2L	1.0322	1	1.03220	0.240814	0.638627
1L by 3L	3.0481	1	3.04814	0.711137	0.426940
2L by 3L	1.2090	1	1.20901	0.282064	0.611779
Error	30.0041	7	4.28630		
Total SS	122.4693	16			

Secondly, the crystallization enthalpy data (Table 4.13) from the cooling cycle were analyzed. The ANOVA results showing the significance of each variable are shown in Table 4.14. It can be seen that only BP concentration (quadratic term) and intensity (quadratic term) were significant at a significance level of 5%.

Table 4.13 – Significance check for the Enthalpy from the Cooling Cycle

	BP	Time	Intensity	Enthalpy (J/g)
Test 1	0.50	60.00	80.60	84.31
1	0.50	60.00	80.60	72.04
2	0.50	60.00	56.60	94.07
3	0.50	30.00	80.60	98.59
4	0.50	30.00	56.60	79.37
5	0.13	60.00	80.60	74.13
6	0.13	60.00	56.60	78.84
7	0.13	30.00	80.60	76.26
8	0.13	30.00	56.60	72.72
9 (05)	0.63	45.00	68.60	75.88
9 (06)	0.63	45.00	68.60	92.45
10 (05)	0.32	70.20	68.60	105.40
10 (06)	0.32	70.20	68.60	103.70
11	0.32	45.00	90.20	71.03
12 (05)	0.00	45.00	68.60	105.10
12 (06)	0.00	45.00	68.60	103.70
13 (05)	0.32	19.80	68.60	118.10
13 (06)	0.32	19.80	68.60	111.80
14	0.32	45.00	47.00	103.30
15	0.32	45.00	68.60	105.80
16	0.32	45.00	68.60	104.00
17	0.32	45.00	68.60	107.50
18	0.32	45.00	68.60	107.10
19	0.32	45.00	68.60	101.70
Av. 20	0.32	45.00	68.60	111.01

Table 4.14 – Statistica results for the Enthalpy from the Cooling Cycle

ANOVA; Var.:Enthalpy; R-sqr=.54095; Adj:.26552 (Spreadsheet3) 3 factors, 1 Blocks, 25 Runs; MS Residual=166.065					
	SS	**df**	**MS**	**F**	**p**
(1) BP (L)	18.563	1	18.563	0.111783	0.742752
BP (Q)	835.124	1	835.124	5.028900	0.040465
(2) Time (L)	67.818	1	67.818	0.408383	0.532429
Time (Q)	16.976	1	16.976	0.102223	0.753588
(3) Intensity (L)	220.618	1	220.618	1.328505	0.267110
Intensity (Q)	1567.788	1	1567.788	9.440812	0.007738
1L by 2L	11.949	1	11.949	0.071956	0.792164
1L by 3L	2.469	1	2.469	0.014868	0.904570
2L by 3L	247.106	1	247.106	1.488010	0.241358
Error	2490.975	15	166.065		
Total SS	5426.351	24			

Lastly, the crystallization peak data (Table 4.15) from the cooling cycle were analyzed and the ANOVA results are shown in Table 4.16. It can be seen that only BP concentration (linear and quadratic terms) was significant at a significance level of 5%.

Table 4.15 – Significance check for the Highest Peak from the Cooling Cycle

	BP	Time	Intensity	Peak (ºC)
Test 1	1	1	1	94.97
1	1	1	1	94.99
2	1	1	-1	97.27
3	1	-1	1	94.91
4	1	-1	-1	96.92
5	-1	1	1	96.18
6	-1	1	-1	96.24
7	-1	-1	1	94.37
8	-1	-1	-1	94.12
9 (05)	α	0	0	95.79
9 (06)	α	0	0	95.83
10 (05)	0	α	0	94.16
10 (06)	0	α	0	94.19
11	0	0	α	95.91
12 (05)	-α	0	0	93.20
12 (06)	-α	0	0	92.43
13 (05)	0	-α	0	94.46
13 (06)	0	-α	0	94.34
14	0	0	-α	95.48
15	0	0	0	94.12
16	0	0	0	96.18
17	0	0	0	95.08
18	0	0	0	95.00
19	0	0	0	96.17
Av. 20	0	0	0	96.20

Table 4.16 – Statistica results for the Highest Peak from the Cooling Cycle

ANOVA; Var.:Peak; R-sqr=.65301; Adj:.44482 (Spreadsheet2) 3 factors, 1 Blocks, 25 Runs; MS Residual=.7340787					
	SS	**df**	**MS**	**F**	**p**
(1) BP (L)	4.88726	1	4.887260	6.657679	0.020904
BP (Q)	4.47680	1	4.476801	6.098530	0.026023
(2) Time (L)	1.34386	1	1.343858	1.830673	0.196090
Time (Q)	1.99926	1	1.999264	2.723501	0.119658
(3) Intensity (L)	2.02517	1	2.025169	2.758790	0.117474
Intensity (Q)	2.02423	1	2.024231	2.757513	0.117552
1L by 2L	1.75087	1	1.750866	2.385121	0.143328
1L by 3L	2.83085	1	2.830848	3.856327	0.068370
2L by 3L	0.06381	1	0.063811	0.086926	0.772163
Error	11.01118	15	0.734079		
Total SS	31.73372	24			

Finally, second heating cycle data were analyzed. Data and ANOVA results for the onset of melting (max temperature) and melting peak are shown in Tables 4.17/4.18 and Tables 4.19/4.20, respectively.

Table 4.17 – Significance check for the Max. Temp. from the Second Heating Cycle

	BP	Time	Intensity	Max. Temp. (ºC)
Test 1	0.50	60.00	80.60	128.23
1	0.50	60.00	80.60	126.89
2	0.50	60.00	56.60	132.69
3	0.50	30.00	80.60	132.88
4	0.50	30.00	56.60	127.88
5	0.13	60.00	80.60	134.49
6	0.13	60.00	56.60	127.26
7	0.13	30.00	80.60	128.29
8	0.13	30.00	56.60	127.95
9 (05)	0.63	45.00	68.60	130.06
9 (06)	0.63	45.00	68.60	129.62
10 (05)	0.32	70.20	68.60	129.94
10 (06)	0.32	70.20	68.60	127.95
11	0.32	45.00	90.20	133.32
12 (05)	0.00	45.00	68.60	131.72
12 (06)	0.00	45.00	68.60	128.63
13 (05)	0.32	19.80	68.60	128.51
13 (06)	0.32	19.80	68.60	130.41
14	0.32	45.00	47.00	127.95
15	0.32	45.00	68.60	131.00
16	0.32	45.00	68.60	131.00
17	0.32	45.00	68.60	130.06
18	0.32	45.00	68.60	128.53
19	0.32	45.00	68.60	130.65
20 (1)	0.32	45.00	68.60	132.41

It can be seen from Table 4.18 that only intensity (linear term) was significant for the onset of melting at a significance level of 5%.

Table 4.18 – Statistica results for the Max. Temp. from the Second Heating Cycle

ANOVA; Var.:Max. Temp.; R-sqr=.42024; Adj:.07239 (Spreadsheet2) 3 factors, 1 Blocks, 25 Runs; MS Residual=4.047049					
	SS	**df**	**MS**	**F**	**p**
(1) BP (L)	0.0372	1	0.03721	0.009195	0.924876
BP (Q)	1.1463	1	1.14627	0.283235	0.602383
(2) Time (L)	0.3314	1	0.33143	0.081893	0.778662
Time (Q)	5.6771	1	5.67705	1.402764	0.254689
(3) Intensity (L)	19.0061	1	19.00606	4.696276	0.046734
Intensity (Q)	0.0128	1	0.01278	0.003158	0.955927
1L by 2L	6.9176	1	6.91758	1.709289	0.210764
1L by 3L	10.2032	1	10.20322	2.521152	0.133180
2L by 3L	2.4975	1	2.49747	0.617109	0.444356
Error	60.7057	15	4.04705		
Total SS	104.7089	24			

From Table 4.20, it can be seen that only exposure time (linear and quadratic terms) was of significance for the melting peak at a significance level of 5%.

Table 4.19 – Significance check for the Highest Peak from the Second Heating Cycle

	BP	Time	Intensity	Peak (ºC)
Av. 1	0.50	60.00	80.60	90.88
2	0.50	60.00	56.60	91.11
3	0.50	30.00	80.60	91.91
4	0.50	30.00	56.60	91.33
5	0.13	60.00	80.60	92.08
6	0.13	60.00	56.60	92.13
7	0.13	30.00	80.60	90.84
8	0.13	30.00	56.60	90.81
Av. 9	0.63	45.00	68.60	91.53
Av. 10	0.32	70.20	68.60	97.61
11	0.32	45.00	90.20	92.30
Av. 12	0.00	45.00	68.60	91.17
Av. 13	0.32	19.80	68.60	91.06
14	0.32	45.00	47.00	91.25
15	0.32	45.00	68.60	91.16
16	0.32	45.00	68.60	91.65
17	0.32	45.00	68.60	90.72
18	0.32	45.00	68.60	91.47
19	0.32	45.00	68.60	91.48
20 (1)	0.32	45.00	68.60	92.30

Table 4.20 – Statistica results for the Highest Peak from the Second Heating Cycle

ANOVA; Var.:Peak; R-sqr=.58515; Adj:.21178 (Spreadsheet74) 3 factors, 1 Blocks, 20 Runs; MS Residual=1.696965					
	SS	**df**	**MS**	**F**	**p**
(1) BP (L)	0.00020	1	0.00020	0.000116	0.991631
BP (Q)	1.10702	1	1.10702	0.652351	0.438064
(2) Time (L)	11.23656	1	11.23656	6.621565	0.027736
Time (Q)	8.43465	1	8.43465	4.970433	0.049889
(3) Intensity (L)	0.33763	1	0.33763	0.198961	0.665064
Intensity (Q)	0.14905	1	0.14905	0.087834	0.773012
1L by 2L	1.66506	1	1.66506	0.981200	0.345265
1L by 3L	0.01942	1	0.01942	0.011444	0.916922
2L by 3L	0.09901	1	0.09901	0.058347	0.814009
Error	16.96965	10	1.69696		
Total SS	40.90523	19			

Similar analysis of the melting enthalpy from the second heating cycle showed that there were not any significant effects.

In summary, a list of the significant effects for the different variables in the cooling and second heating cycles is presented in Table 4.21/4.22.

Table 4.21 – Comparison of Significance of Variables in the Cooling Cycle

Cooling Cycle	Significance
Maximum Temperature	Linear and Quadratic BP, Quadratic Intensity
Enthalpy	Quadratic BP and Quadratic Intensity
Highest Peak	Linear and Quadratic BP

Table 4.22 – Comparison of Significance of Variables in the Second Heating Cycle

Second Heating Cycle	Significance
Maximum Temperature	Linear Intensity
Enthalpy	No Significance
Highest Peak	Linear and Quadratic Time

All the graphs with extracted values for cooling and second heating cycles in the DSC for all sample runs are cited in Appendix A and B, respectively.

Finally, the percent crystallinity of all samples was calculated by using the following equation:

$$X_C = \frac{\Delta H_f\ (Sample)}{\Delta H_f\ (100\%\ Crystalline\ Material)} \times 100 \qquad [4.7]$$

According to the literature, ΔH_f of 100% crystalline material is 287.3 J/g [40-41], and the calculated crystallinities are tabulated in Table 4.23 using Equation 4.7. Table 4.23 contains sample runs and their specific crystallinity, while Table 4.24 contains the calculated/averaged

values of sample runs which were not possible to be conducted due to UV lamp limitations, discussed earlier in Chapter 3. Highest crystallinity is seen in sample runs 13(05) and 13(06) which were slightly higher than that of the virgin material [42].

Table 4.23 – Sample Runs and their Crystallinity for actual values

	Enthalpy (J/g)	Xc (%)
Test 01	115.50	40.20
1	107.20	37.31
2	112.30	39.09
3	92.27	32.12
4	105.90	36.86
5	114.50	39.85
6	115.90	40.34
7	112.80	39.26
8	103.40	35.99
09 (05)	113.90	39.64
09 (06)	109.50	38.11
10 (05)	115.80	40.31
10 (06)	54.33	18.91
11	104.80	36.48
12 (05)	93.68	32.61
12 (06)	114.50	39.85
13 (05)	131.70	45.84
13 (06)	132.00	45.95
14	109.70	38.18
15	124.30	43.26
16	115.50	40.20
17	102.60	35.71
18	110.00	38.29
19	107.30	37.35
20 (1)	115.40	40.17
20 (2)	97.34	33.88

Table 4.24 – Sample Runs and their Crystallinity for averaged values

	Enthalpy (J/g)	Xc (J/g)
Av. 01	111.35	38.76
Av. 09	111.70	38.88
Av. 10	85.07	29.61
Av. 12	104.09	36.23
Av. 13	131.85	45.89
Av. 15 & 18	117.15	40.78
Av. 16 & 19	111.40	38.77
Av. 17 & 20 (1)	109.00	37.94
Av. 17 & 20 (2)	99.97	34.80
Av. 15 & 19	115.80	40.31
Av. 16 & 20 (1)	115.45	40.18
Av. 16 & 20 (2)	106.42	37.04
Av. 17 & 18	106.30	37.00
Av. 15 & 20 (1)	119.85	41.72
Av. 15 & 20 (2)	110.82	38.57
Av. 16 & 18	112.75	39.24
Av. 17 & 19	104.95	36.53
Av. 15-17	114.13	39.73
Av. 18-20 (1)	110.90	38.60
Av. 18-20 (2)	104.88	36.51
Av. 18-(Av. 20)	107.89	37.55
Av. 15-(Av. 20)	111.01	38.64
Av. 20	106.37	37.02
Av. 15-20	110.35	38.41

Table 4.24 contains sample runs which have been averaged using the actual sample runs performed; the names indicate which sample runs were averaged. This is because these samples were comprised of moderate BP of 0.32% by weight and exposed to a moderate UV lamp intensity of 68.6%, and the time that the sample was irradiated over was the minimum in any of the sample runs. Therefore, the photo – initiator was not given enough time to induce LCB in both samples. Sample run 10(06) shows the minimum crystallinity among all the sample runs under review. This sample had the same BP and lamp intensity as sample 13(05) and 13(06) but the time of exposure

to the UV lamp was the maximum in all the sample runs conducted. The reason for highest percentage of LCBs and/or crosslinking in sample run 10 is because it was given more than enough time to gradually form branches.

Looking at the values of crystallinity in the samples, it is seen that the measured and calculated values of X_C are between 19% and 46%. The virgin sample had 42% crystallinity. Therefore, in comparison, only two samples (13(05) and 13(06)) appeared to have had a slightly higher value than the virgin material. This may be attributed to some chain scission in favor to LCB. However, if the error in crystallinity determination is estimated using center-point runs (3.8 for runs 15-17 and 2.6 for runs 18-20), one can conclude that there is not a significant difference between the virgin material and runs 13(05) and 13(06).Other than that, all samples had a lower crystallinity as expected due to increased branching [40-41].

CHAPTER 5

CONCLUSIONS AND RECOMMENDATIONS

5.1 Conclusions

A LLDPE resin has been modified through UV irradiation and the effects of photo-initiator (BP) concentration, irradiation time and lamp intensity on rheological and thermal properties have been studied by using a CCD design. In general, it was found that LCB and crosslinking can be induced onto the base LLDPE resin upon UV treatment. Linear viscoelastic rheological characterization experiments were conducted to study properties like power-law index, zero shear viscosity (η_0), and rheological polydispersity through the use of Cole-Cole plots, ER, PI and ModSep. Overall, it was observed that when concentration of BP was increased, η_0 increases, when the sample runs were exposed to UV lamp at certain intensity for a specific duration. If the BP was kept constant along with the UV lamp intensity and only time of exposure increased, it was seen that the η_0 increases and the trend keeps increasing at lower frequencies, which makes it impossible to predict the actual zero shear viscosity. When the BP concentration and time duration were kept constant and only intensity was increased, η_0 increases along with shear thinning in the sample runs, in comparison to the virgin material. Lastly, when the time and UV intensity are kept constant to check for the effect of increase in concentration of BP in sample runs, increase in η_0 is seen. Only when the concentration of BP is zero but sample runs are irradiated for any certain interval at some specific intensity, does the material degrade.

When studying the effect on PI, it is seen that PI will always increase with increase in any one factor (BP concentration, time of exposure or UV intensity), when the other two of the three factors are kept constant.

Statistical analysis of the ER polydispersity index showed that all three factors (BP concentration, time and intensity) were significant at a significance level of 5% and an increase in the value of any factor causes an increase in the ER value, which means a broader distribution of the high molecular weight chains and/or LCB.

The melting and crystallization characteristics of the irradiated samples were analyzed by DSC. The effects of all three processing conditions were evaluated and it was found that:

(i) Onset crystallization temperature and crystallization enthalpy were significantly affected by BP concentration and UV intensity.

(ii) Crystallization temperature was significantly affected by BP concentration.

(iii) Melting temperature was significantly affected by irradiation time.

(iv) Onset melting temperature was significantly affected by UV intensity.

5.2 Recommendations

The UV lamp used for this experimental work allowed only 12 intensity settings which had a fixed set point value. The design of experiments contained two values for the intensity variable which could not be set on the lamp/equipment and iterative calculations were performed to obtain results for those particular sample runs. We assumed that the iteration method provided a good approximation; however, overcoming this limitation could help avert any inaccuracies associated with calculations. Using a variable intensity lamp would be preferable in future experiments. This way any value of intensity according to the calculated DOE could be inputted on the variable lamp

controller without additional experiments to be done, interpolation of values or approximations to be taken into account.

Molecular weight measurements were not performed in this study due to time limitations. A GPC experiment could be useful in providing precise data on MW and MWD for each of the sample runs. The changes in molecular weight and distribution can be important in quantifying the impact of radiation on formation of shorter or longer chains compared to virgin material, along with quantification of branching frequency. MW and PDI measurements would be valuable to confirm observations from the rheological analysis.

In future work, it would be useful to perform Soxhlet extraction experiments to determine the amount of gel being formed (if present) as that could be used to identify conditions leading to gelation versus LCB. Moreover a critical irradiation dose required for the onset of gelation can also be approximated by this method [43]. Also, FTIR measurements can also be useful in studying changing peaks due to formation or destruction of crystals and changes in gel content in the material [44].

Finally, an important development to the work done in this thesis proving changes in chain microstructure would be determination of extent of LCB versus crosslinking by conducting swelling measurements [45] or ^{13}C-NMR experiments [46]. These experiments will help quantify the exact amount of each of these characteristics after the removal of gel through Soxhlet extraction as gel also affects the rheological properties and hinders an accurate calculation of LCBs or crosslinks.

BIBLIOGRAPHY

[1] A. E. Hamielec and J. B. P. Soares , "Metallocene catalyzed polymerization: industrial technology," in *Propylene*, vol. 2, Springer Netherlands, 1999, pp. 446-453.

[2] C. W. Macosko , Rheology: Principles, Measurements and Applications, New York: Wiley-VCH, 1994.

[3] A. Shyichuk, J. R. White, I. Craig and I. Syrotynska, "Comparison of UV-degradation depth-profiles in polyethylene, polypropylene and an ethylene-propylene copolymer," *Polymer Degradation and Stability,* vol. 88, no. 3, pp. 415-419, 2005.

[4] S. V. D. Ven, Polypropylene and other Polyolefins: Polymerization and Characterization, New York: Elsevier Science Publishing Company Inc., 2012.

[5] P. Lepoutre, "http://nzic.org.nz/," [Online]. Available: http://nzic.org.nz/ChemProcesses/polymers/10J.pdf. [Accessed 16 July 2015].

[6] M. P. Sepe, "http://www.ptonline.com/," July 2014. [Online]. Available: http://www.ptonline.com/columns/materials-performance-in-polyethylene-density-matters. [Accessed 9 March 2016].

[7] Y. Amintowlieh, C. Tzoganakis and A. Penlidis, "The Effect of Depth and Duration of UV Radiation on Polypropylene Modification via Photoinitiation," *Journal of Polymer Science,* vol. 131, no. 21, 2014.

[8] G. Oster, "Crosslinking of polyethylene with selective wave lengths of ultraviolet light," *Journal of Polymer Science,* vol. 22, no. 100, p. 185, 1956.

[9] G. Oster, G. K. Oster and H. Moroson, "Ultraviolet induced crosslinking and grafting of solid high polymers," *Journal of Polymer Science,* vol. 34, no. 127, pp. 671-684, 1959.

[10] B. Ranby, B. J. Qu and W. F. Shi, Photocrosslinking (overview) in Polymeric Materials Encyclopedia, Florida: 5155, 1997.

[11] Y. L. Chen and B. Ranby, "Photocrosslinking of Polyethylene: Photoinitiators, Crosslinking Agent, and Reaction Kinetics," *Journal of Polymer Science Part A: Polymer Chemistry,* vol. 27, no. 12, pp. 4051-4075, 1989.

[12] B. J. Qu, "Recent developments in photoinitiated crosslinking of polyethylene and its industrial applications," *Chinese Journal of Polymer Science,* vol. 19, no. 2, pp. 189-207, 2001.

[13] G. He and C. Tzoganakis, "A UV-Initiated Reactive Extrusion Process for Production of Controlled-Rheology Polypropylene," *Polymer Engineering & Science,* vol. 51, no. 1, pp. 151-157, 2011.

[14] M. Rätzsch, M. Arnold, E. Borsig, H. Bucka and N. Reichelt, "Radical reactions on polypropylene in the solid state," *Progress in Polymer Science,* vol. 27, no. 7, pp. 1195-1282, 2002.

[15] Y. Amintowlieh, Rheological Modification of Polypropylene by Incorporation of Long Chain Branches Using UV Radiation, PhD. Thesis, Department of Chemical Engineering, University of Waterloo, 2014.

[16] Y. Amintowlieh, C. Tzoganakis, S. G. Hatzikiriakos and A. Penlidis, "Effects of processing variables on Polypropylene degradation and long chain branching with UV irradiation," *Polymer Degradation and Stability,* vol. 104, pp. 1-10, 2014.

[17] R. Garrido, V. Hugo, M. Zatloukal and M. H. Wagner, "Increase of long-chain branching by thermo-oxidative treatment of LDPE: Chromatographic, spectroscopic and rheological evidence," *Journal of Rheology,* vol. 57, no. 1, pp. 105-129, 2013.

[18] A. Holmstrom and E. M. Sorvik, "Thermal degradation of polyethylene in a nitrogen atmosphere of low oxygen content. II. Structural changes occuring in low-density polyethylene at an oxygen content less than 0.0005%," *Journal of Applied Polymer Science,* vol. 18, no. 3, pp. 761-778, 1974.

[19] A. Holmstrom and E. M. Sorvik, "Thermooxidative degradation of polyethylene. I and II. Structural changes occurring in low-density polyethylene, high-density polyethylene, and tetratetracontane heated in air," *Journal of Polymer Science, Part A Polymer Chemistry,* vol. 16, no. 10, pp. 2555-2586, 1978.

[20] A. Drozdov, "The effect of thermal oxidative degradation of polymers on their viscoelastic response," *International Journal of Engineering Science,* vol. 45, no. 11, pp. 882-904, 2007.

[21] T. V. Sepulveda, E. F. Torres, A. M. Guzman, M. L. Gonzalez and G. T. Quintero, "Microbial degradation of thermo-oxidized low-density polyethylene," *Journal of Applied Polymer Science,* vol. 73, no. 8, pp. 1435-1440, 1999.

[22] Y. Shangguan, C. Zhang, Y. Xie, R. Chen, L. Jin and Q. Zheng, "Study on degradation and crosslinking of impact polypropylene copolymer by dynamic rheological measurement," *Polymer,* vol. 51, no. 2, pp. 500-506, 2010.

[23] P. Sardashti, C. Tzoganakis, M. A. Polak and A. Penlidis, "Radiation Induced Long Chain Branching in High-Density Polyethylene through a Reactive Extrusion Process," *Macromolecular Reaction Engineering,* vol. 8, no. 2, pp. 100-111, 2014.

[24] A. Rudin and P. Choi, The Elements of Polymer Science & Engineering, New York: Academic Press, 2012.

[25] K. Xiao, C. Tzoganakis and H. Budman, "Modification of Rheological Properties of LDPE for Coating Applications," *Industrial and Engineering Chemistry Research*, vol. 39, no. 12, p. 4928–4932, 2000.

[26] R. Shroff and H. Mavridis, "New measures of polydispersity from rheological data on polymer melts," *Journal of Applied Polymer Science*, vol. 57, no. 13, pp. 1605-1626, 1995.

[27] A. J. Peacock, Handbook of Polyethylene: Structures, Properties and Applications, New York: Marcel Dekker, 2000.

[28] F. G. D. Ferreira, M. A. G. A. Lima, Y. M. B. Almeida and G. M. Vinhas, "Effect of the Radiolitic Sterilization in Polyethylene/Starch Blends," *Quimica Nova*, vol. 31, no. 5, pp. 1043-1047, 2008.

[29] N. S. Allen, A. C. Padron and T. J. Henman, "The Photo-stabilization of Polypropylene: A review," *Polymer Degradation and Stability*, vol. 13, no. 1, pp. 31-76, 1985.

[30] B. Qu, L. Tang, M. Yan and C. Liu, "Effect of UV-Photocrosslinking on the Nonisothermal Crystallization Kinetics of Polyethylene," *Journal of Applied Polymer Science*, vol. 108, no. 1, pp. 174-180, 2008.

[31] C. Tzoganakis, J. Vlachopoulos and A. E. Hamielec, "Modelling of the Peroxide Degradation of Polypropylene," *International Polymer Processing*, vol. 3, no. 3, pp. 141-150, 1988.

[32] C. Tzoganakis, J. Vlachopoulos, A. E. Hamielec and D. M. Shinozak, "Effect of molecular weight distribution on the rheological and mechanical properties of polypropylene," *Polymer Engineering & Science*, vol. 29, no. 6, pp. 390-396, 1989.

[33] C. Tzoganakis, "A Rheological Evaluation of Linear and Branched Controlled-Rheology Polypropylenes," *The Canadian Journal of Chemical Engineering*, vol. 72, no. 4, pp. 749-754, 1994.

[34] J. Huang, G. He, X. Liao, Y. Huang and Q. Yang, "The rheological property and foam morphology of linear polypropylene and long chain branching polypropylene.," *Journal of Wuhan University of Technology-Mater. Sci. Ed.*, vol. 28, no. 4, pp. 798-803, 2013.

[35] G. Barakos, E. Mitsoulis, C. Tzoganakis and T. Kajiwara, "Rheological Characterization Of Controlled-Rheology Polypropylenes Using Integral Constitutive Equations," *Journal of applied polymer science*, vol. 59, no. 3, pp. 543-556, 1996.

[36] W. L. Hawkins, "Thermal and Oxidative Degradation of Polymers," *Polymer Engineering & Science*, vol. 4, no. 3, p. 187–192, 1964.

[37] D. C. Montgomery and G. C. Runger, Applied Statistics and Probability for Engineers, Hoboken: John Wiley & Sons, Inc., 2010.

[38] H. Wyss, "http://www.mate.tue.nl~wyssfilesWyss_GIT_Lab_J_2007.pdf," [Online]. Available: http://www.mate.tue.nl/~wyss/home/. [Accessed 20 February 2016].

[39] J. D. Ferry, Viscoelastic Properties of Polymers, 3rd ed., New York: John Wiley & Sons, Inc., 1980.

[40] F. M. Mirabella and A. Bafna, "Determination of the Crystallinity of Polyethylene/a-Olefin Copolymers by Thermal Analysis: Relationship of the Heat of Fusion of 100% Polyethylene Crystal and the Density," *Journal of Polymer Science: Part B: Polymer Physics,* vol. 40, no. 15, pp. 1637-1643, 2002.

[41] J. Zhang, G. M. Rizvi and C. B. Park, "Extruded WPC Foams," *Bioresources,* vol. 6, no. 4, pp. 4979-4989, 2011.

[42] R. Larson, The structure and rheology of complex fluids, New York: Oxford University Press, 1998.

[43] E. M. Valles, J. M. Carella, H. H. Winter and M. Baumgaertel, "Gelation of a radiation crosslinked model polyethylene," *Rheologica Acta,* vol. 29, no. 6, pp. 535-542, 1990.

[44] L. Guadagnoa, C. Naddeo, V. Vittoria, G. Camino and C. Cagnani, "Chemical and morphologial modifications of irradiated linear low density polyethylene (LLDPE)," *Polymer Degradation and Stability,* vol. 72, no. 1, pp. 175-186, 2001.

[45] Cambridge Polymer Group Inc., "http://www.campoly.com/," [Online]. Available: http://www.campoly.com/files/3013/5216/6056/005.pdf. [Accessed 18 03 2016].

[46] K. Klimke, Optimised Polyolefin Branch Quantification by C NMR Spectroscopy, Sc. D University of Mainz , 2006.

[47] Y. Amintowlieh, "Modification of Polypropylene by UV-Radiation," in *IPR symposium, Dept. of Chemical Engineering, University of Waterloo,* 2012.

APPENDICES

APPENDIX A: DSC Plots for Cooling Cycle

Runs can be found in Table 4.9

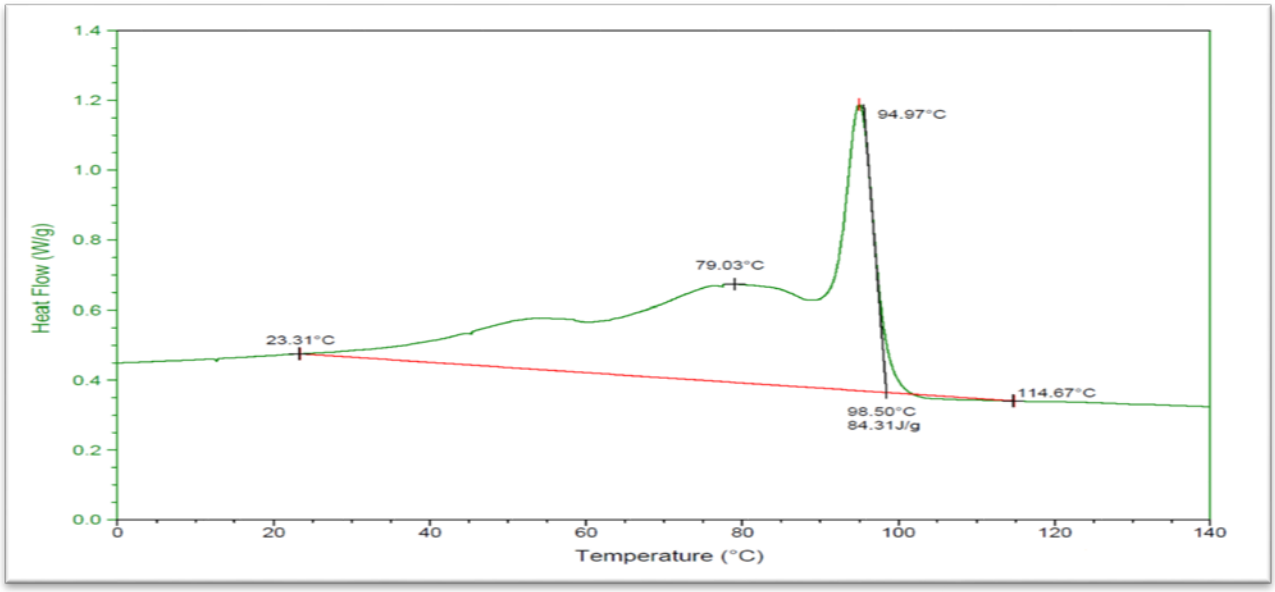

Figure A.1 – DSC plot for Cooling Cycle of sample run, Test 1 with Extracted Values

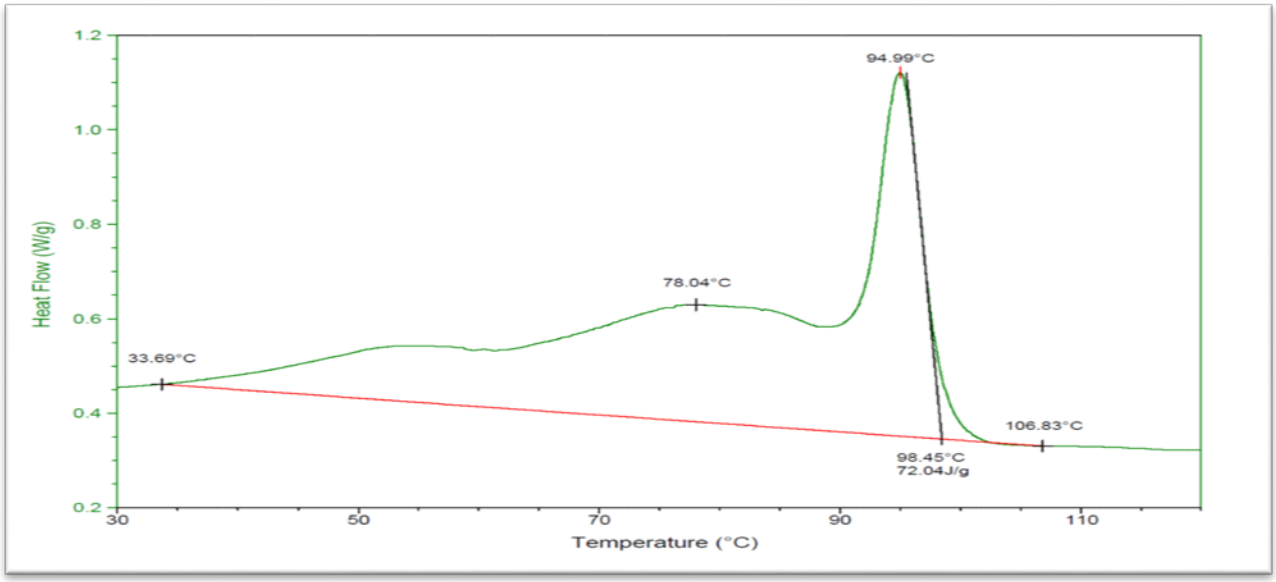

Figure A.2 – DSC plot for Cooling Cycle of sample run 1 with Extracted Values

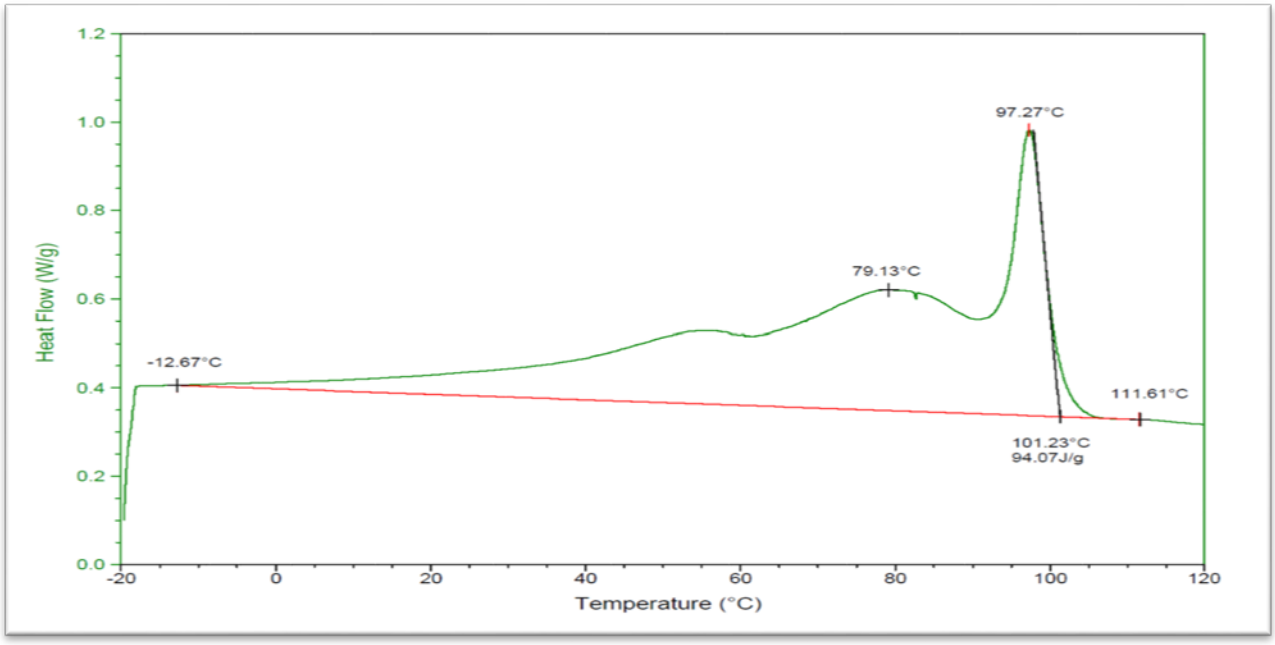

Figure A.3 – DSC plot for Cooling Cycle of sample run 2 with Extracted Values

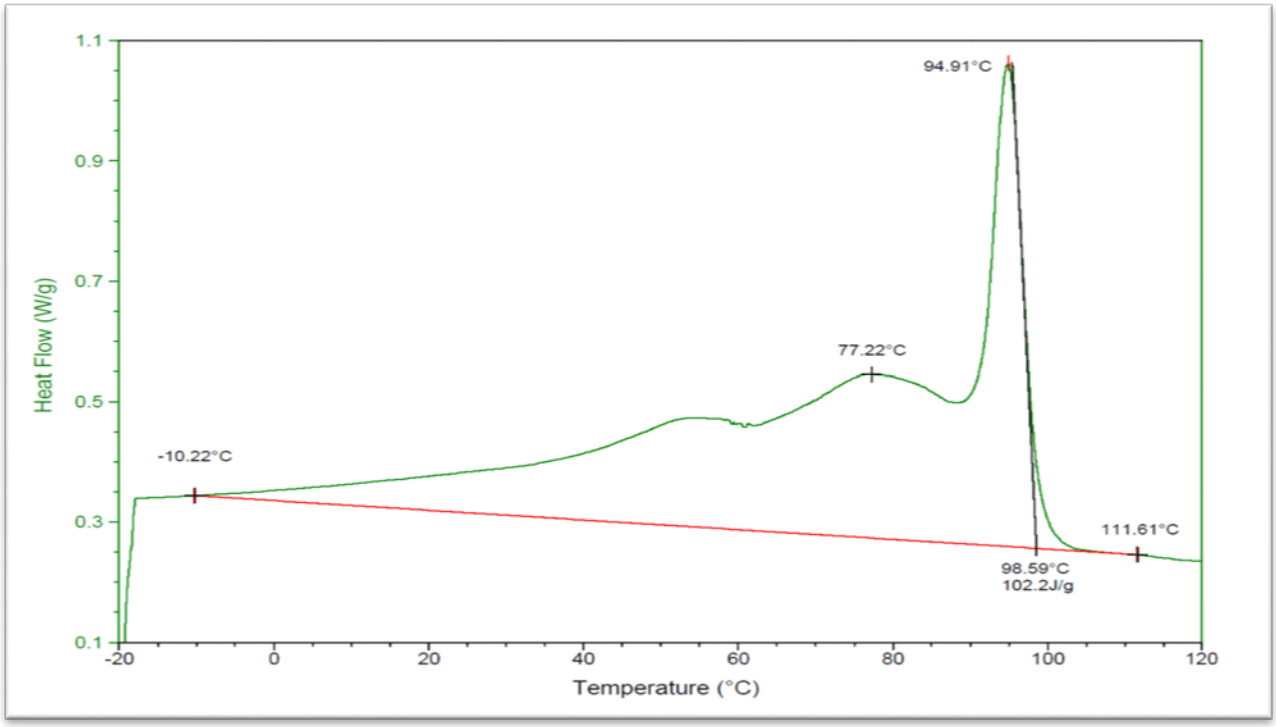

Figure A.4 – DSC plot for Cooling Cycle of sample run 3 with Extracted Values

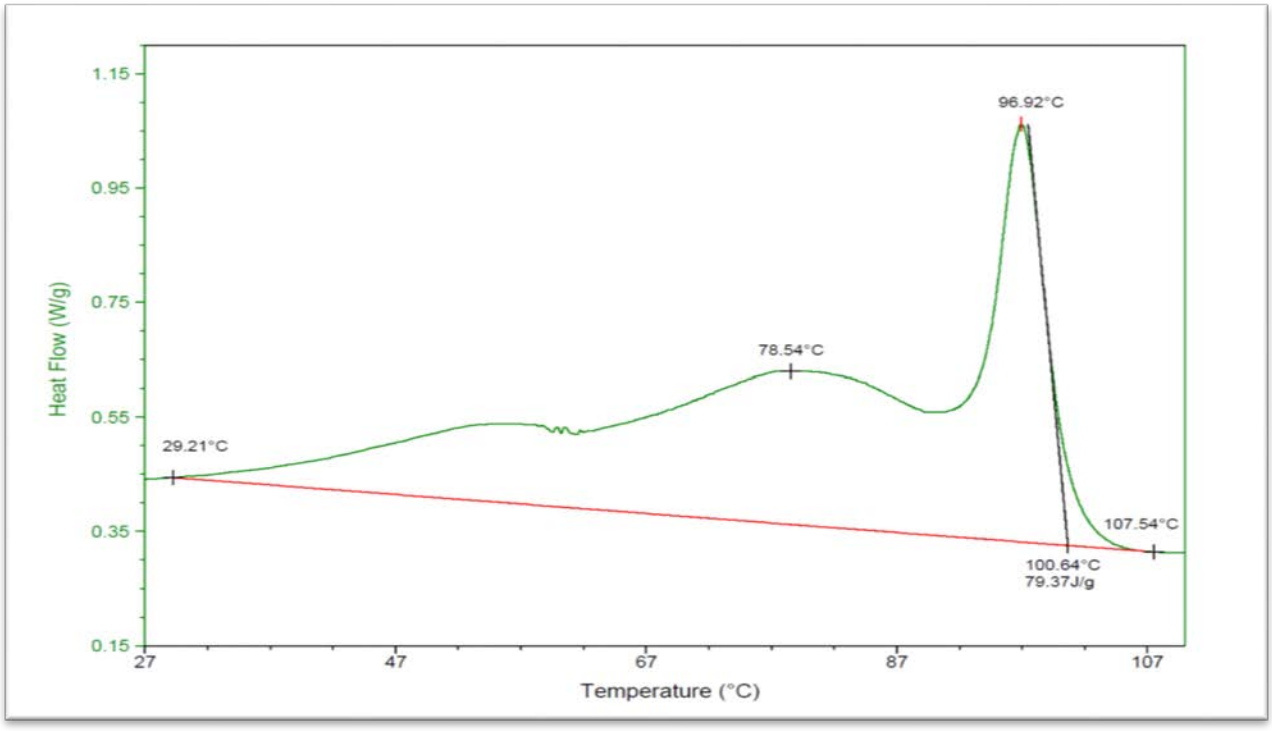

Figure A.5 – DSC plot for Cooling Cycle of sample run 4 with Extracted Values

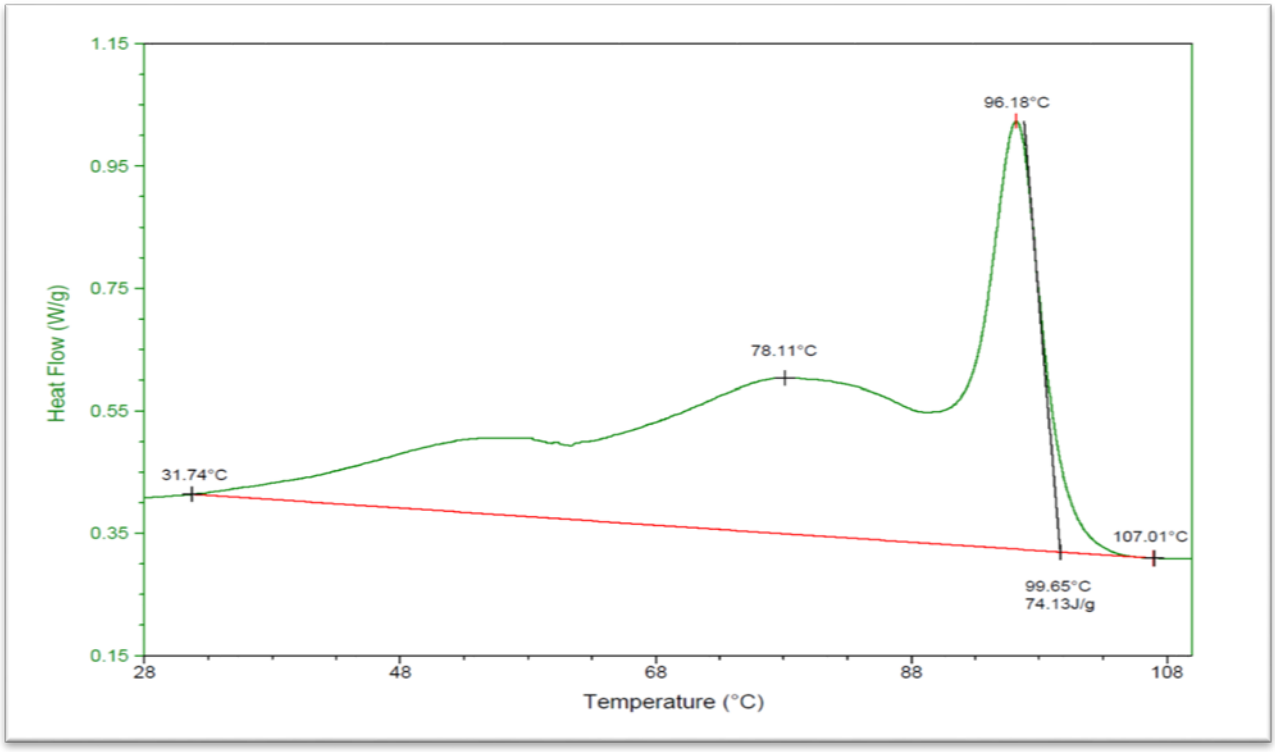

Figure A.6 – DSC plot for Cooling Cycle of sample run 5 with Extracted Values

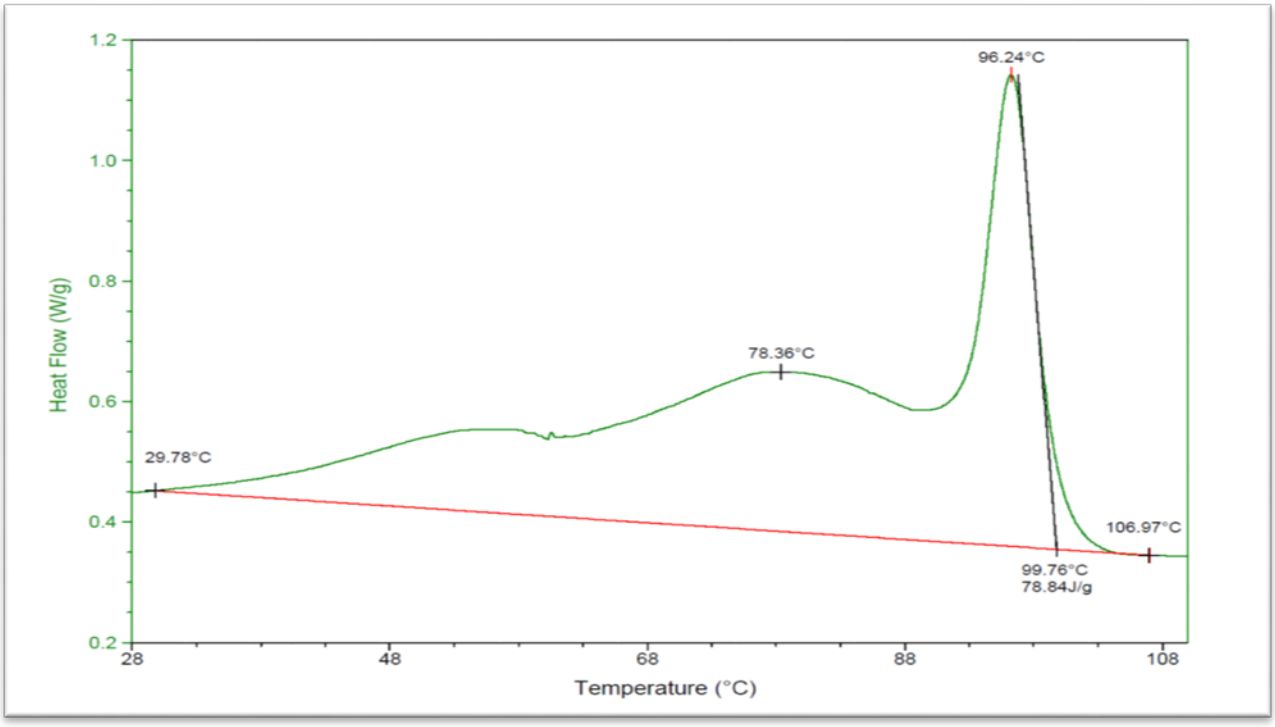

Figure A.7 – DSC plot for Cooling Cycle of sample run 6 with Extracted Values

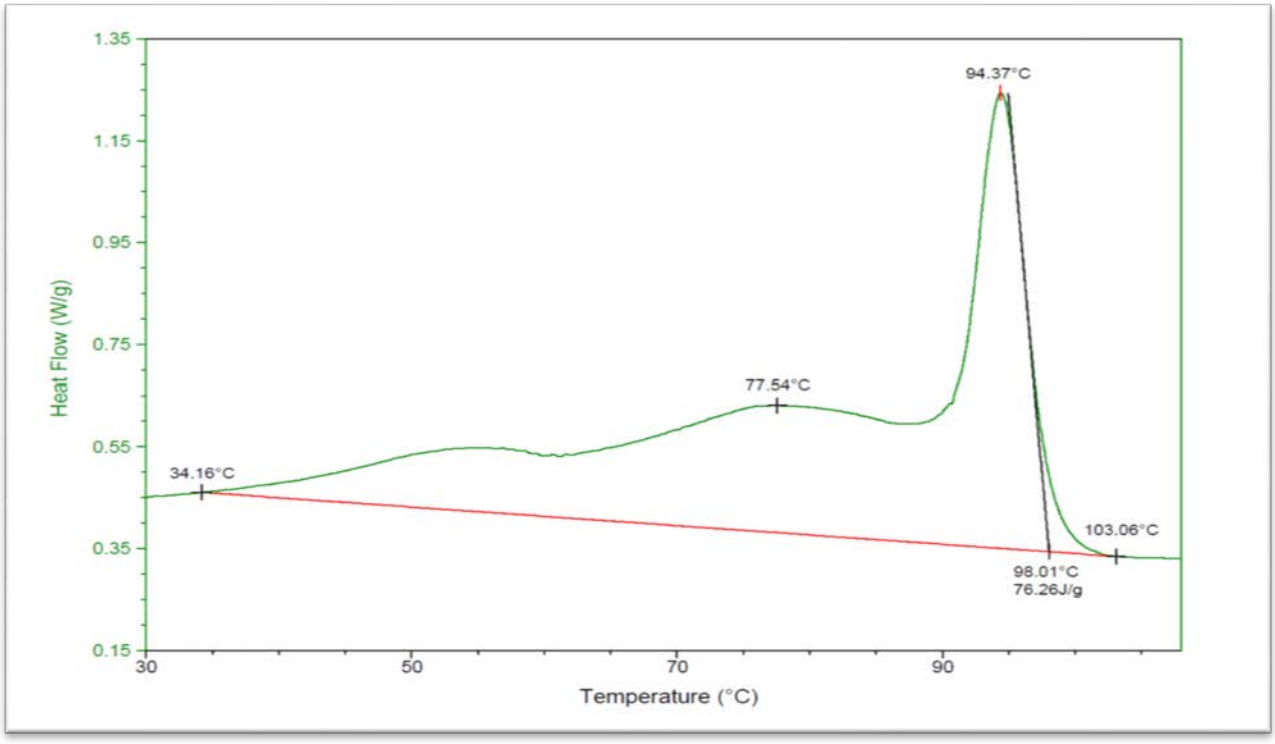

Figure A.8 – DSC plot for Cooling Cycle of sample run 7 with Extracted Values

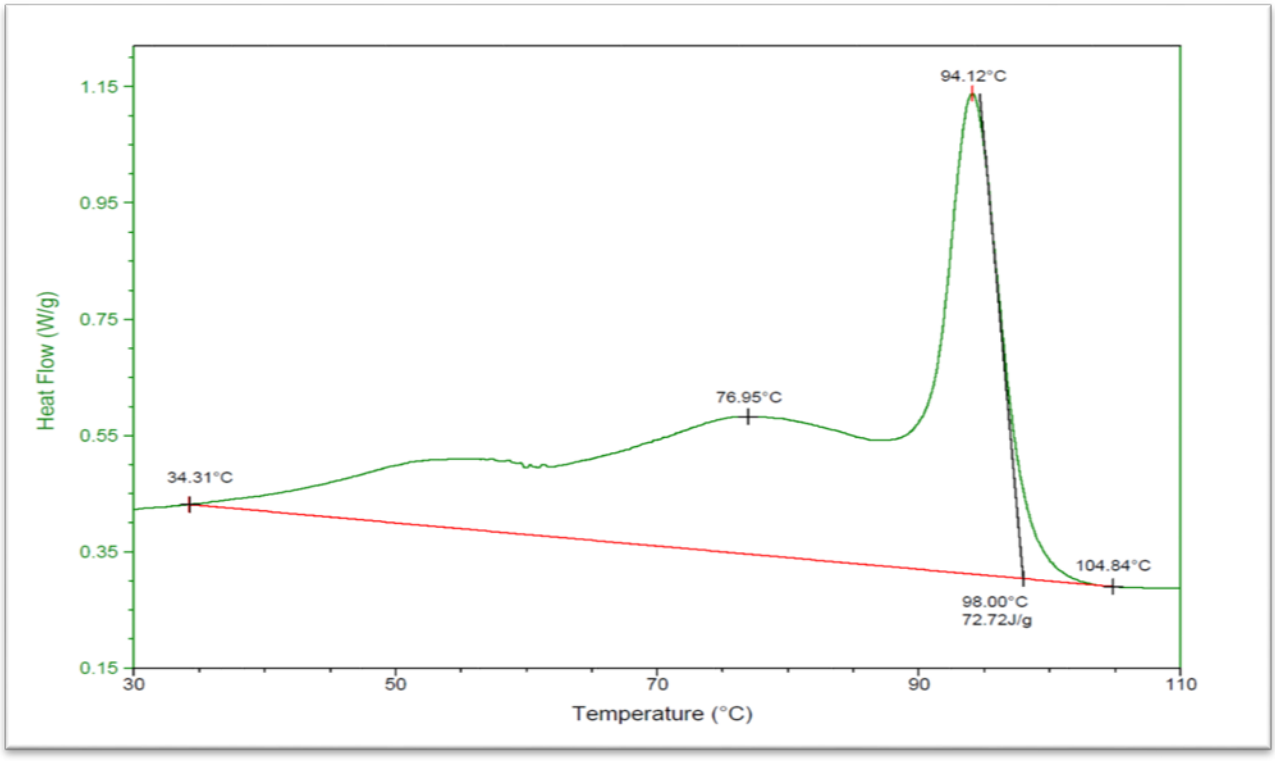

Figure A.9 – DSC plot for Cooling Cycle of sample run 8 with Extracted Values

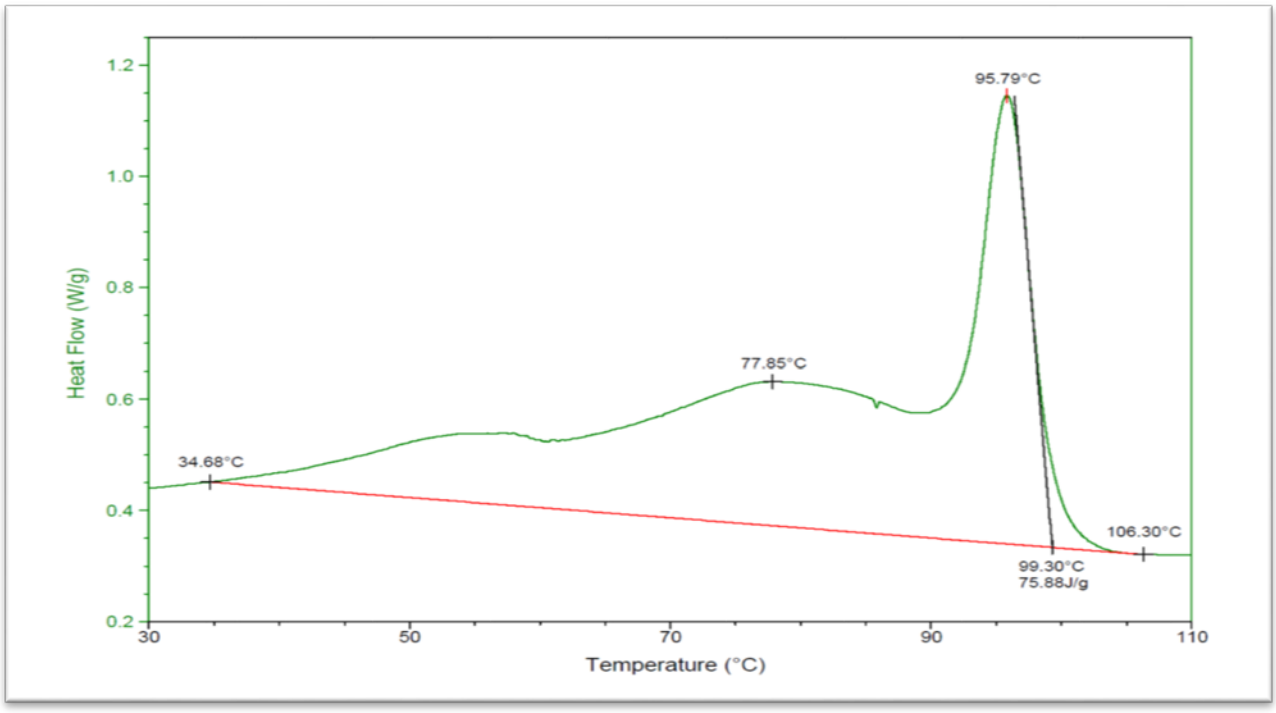

Figure A.10 – DSC plot for Cooling Cycle of sample run 9(05) with Extracted Values

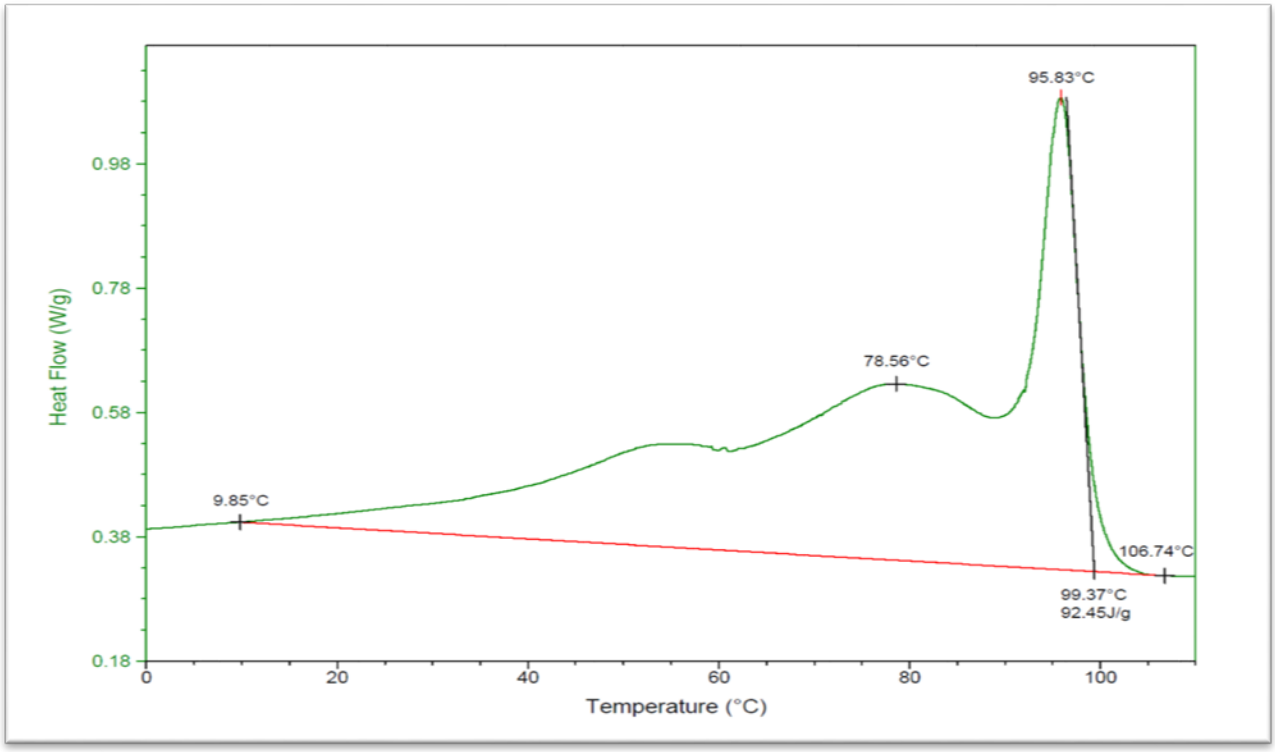

Figure A.11 – DSC plot for Cooling Cycle of sample run 9(06) with Extracted Values

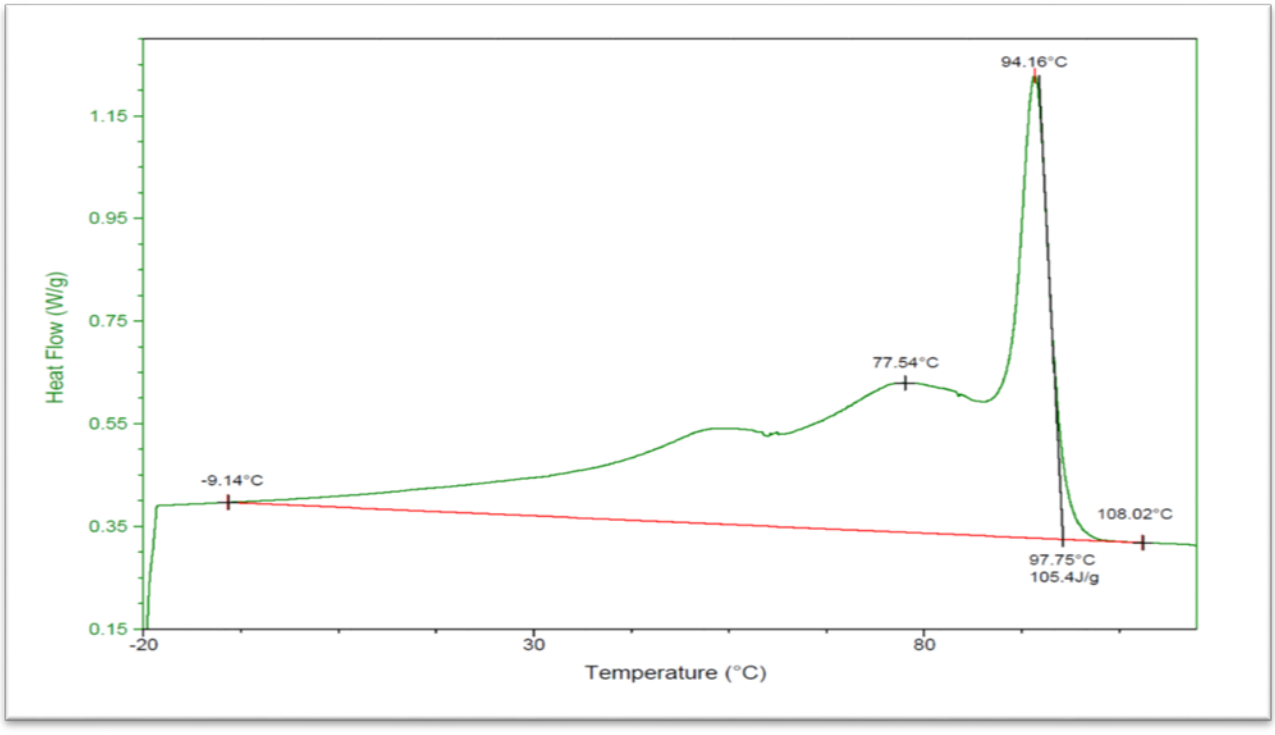

Figure A.12 – DSC plot for Cooling Cycle of sample run 10(05) with Extracted Values

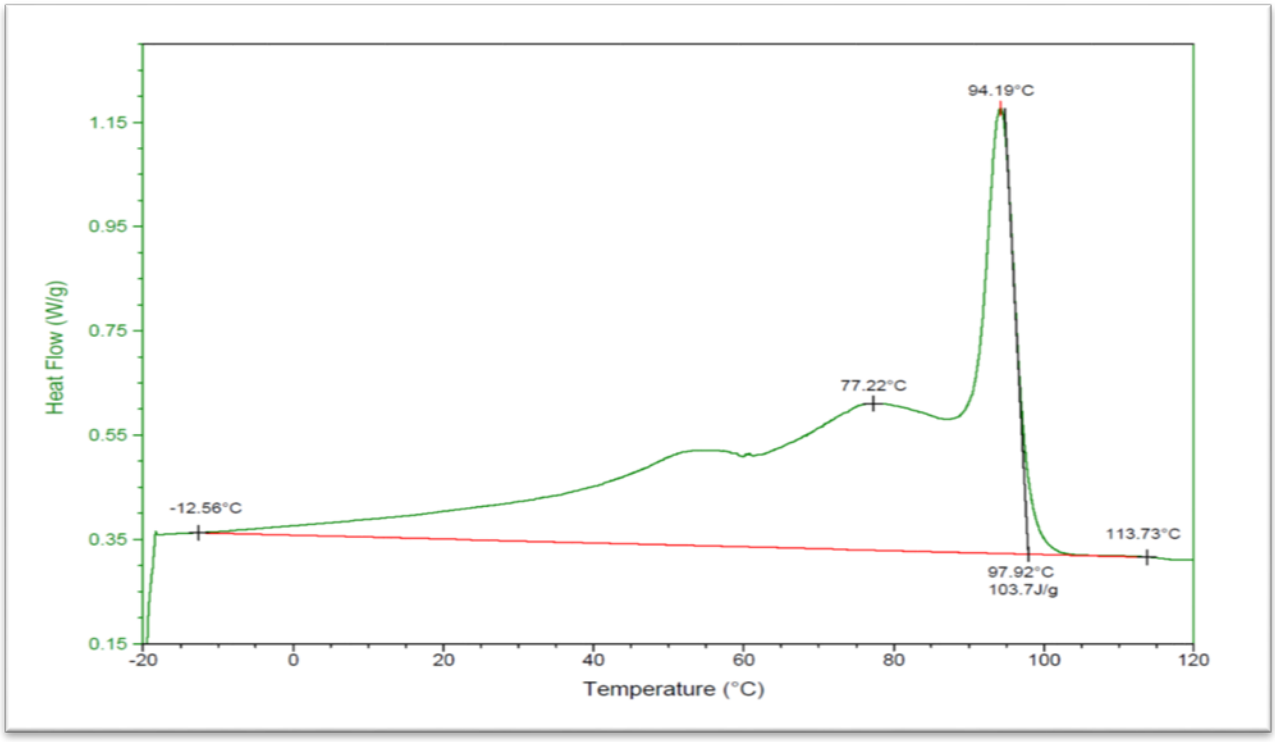

Figure A.13 – DSC plot for Cooling Cycle of sample run 10(06) with Extracted Values

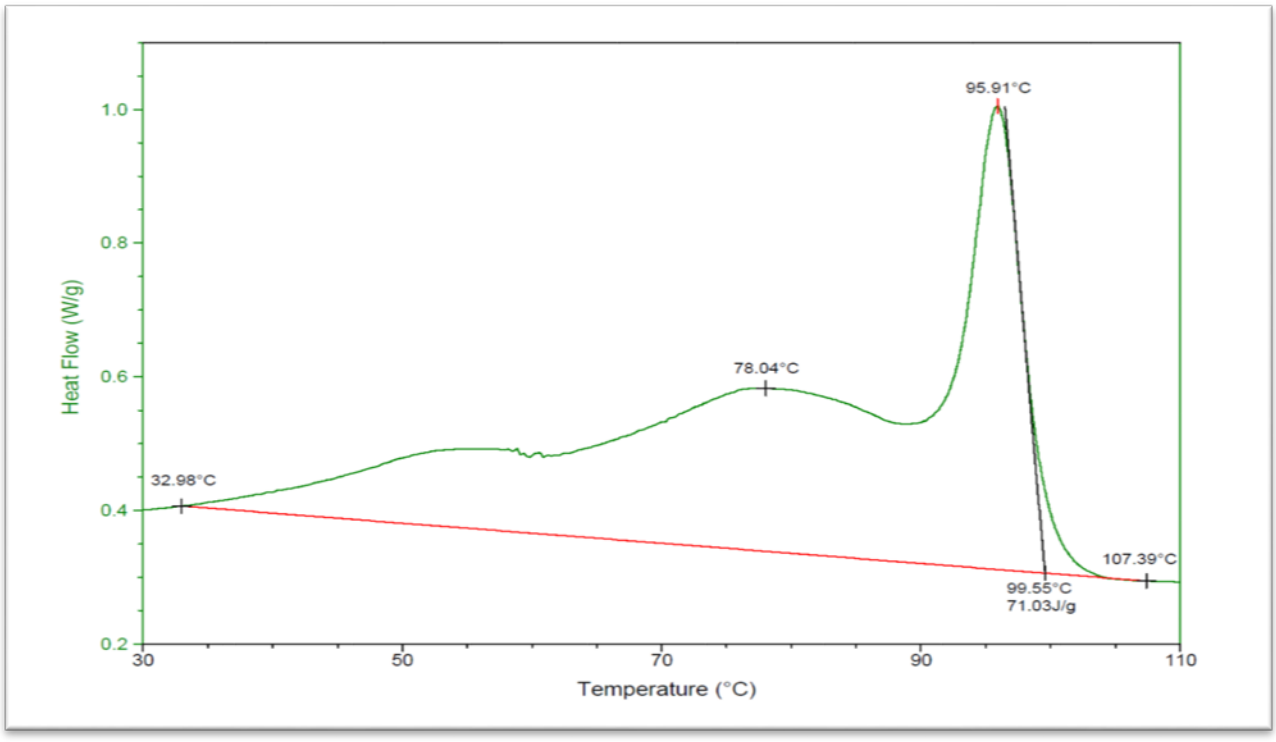

Figure A.14 – DSC plot for Cooling Cycle of sample run 11 with Extracted Values

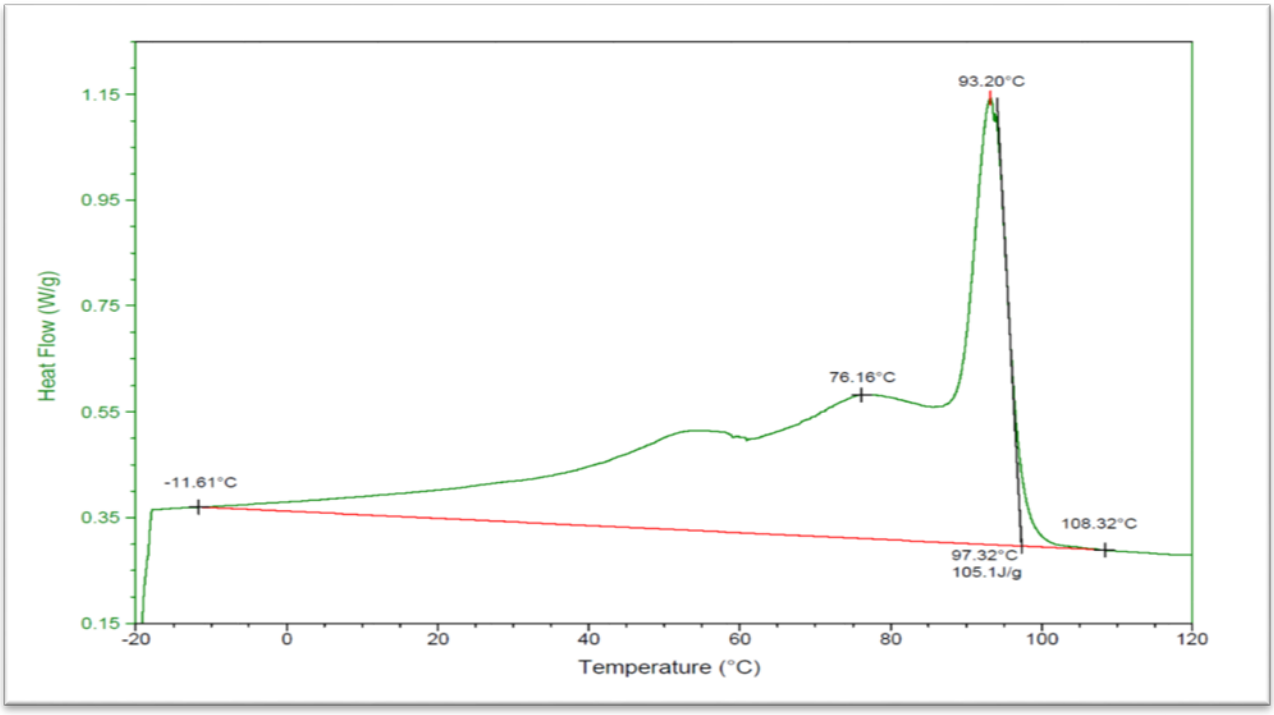

Figure A.15 – DSC plot for Cooling Cycle of sample run 12(05) with Extracted Values

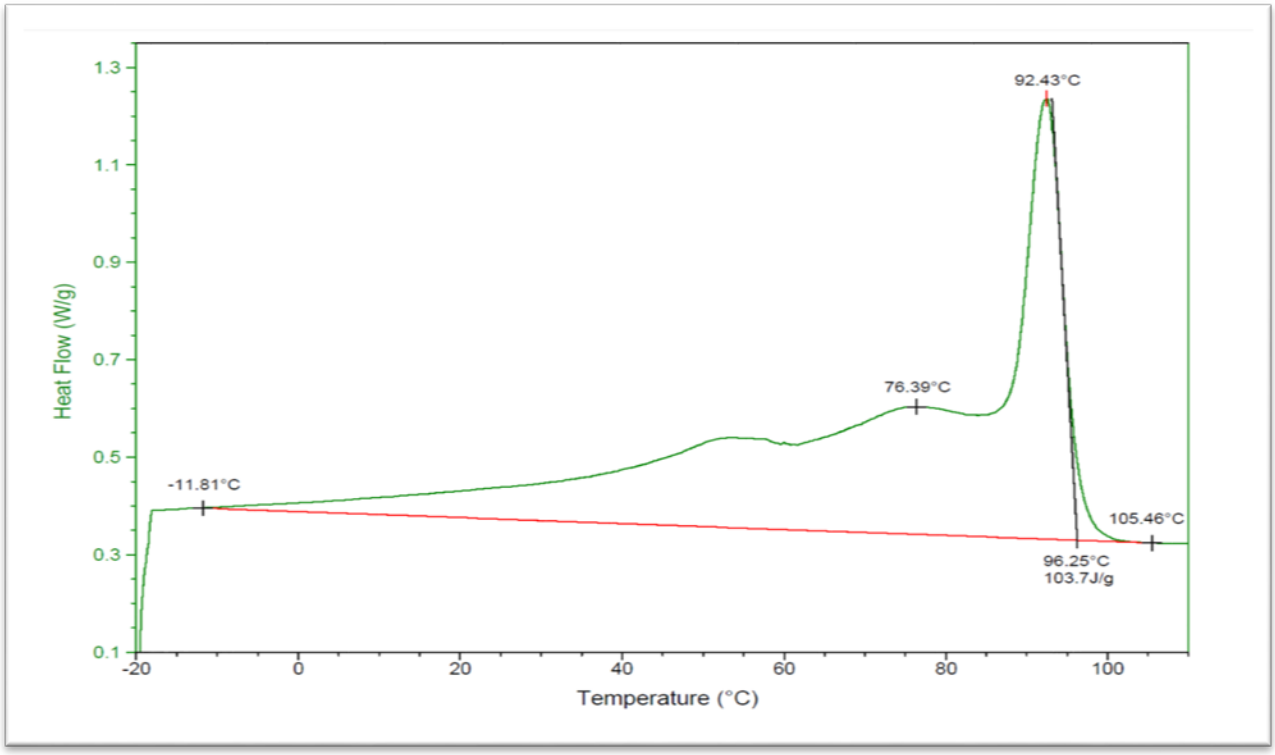

Figure A.16 – DSC plot for Cooling Cycle of sample run 12(06) with Extracted Values

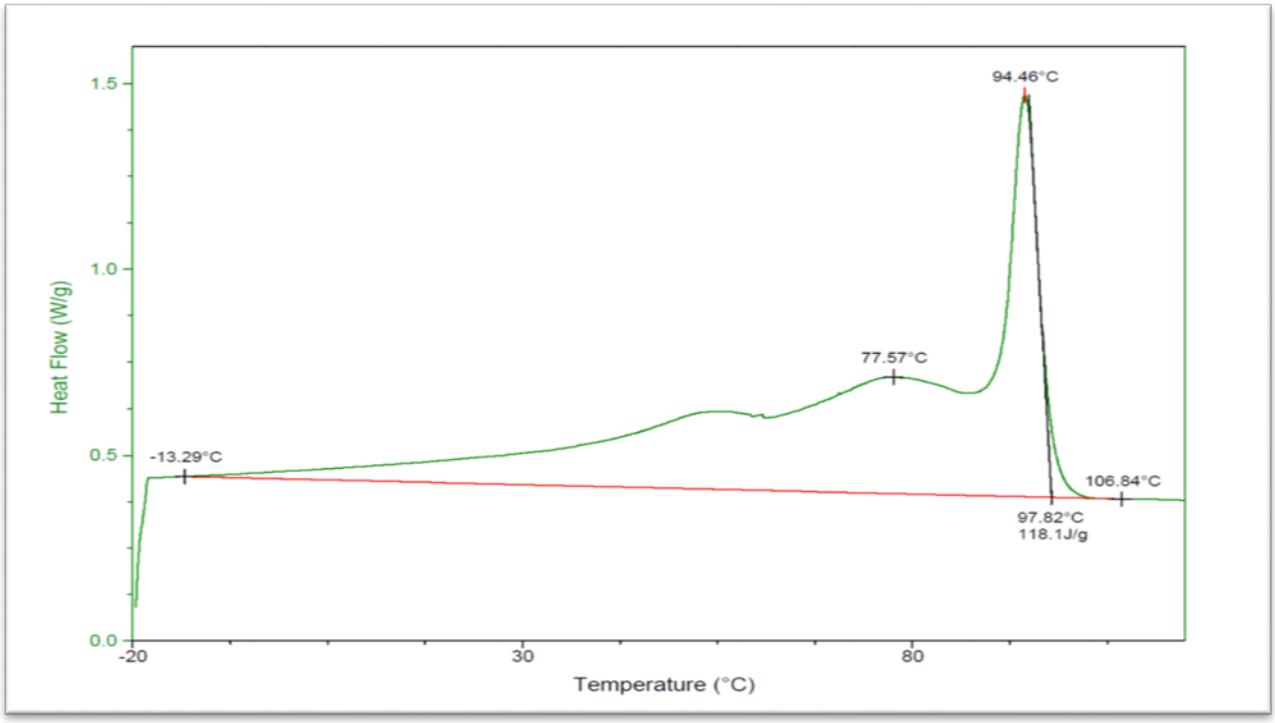

Figure A.17 – DSC plot for Cooling Cycle of sample run 13(05) with Extracted Values

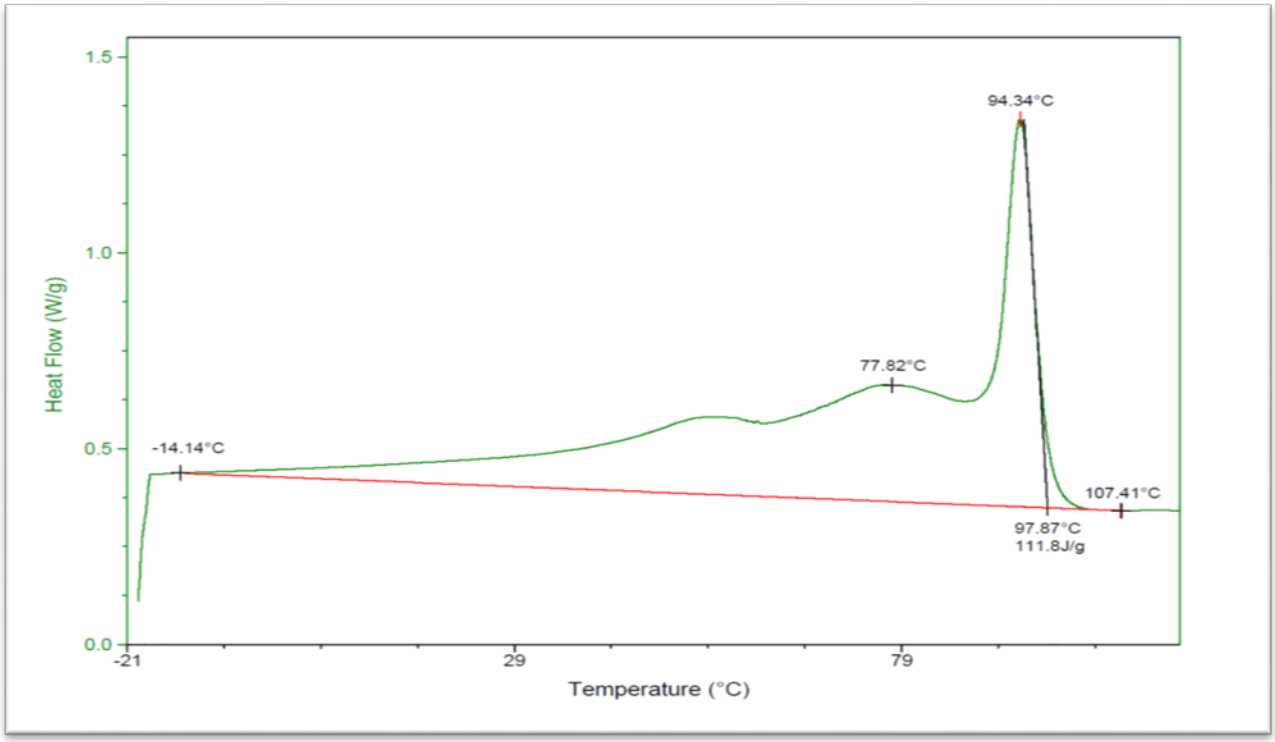

Figure A.18 – DSC plot for Cooling Cycle of sample run 13(06) with Extracted Values

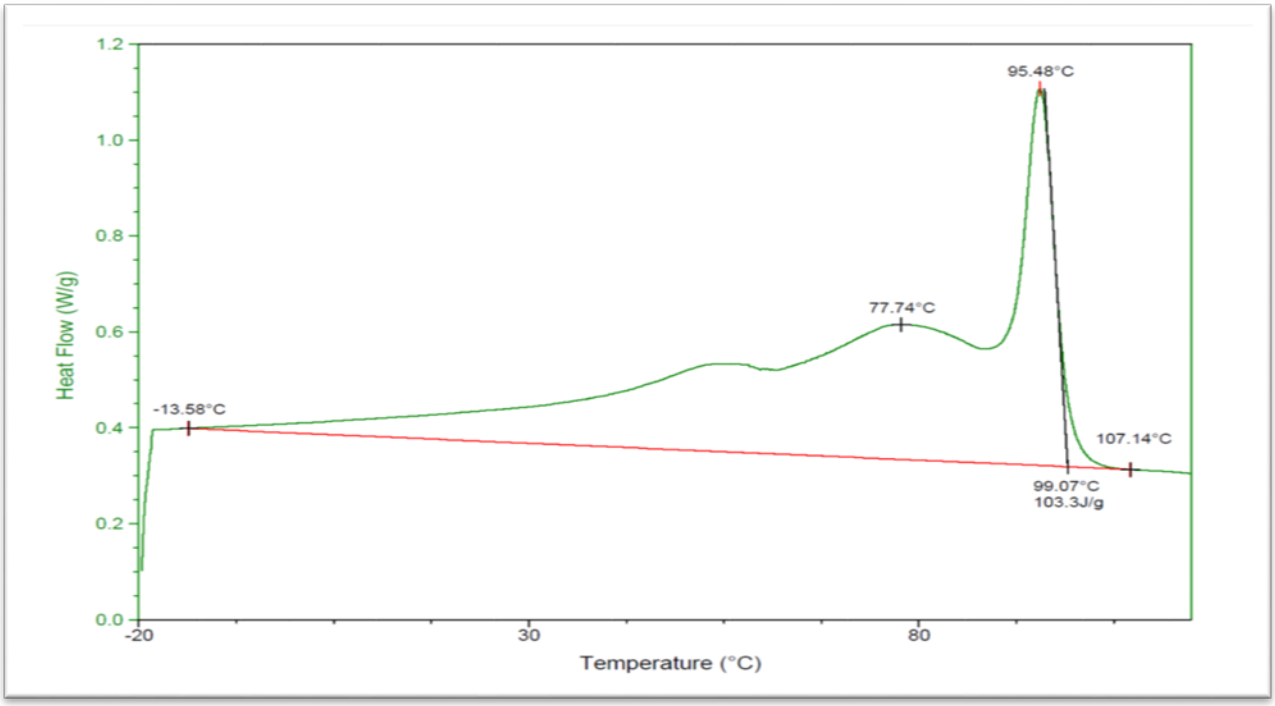

Figure A.19 – DSC plot for Cooling Cycle of sample run 14 with Extracted Values

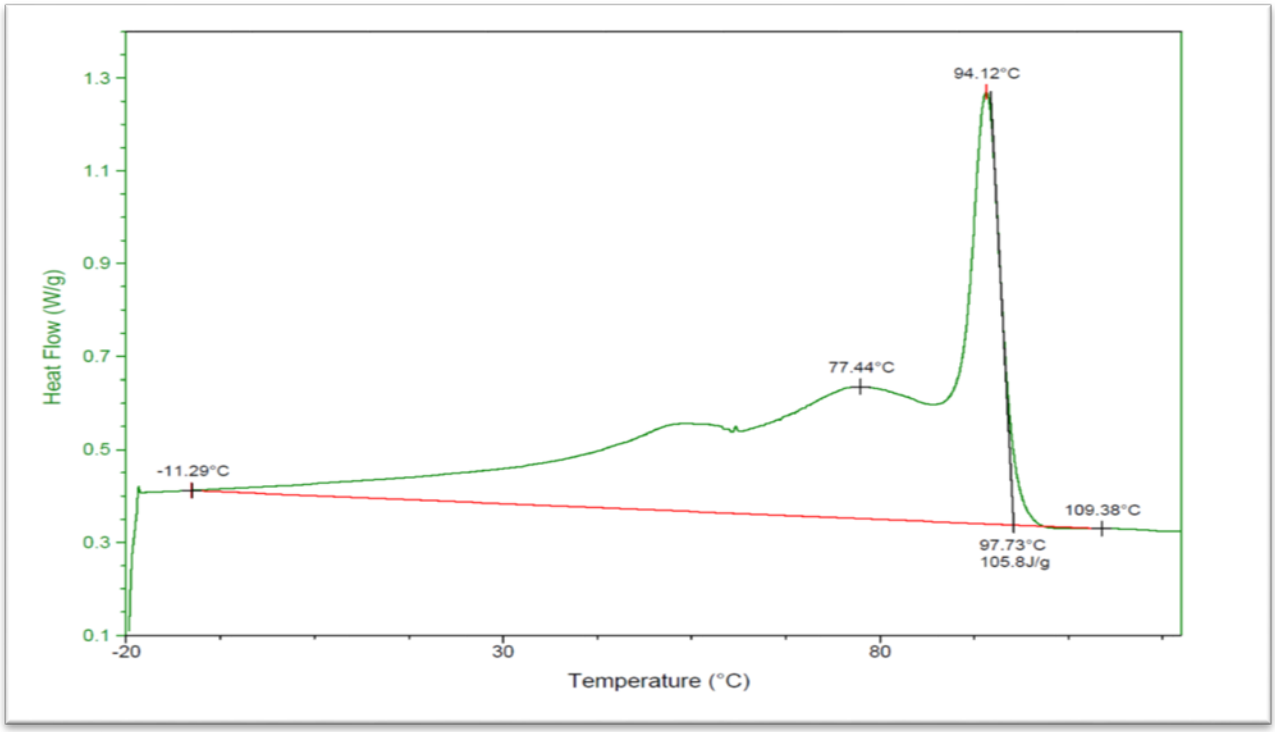

Figure A.20 – DSC plot for Cooling Cycle of sample run 15 with Extracted Values

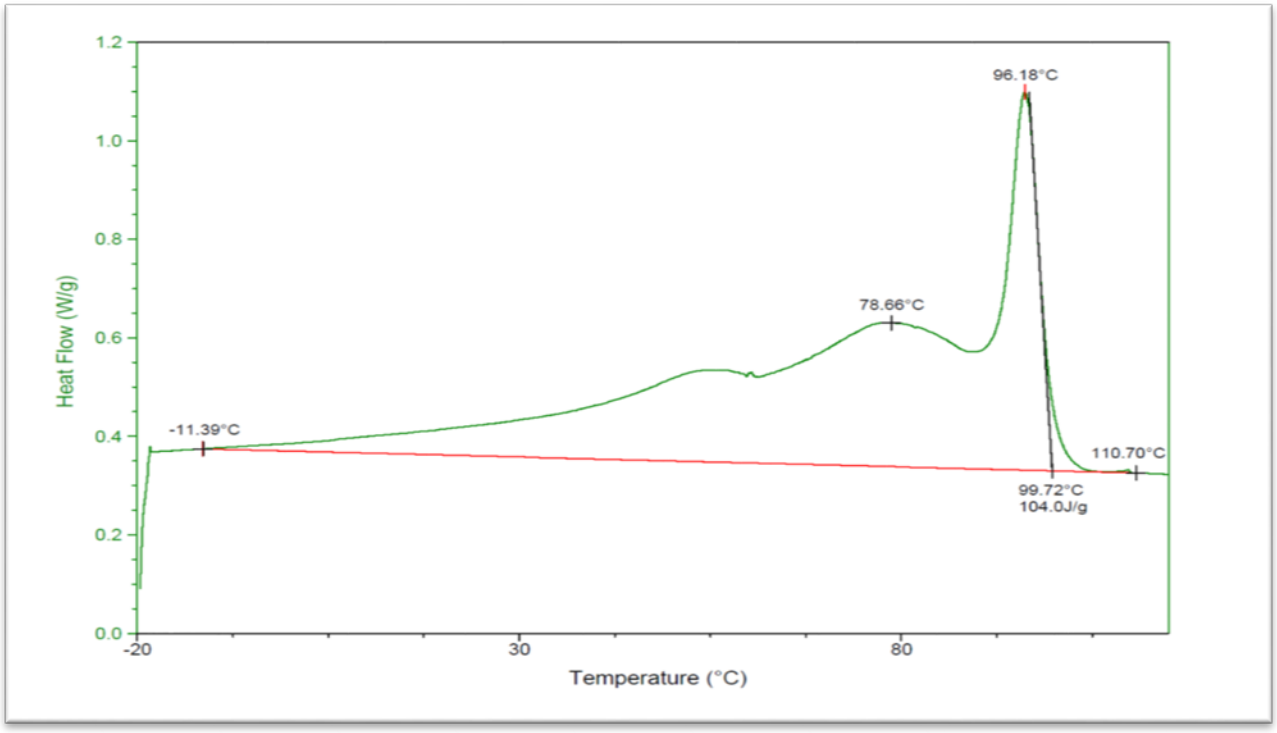

Figure A.21 – DSC plot for Cooling Cycle of sample run 16 with Extracted Values

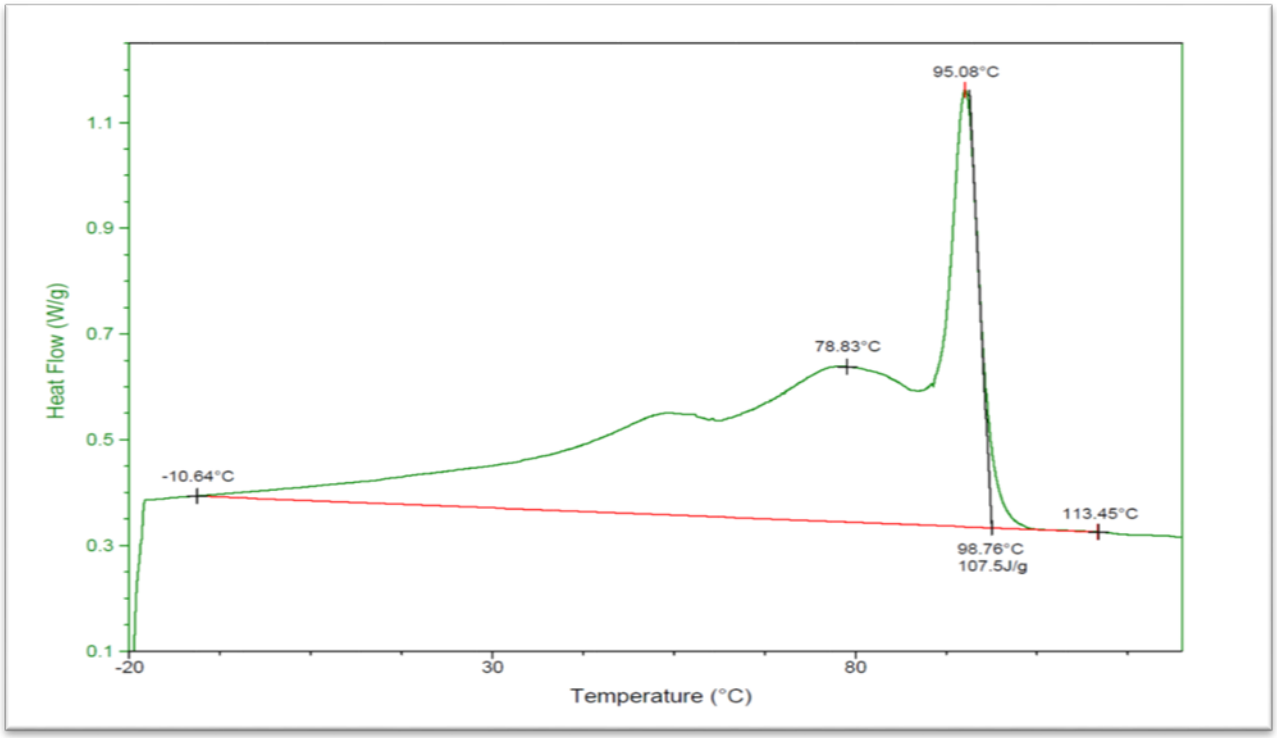

Figure A.22 – DSC plot for Cooling Cycle of sample run 17 with Extracted Values

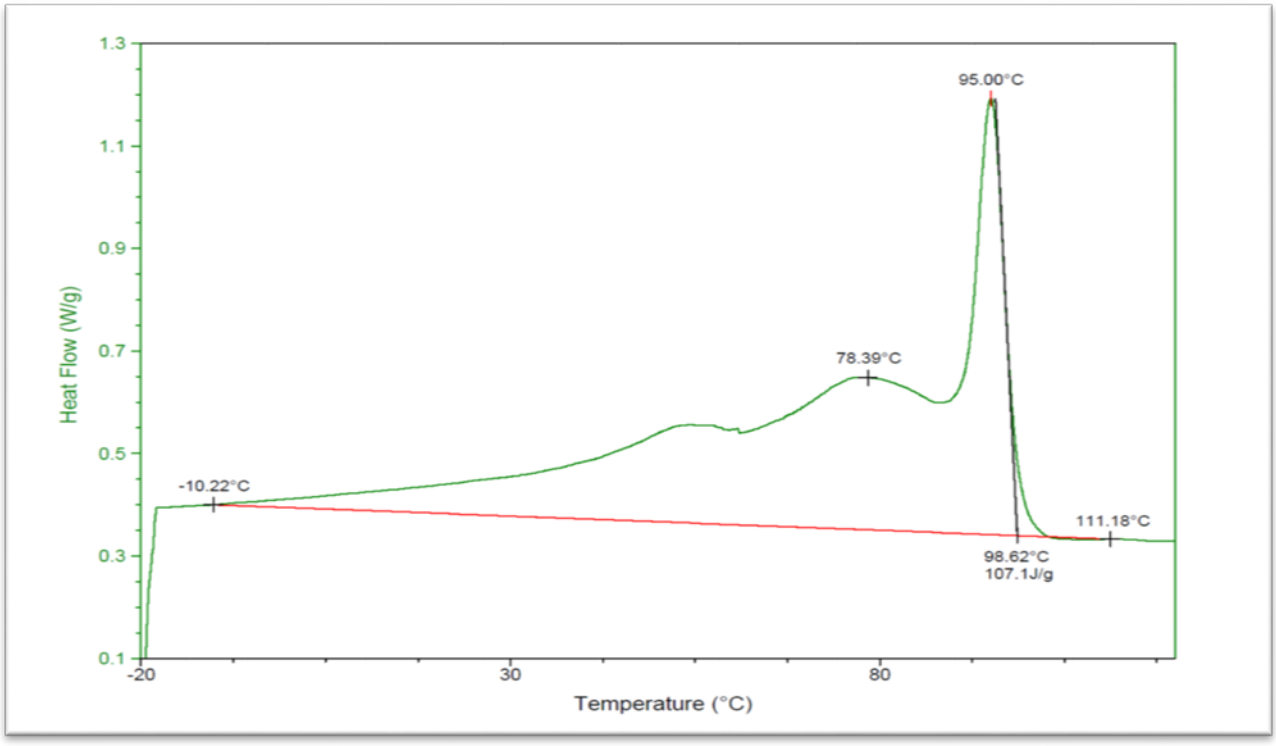

Figure A.23 – DSC plot for Cooling Cycle of sample run 18 with Extracted Values

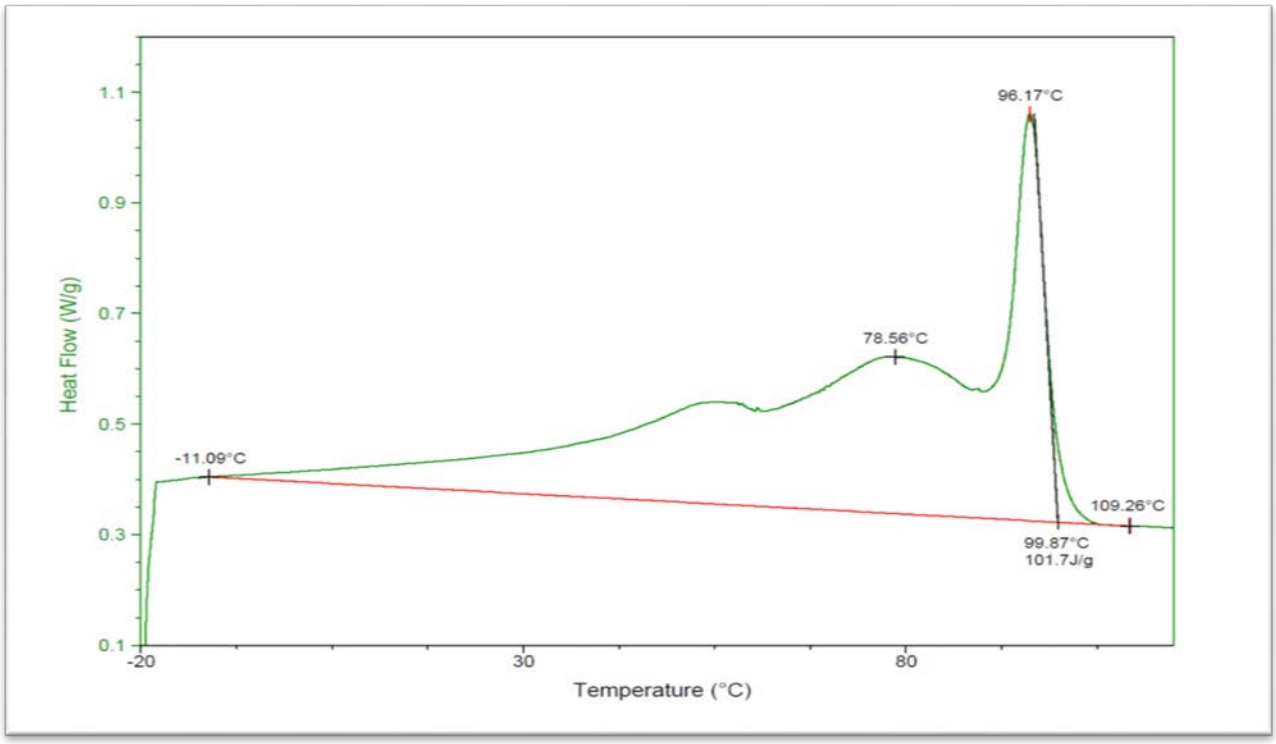

Figure A.24 – DSC plot for Cooling Cycle of sample run 19 with Extracted Values

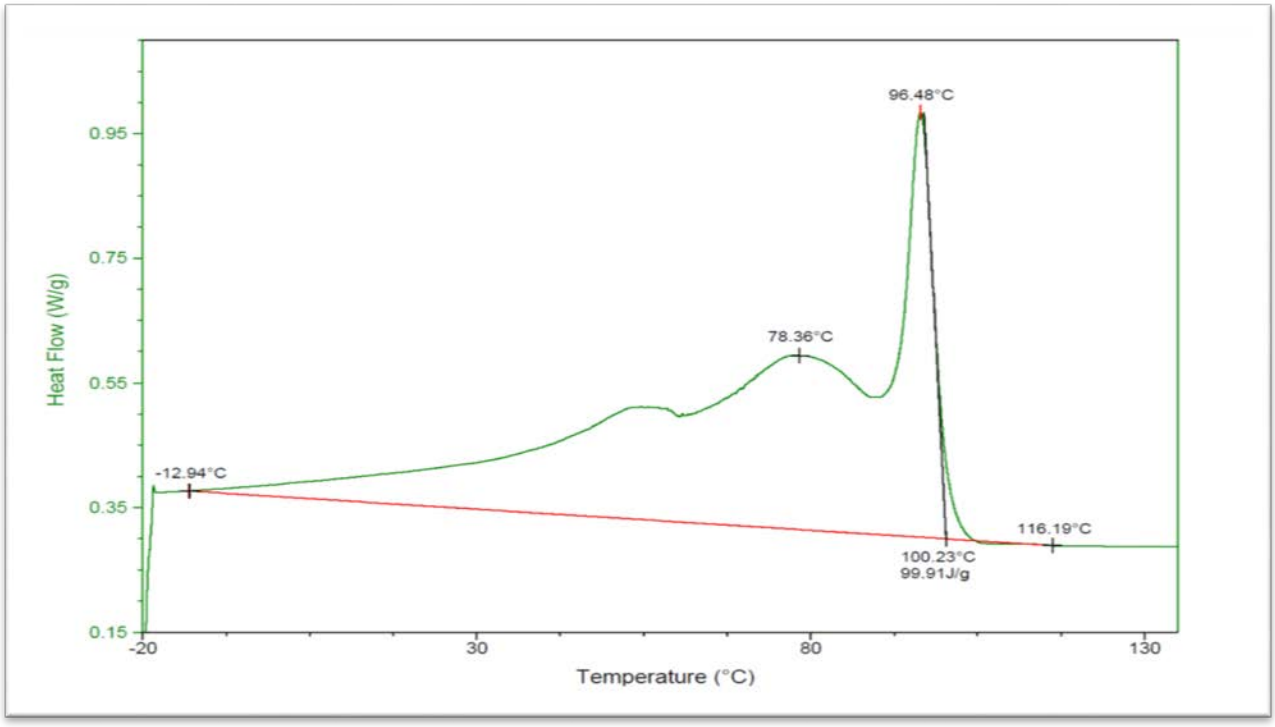

Figure A.25 – DSC plot for Cooling Cycle of sample run 20(1) with Extracted Values

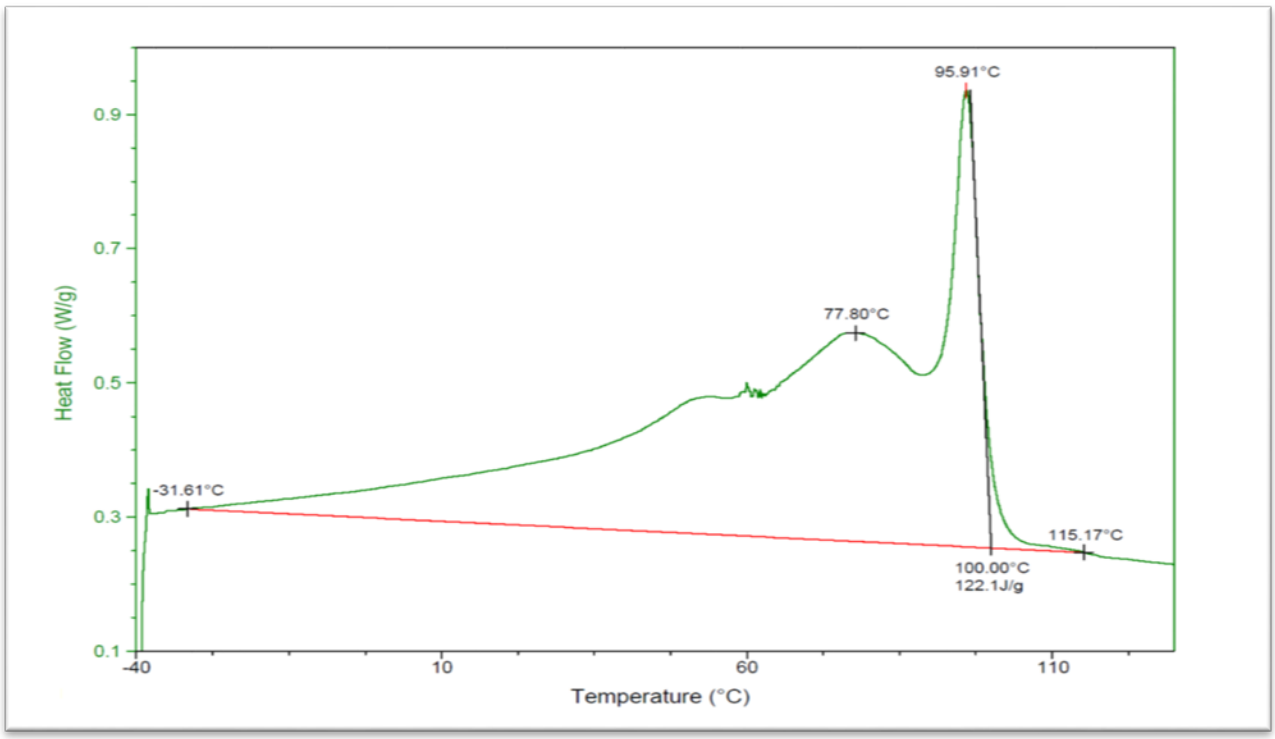

Figure A.26 – DSC plot for Cooling Cycle of sample run 20(2) with Extracted Values

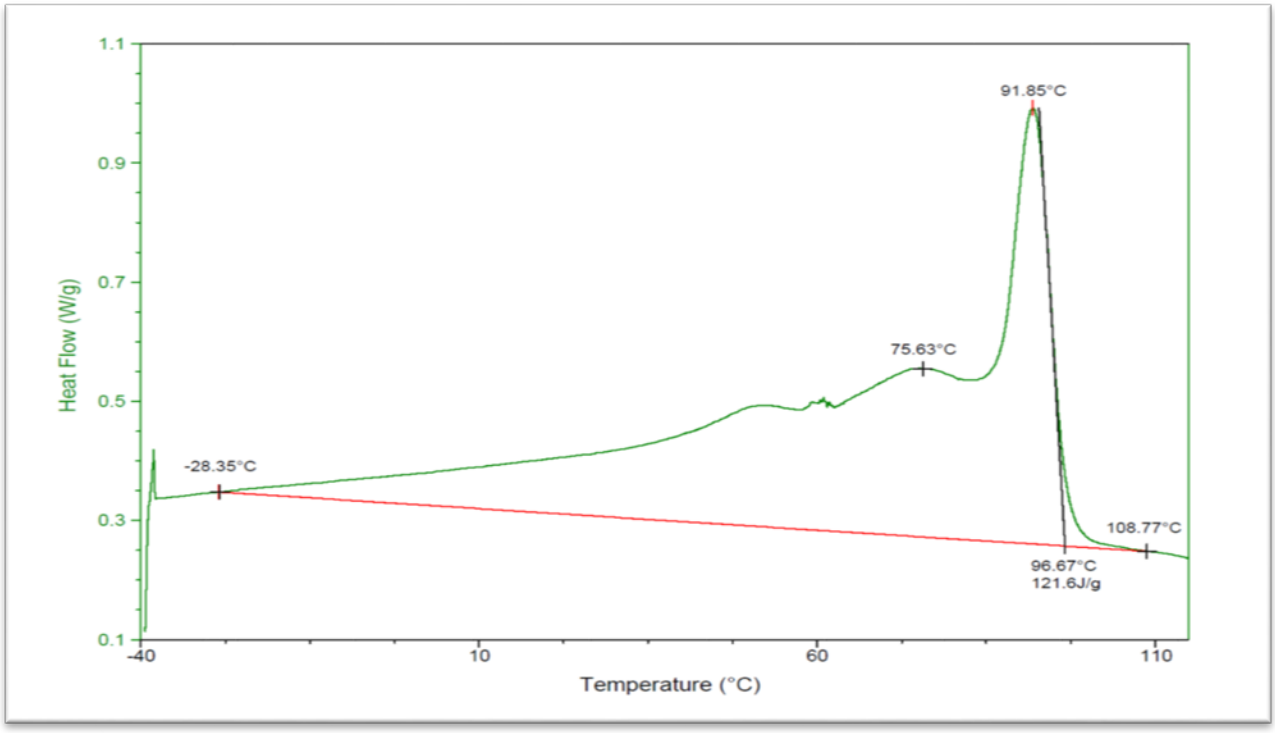

Figure A.27 – DSC plot for Cooling Cycle of Virgin Material with Extracted Values

APPENDIX B: DSC Plots for Second Heating Cycle

Runs can be found in Table 4.10

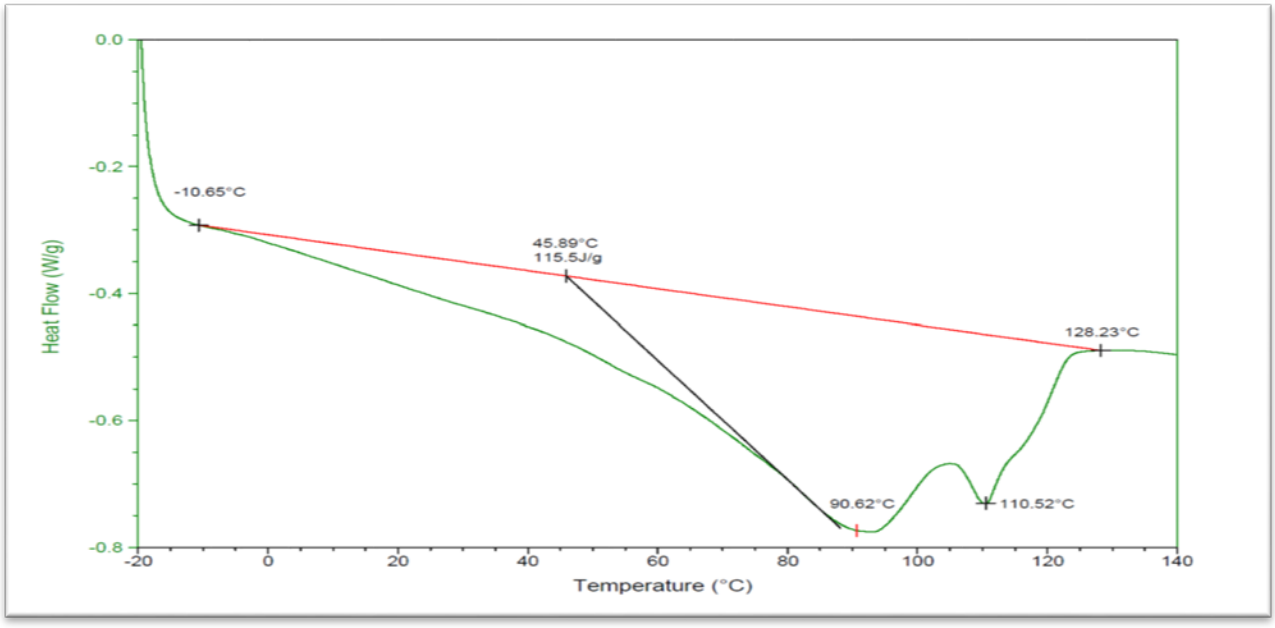

Figure B.1 – DSC plot for Second Heating Cycle of sample run, Test 1 with Extracted Values

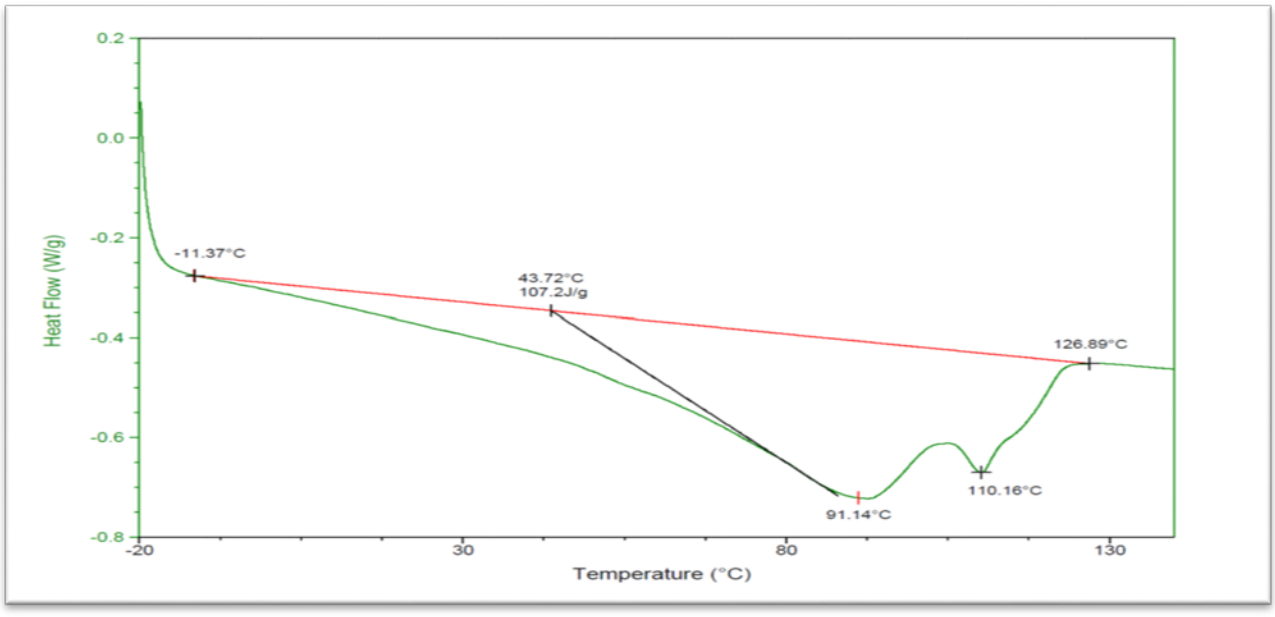

Figure B.2 – DSC plot for Second Heating Cycle of sample run 1 with Extracted Values

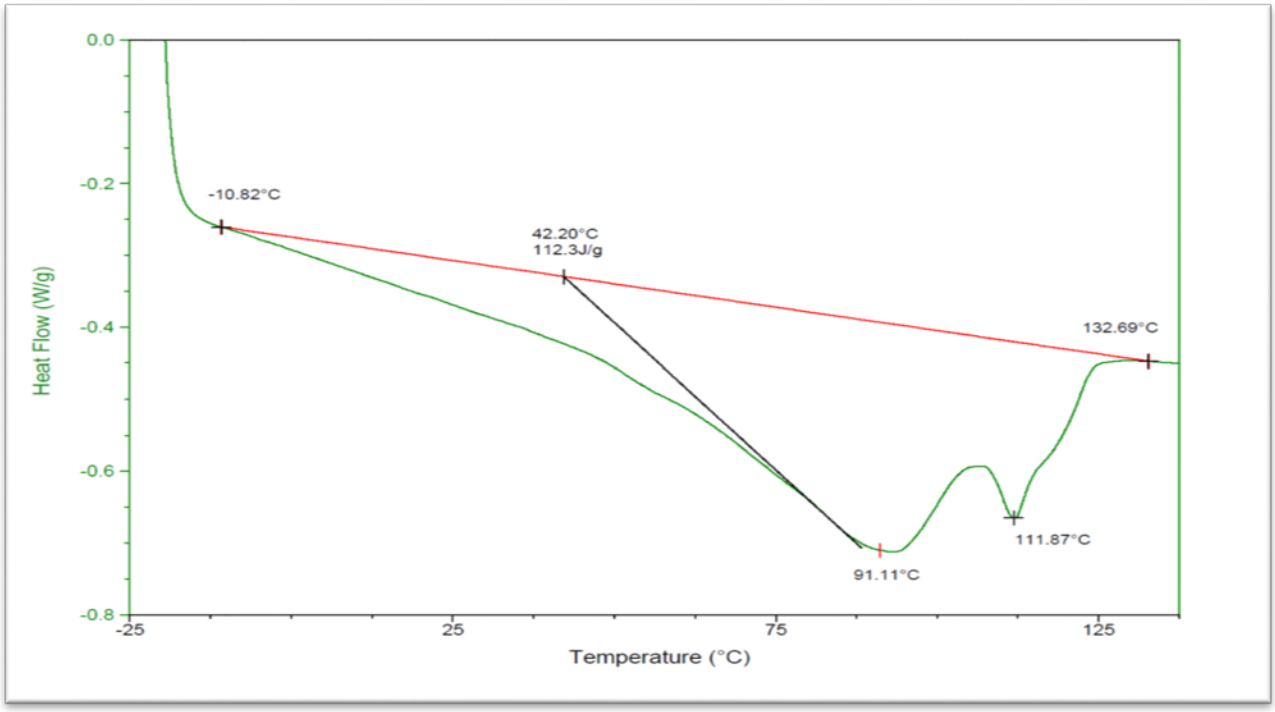

Figure B.3 – DSC plot for Second Heating Cycle of sample run 2 with Extracted Values

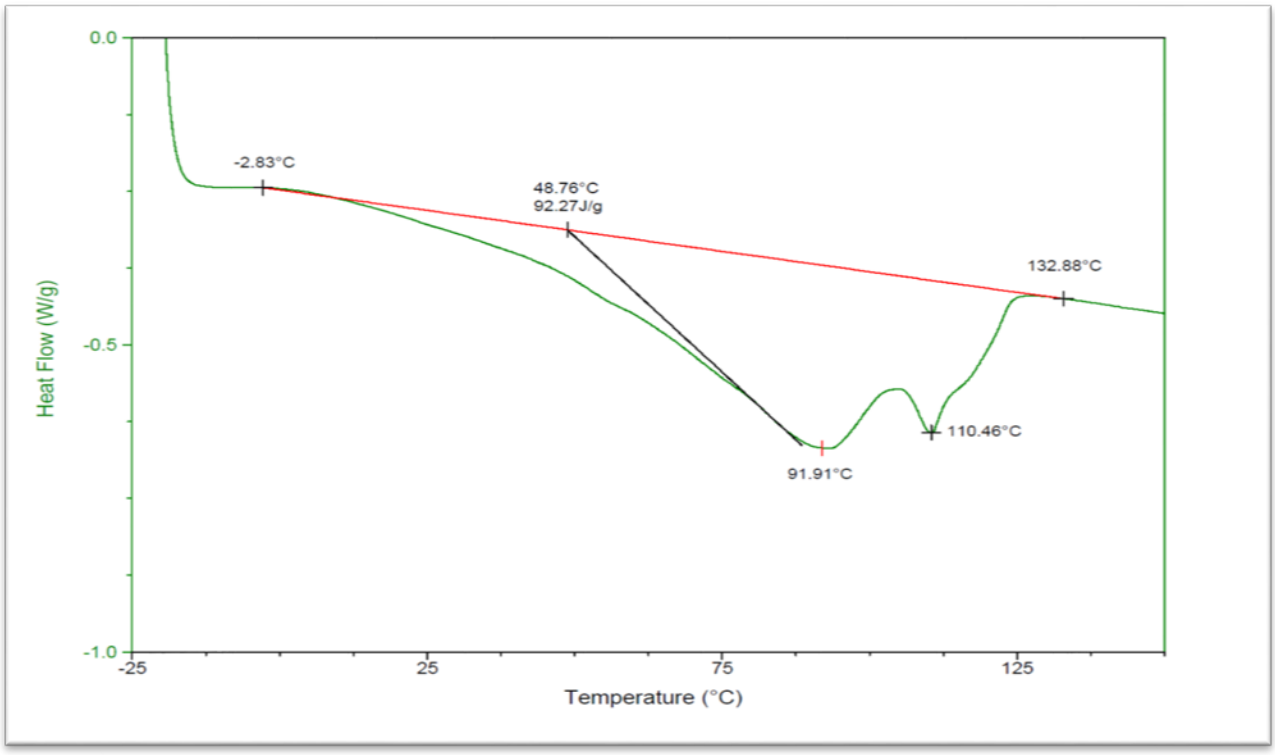

Figure B.4 – DSC plot for Second Heating Cycle of sample run 3 with Extracted Values

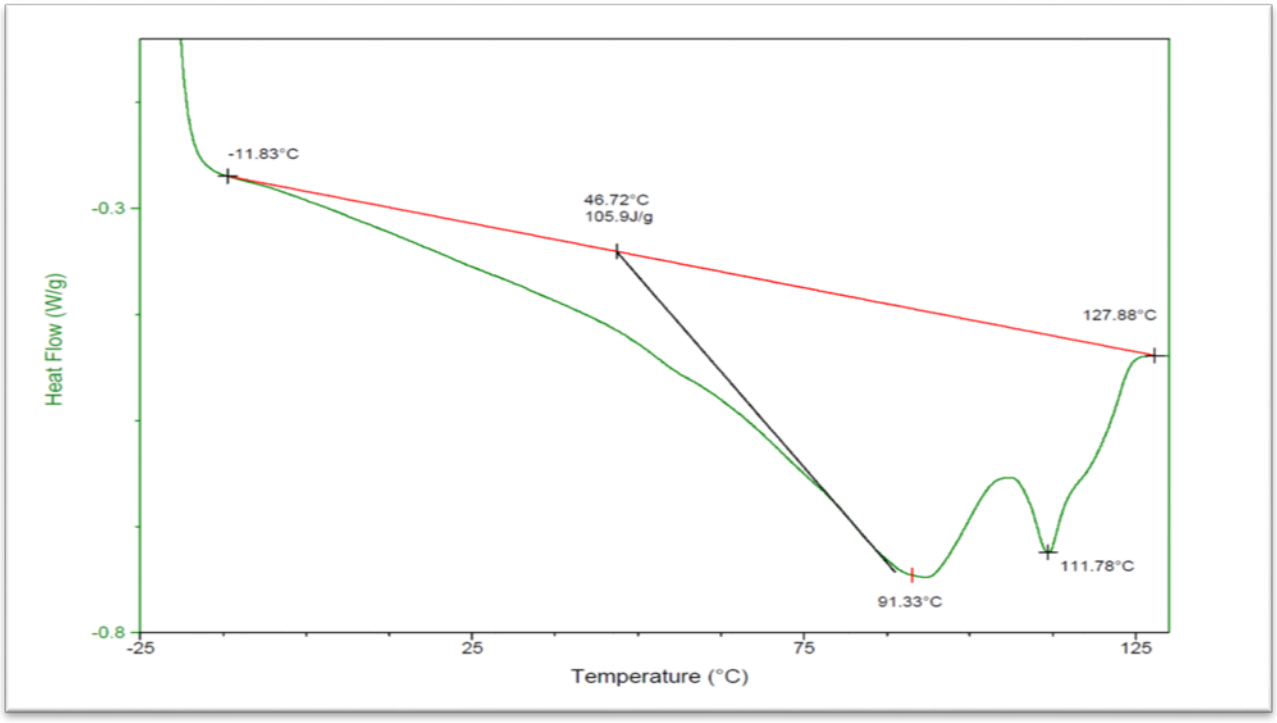

Figure B.5 – DSC plot for Second Heating Cycle of sample run 4 with Extracted Values

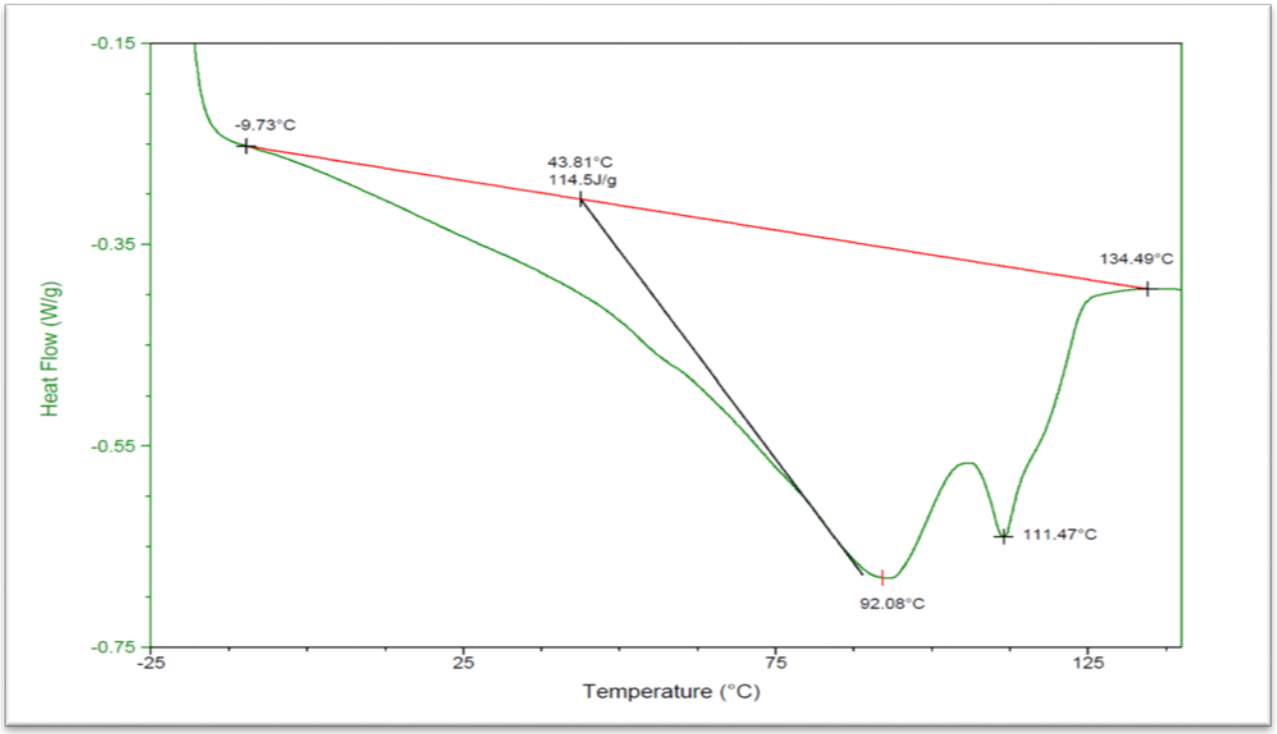

Figure B.6 – DSC plot for Second Heating Cycle of sample run 5 with Extracted Values

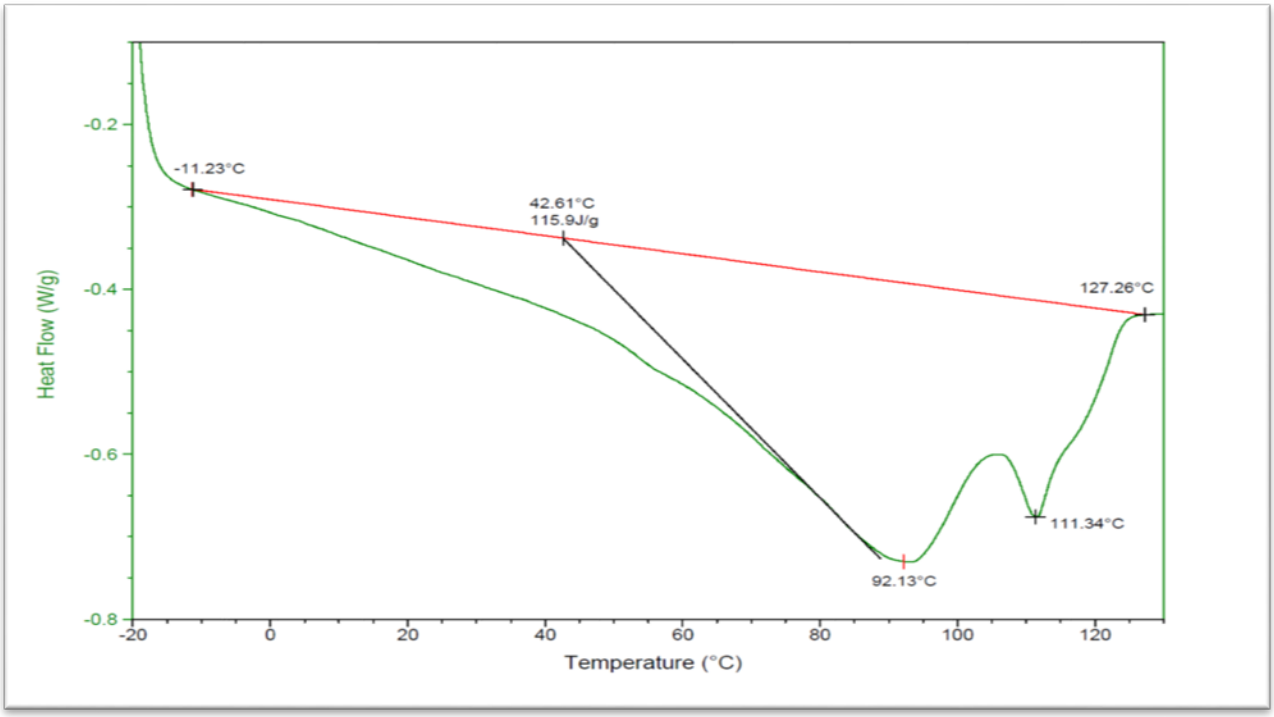

Figure B.7 – DSC plot for Second Heating Cycle of sample run 6 with Extracted Values

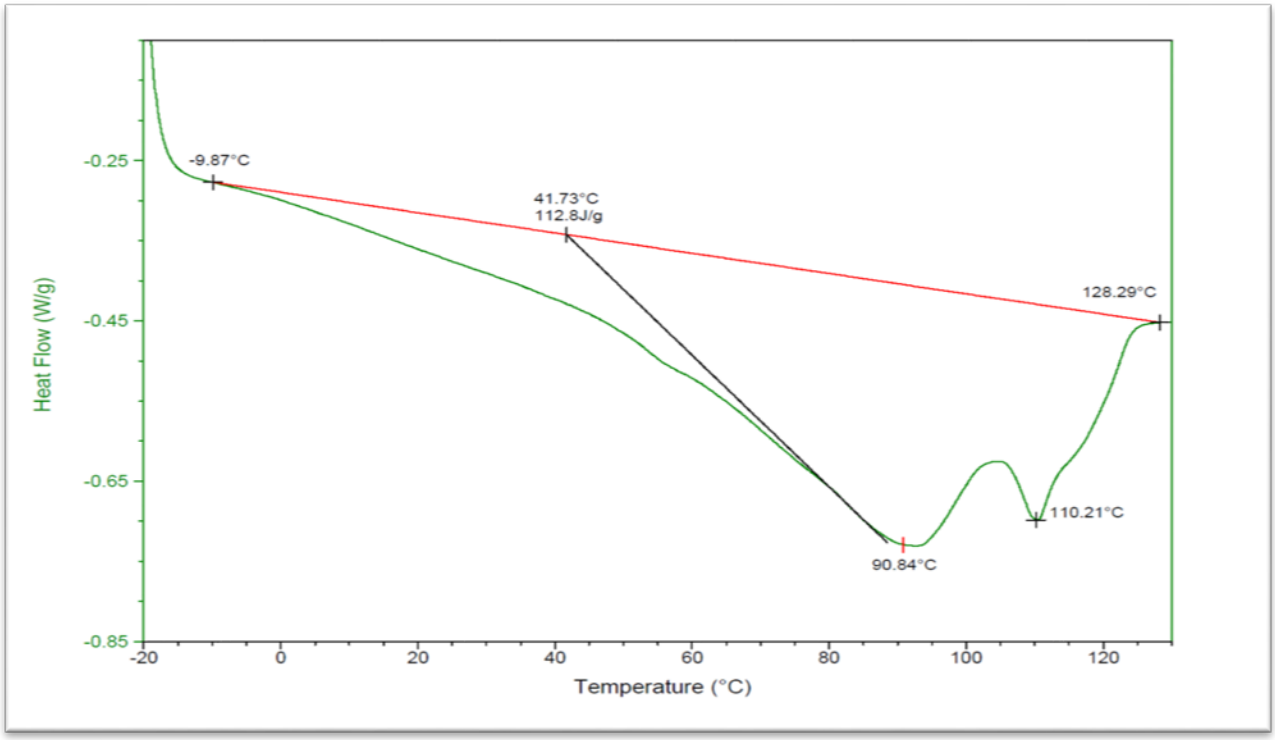

Figure B.8 – DSC plot for Second Heating Cycle of sample run 7 with Extracted Values

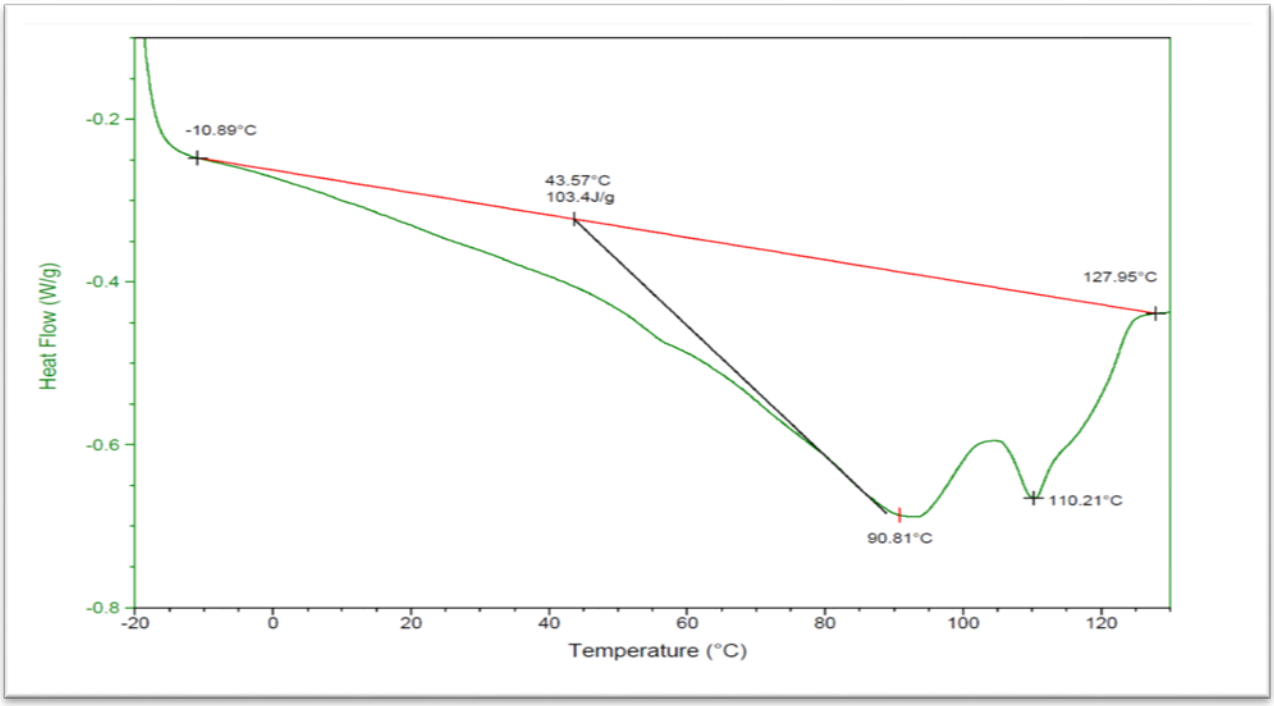

Figure B.9 – DSC plot for Second Heating Cycle of sample run 8 with Extracted Values

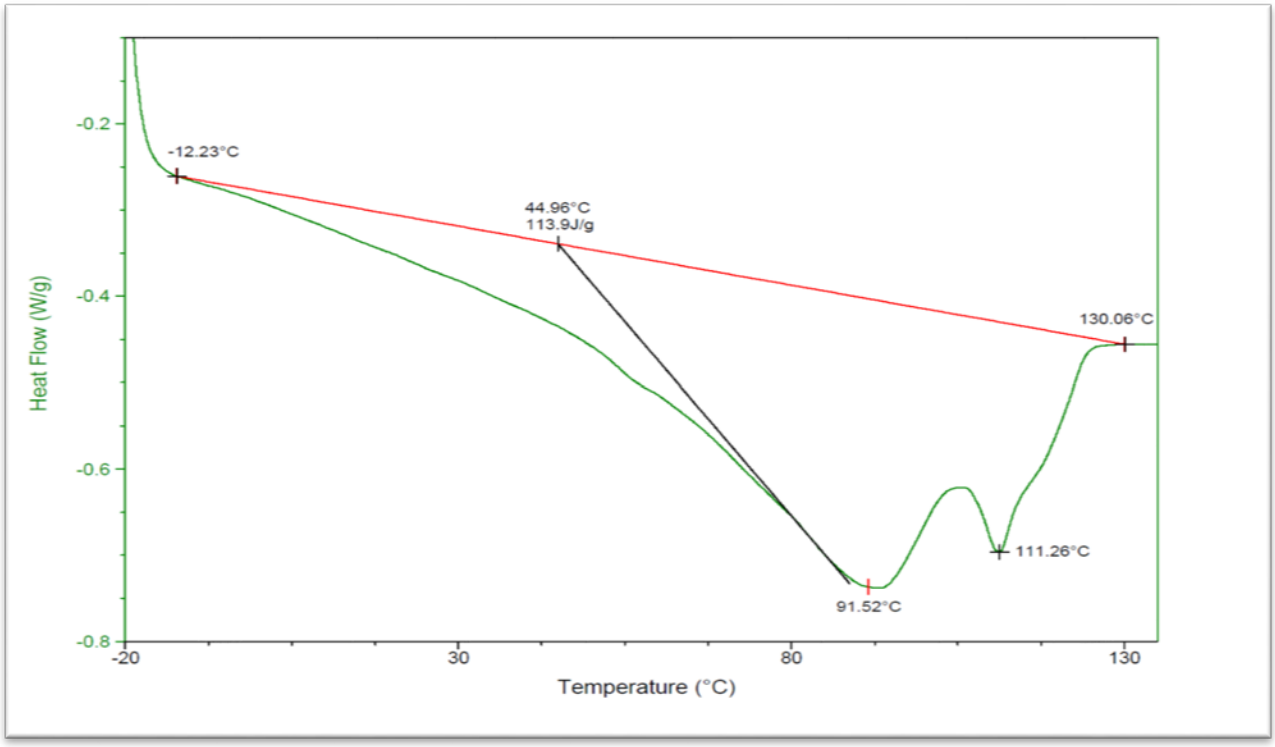

Figure B.10 – DSC plot for Second Heating Cycle of sample run 9(05) with Extracted Values

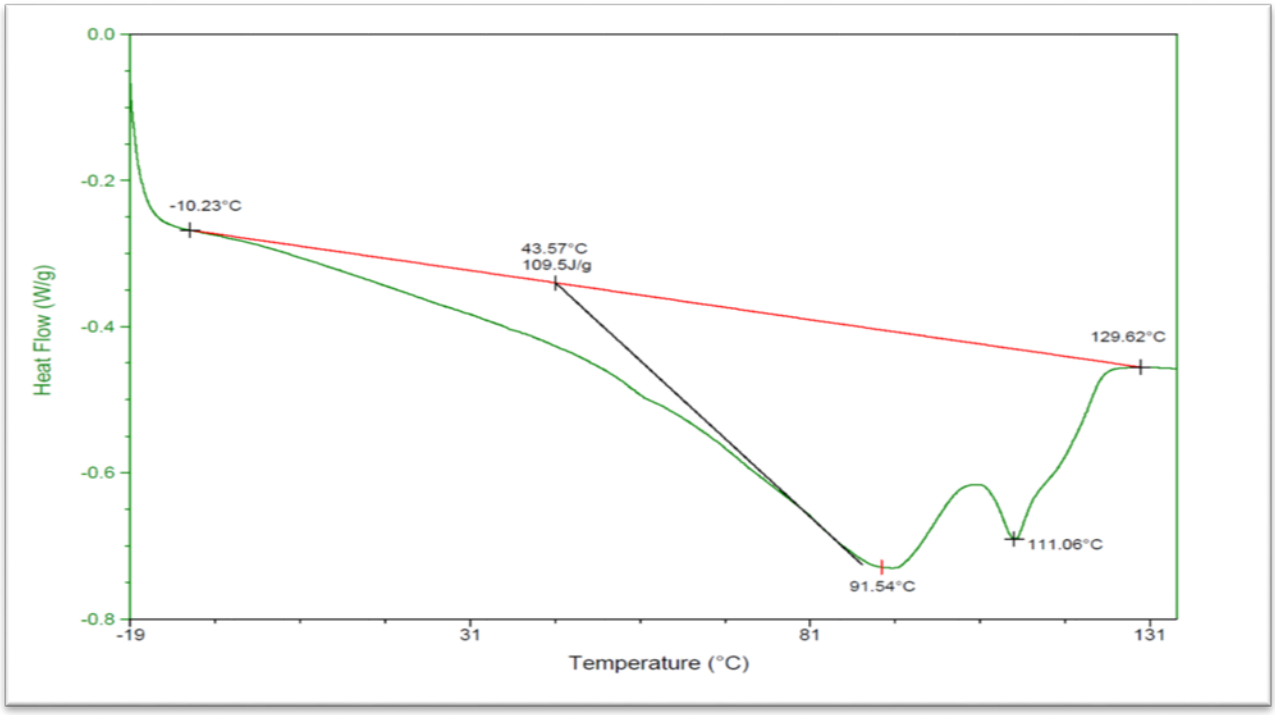

Figure B.11 – DSC plot for Second Heating Cycle of sample run 9(06) with Extracted Values

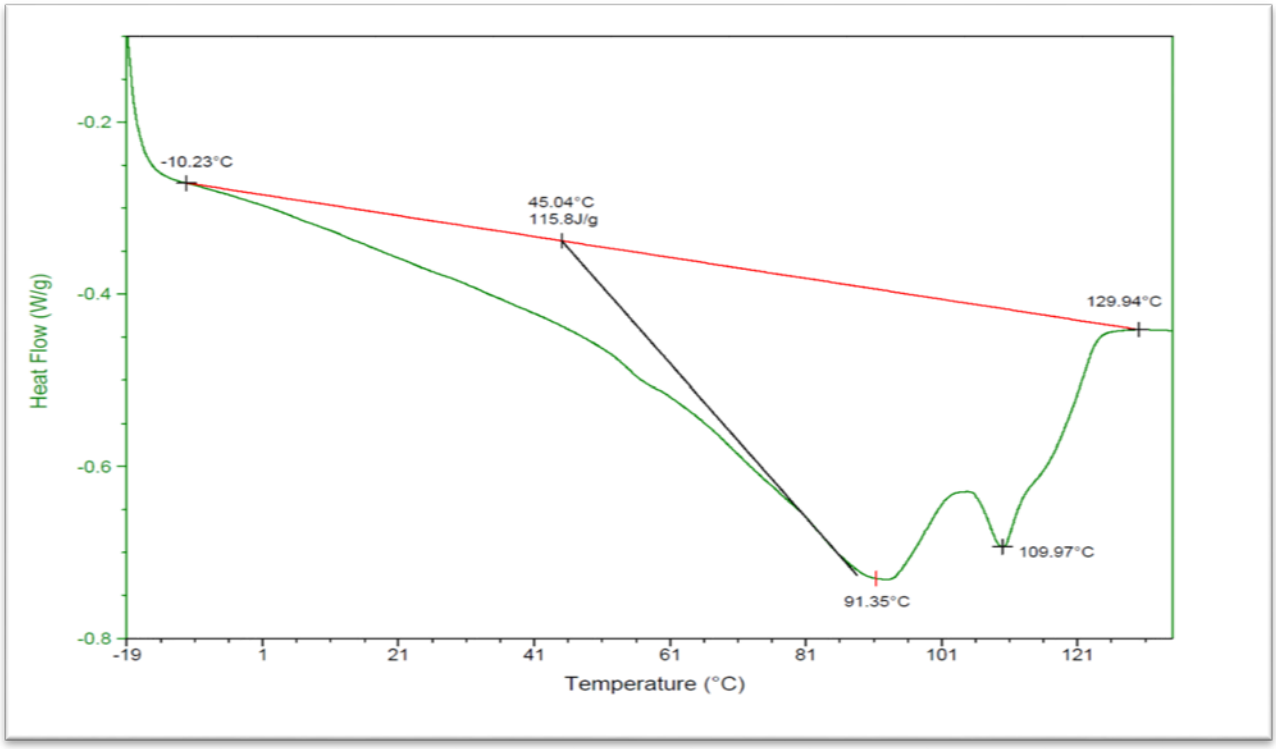

Figure B.12 – DSC plot for Second Heating Cycle of sample run 10(05) with Extracted Values

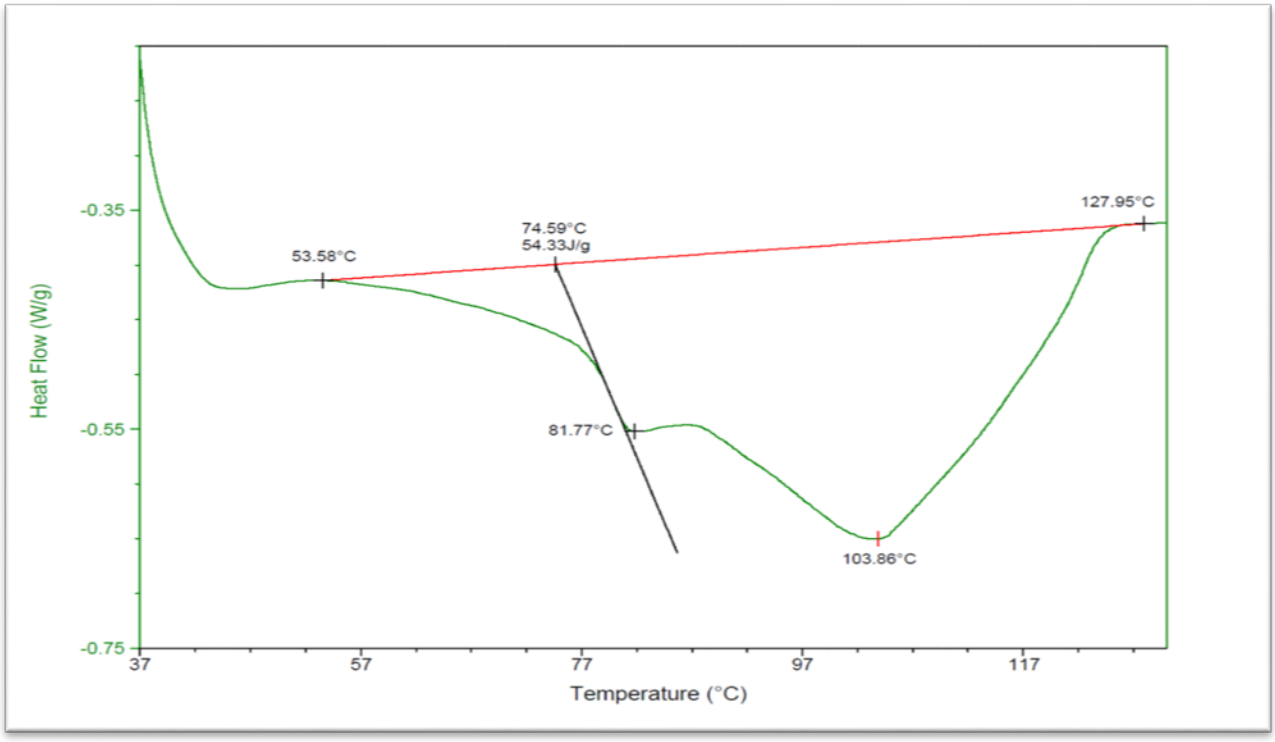

Figure B.13 – DSC plot for Second Heating Cycle of sample run 10(06) with Extracted Values

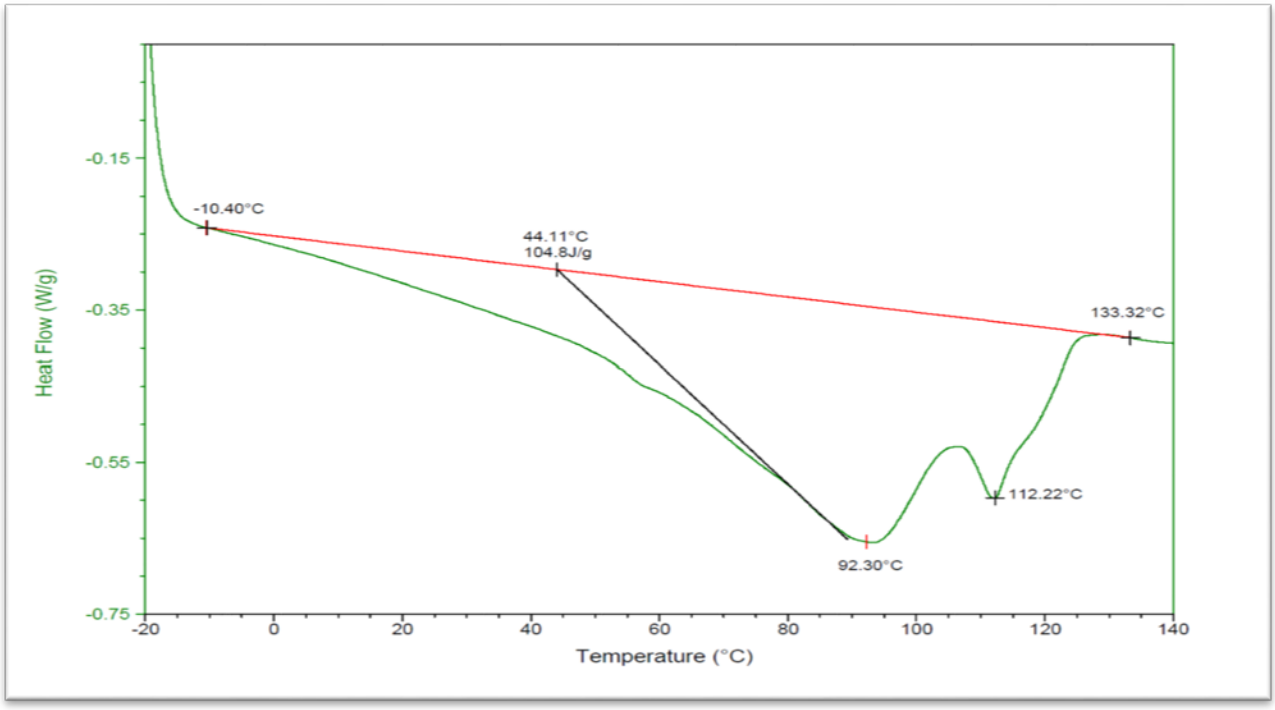

Figure B.14 – DSC plot for Second Heating Cycle of sample run 11 with Extracted Values

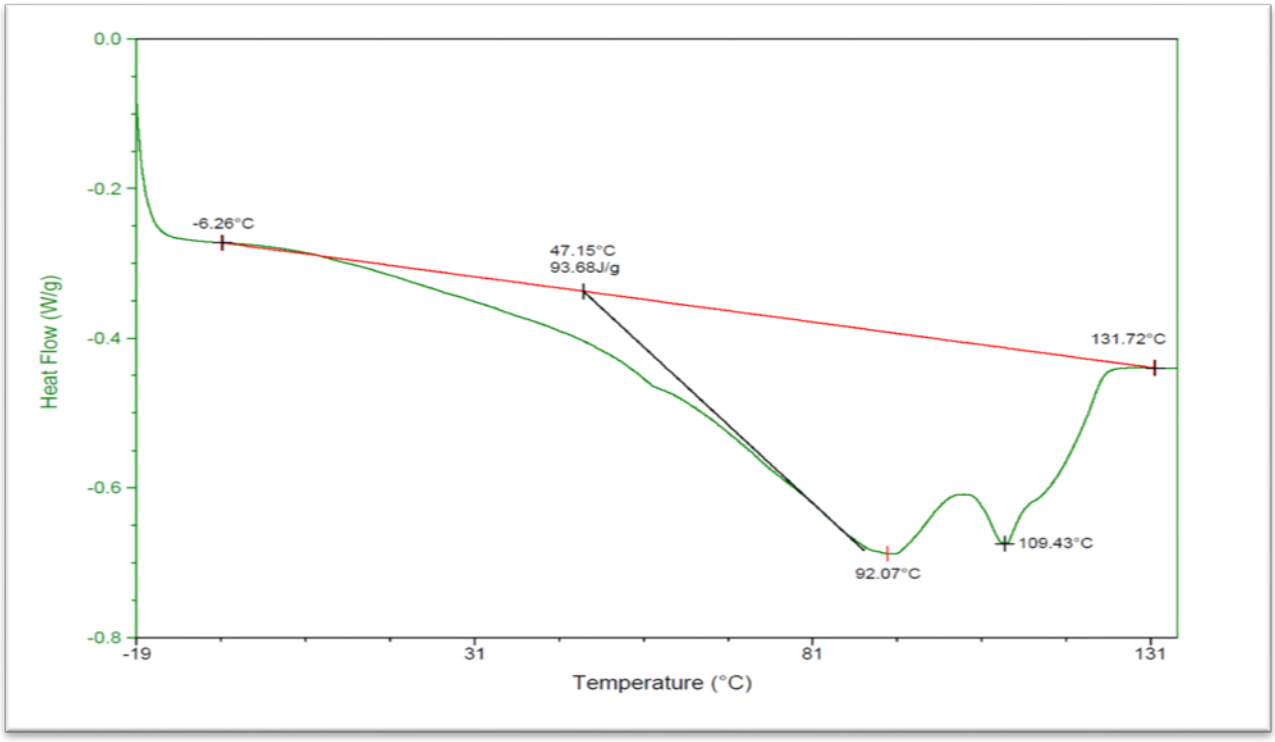

Figure B.15 – DSC plot for Second Heating Cycle of sample run 12(05) with Extracted Values

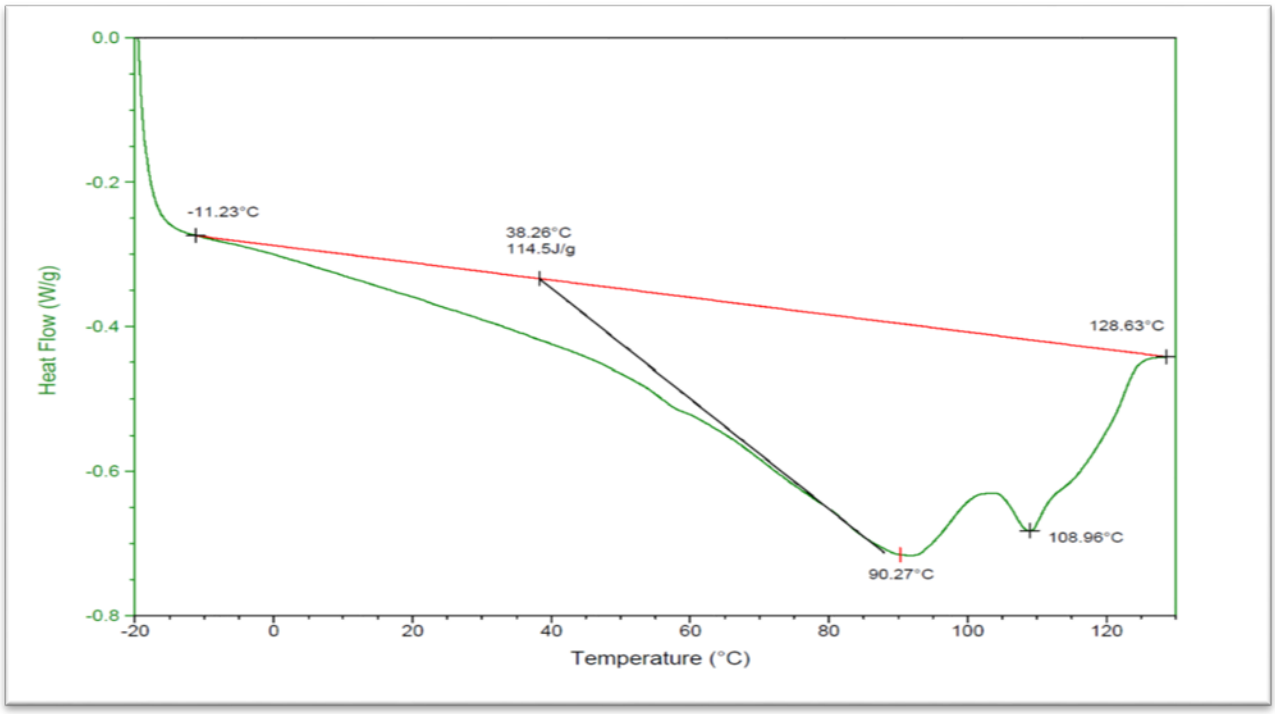

Figure B.16 – DSC plot for Second Heating Cycle of sample run 12(06) with Extracted Values

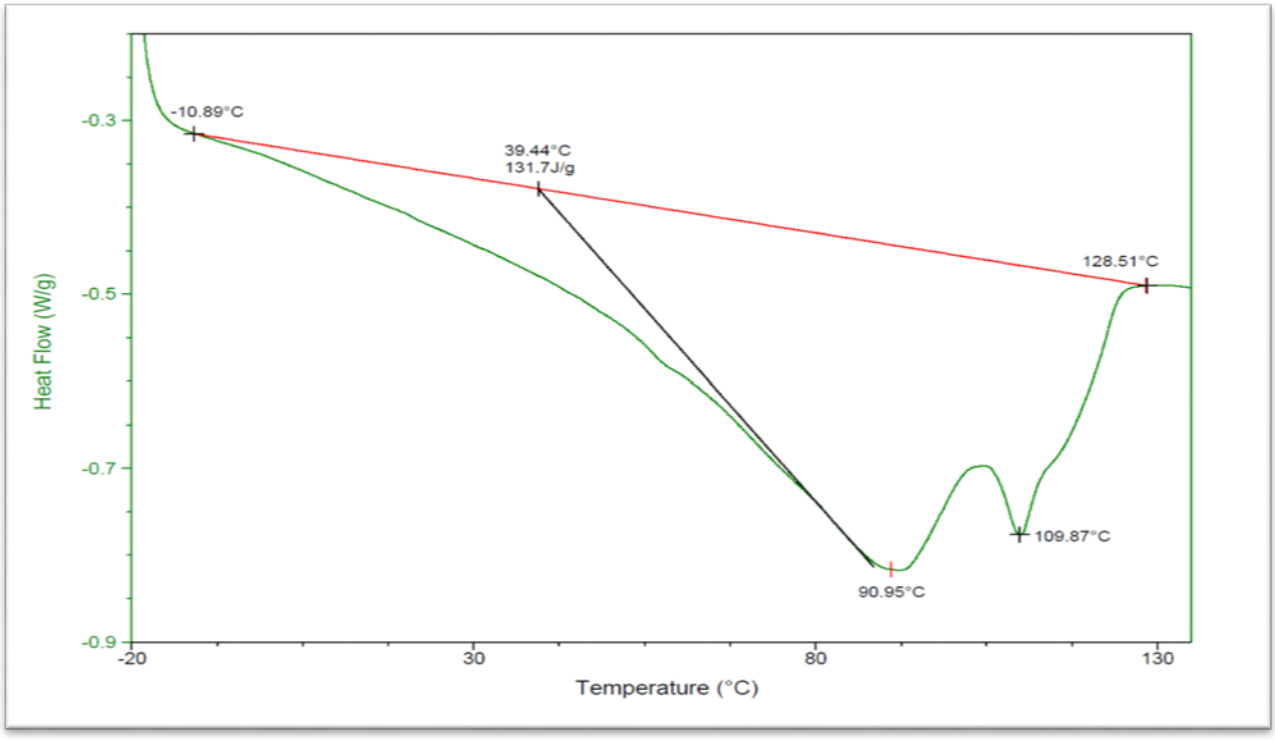

Figure B.17 – DSC plot for Second Heating Cycle of sample run 13(05) with Extracted Values

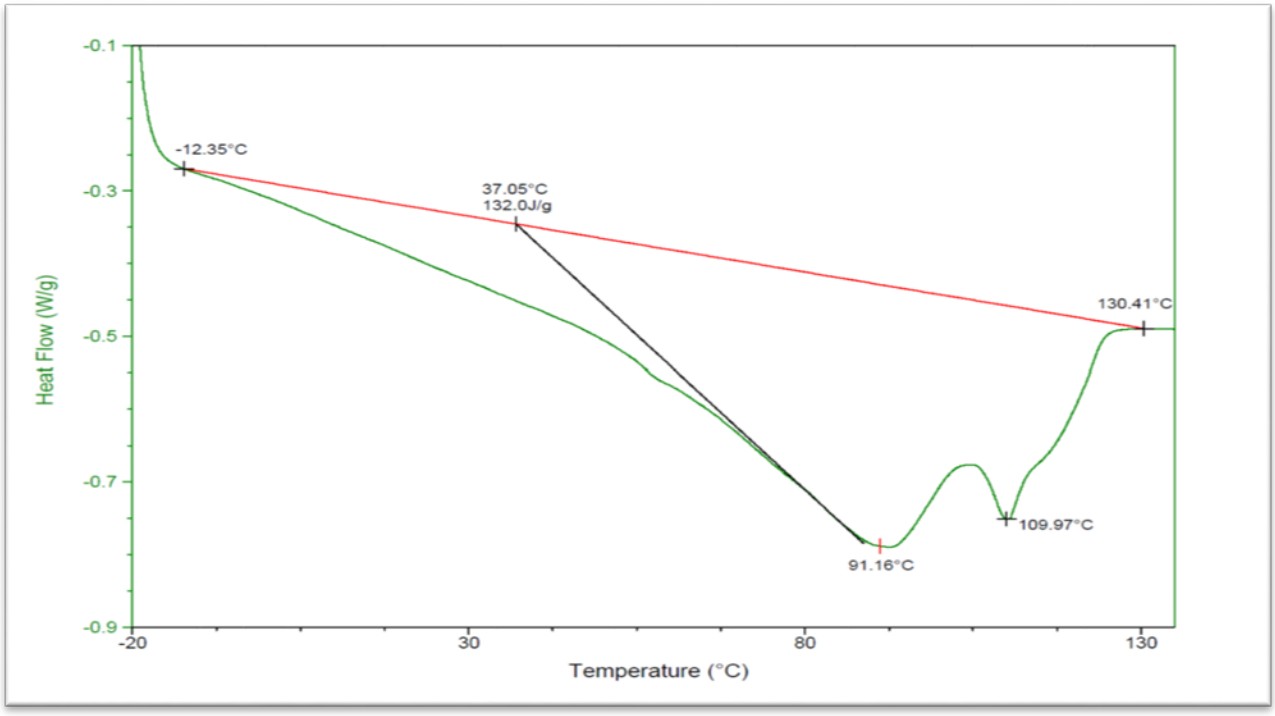

Figure B.18 – DSC plot for Second Heating Cycle of sample run 13(06) with Extracted Values

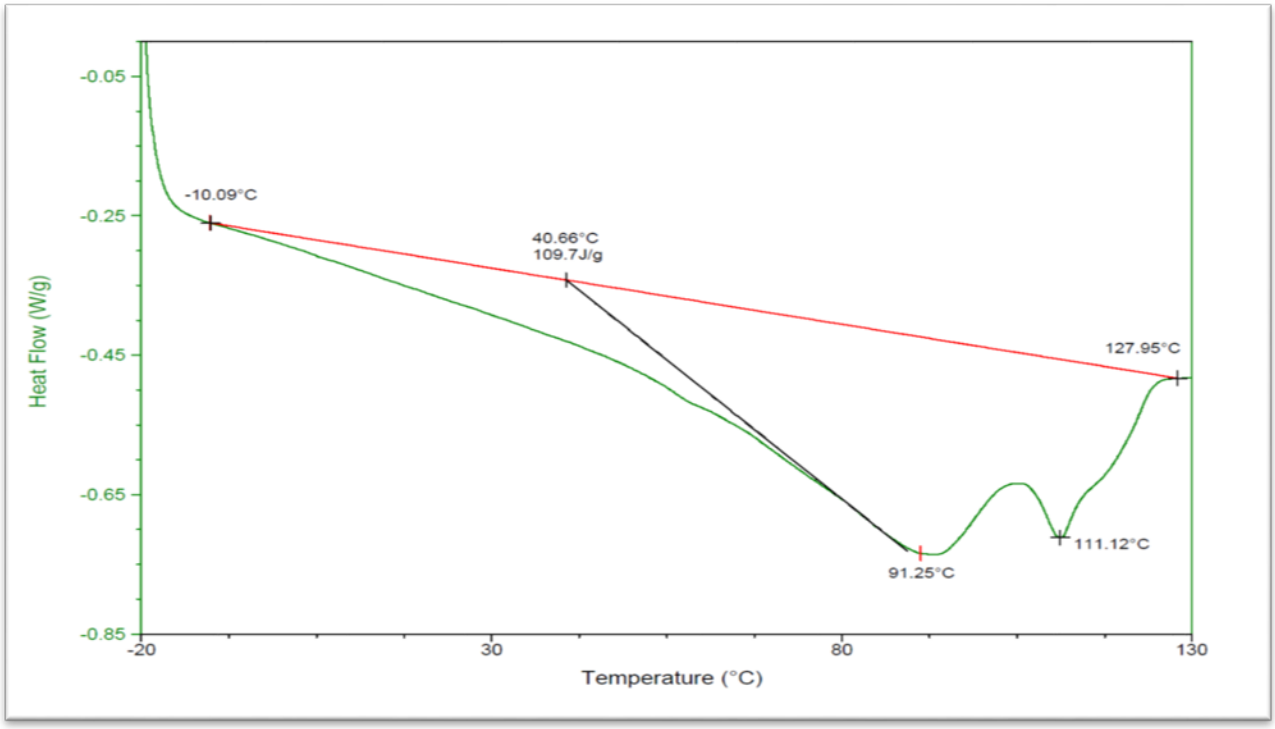

Figure B.19 – DSC plot for Second Heating Cycle of sample run 14 with Extracted Values

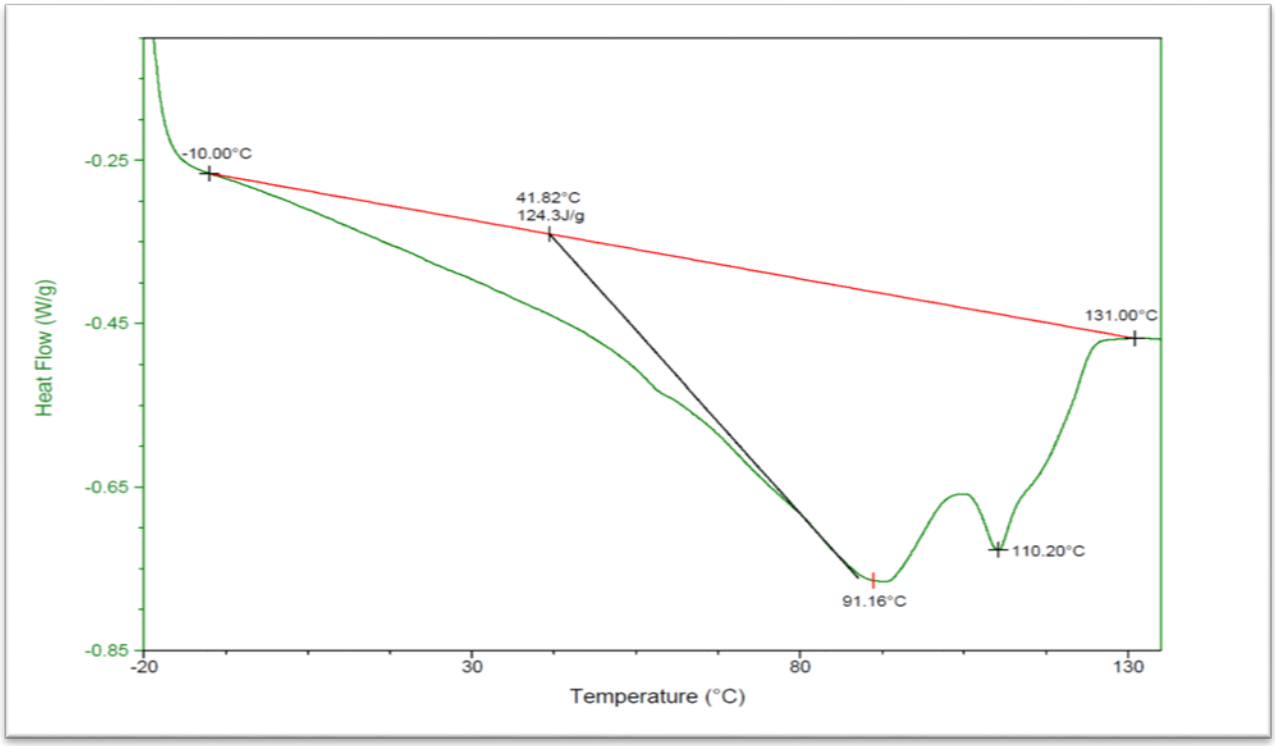

Figure B.20 – DSC plot for Second Heating Cycle of sample run 15 with Extracted Values

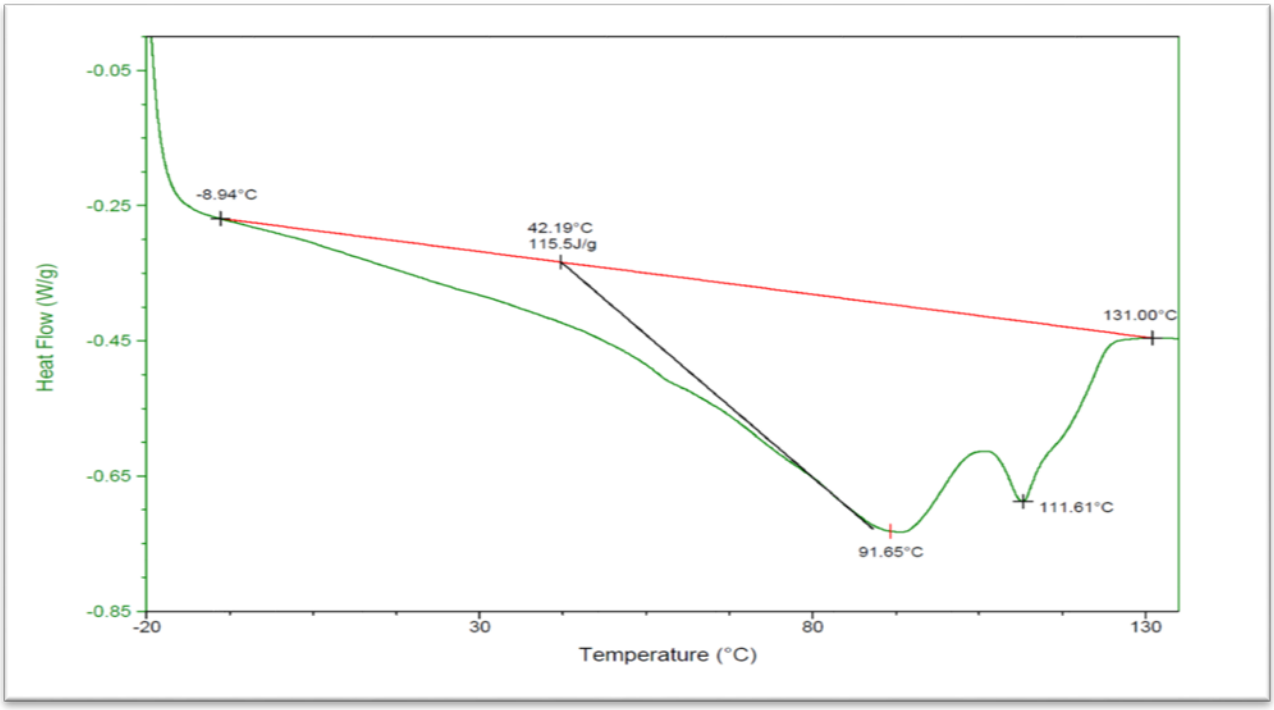

Figure B.21 – DSC plot for Second Heating Cycle of sample run 16 with Extracted Values

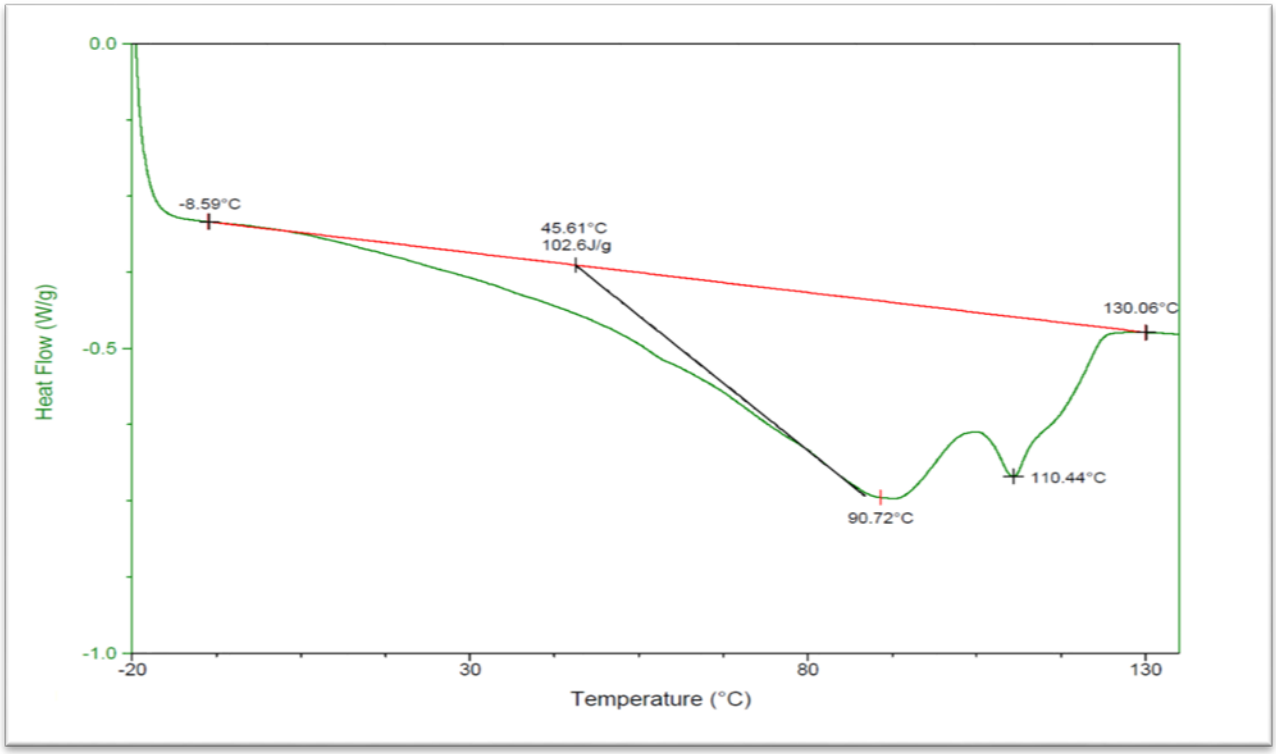

Figure B.22 – DSC plot for Second Heating Cycle of sample run 17 with Extracted Values

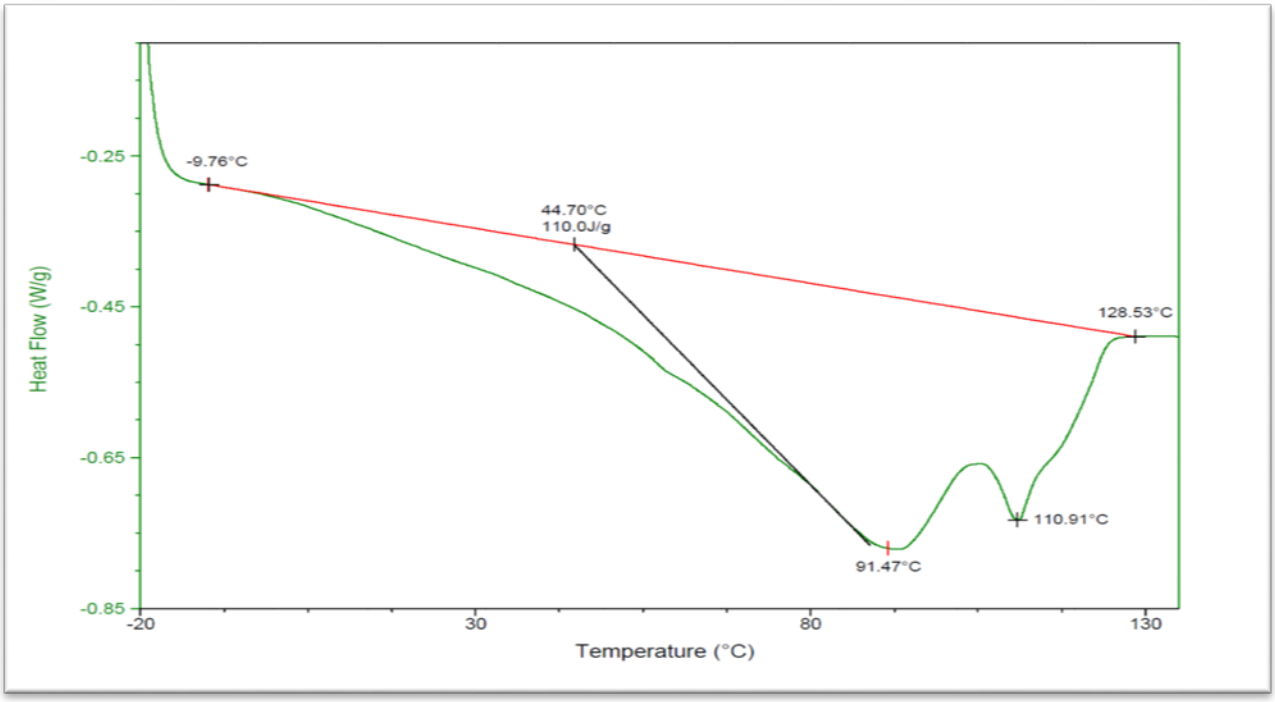

Figure B.23 – DSC plot for Second Heating Cycle of sample run 18 with Extracted Values

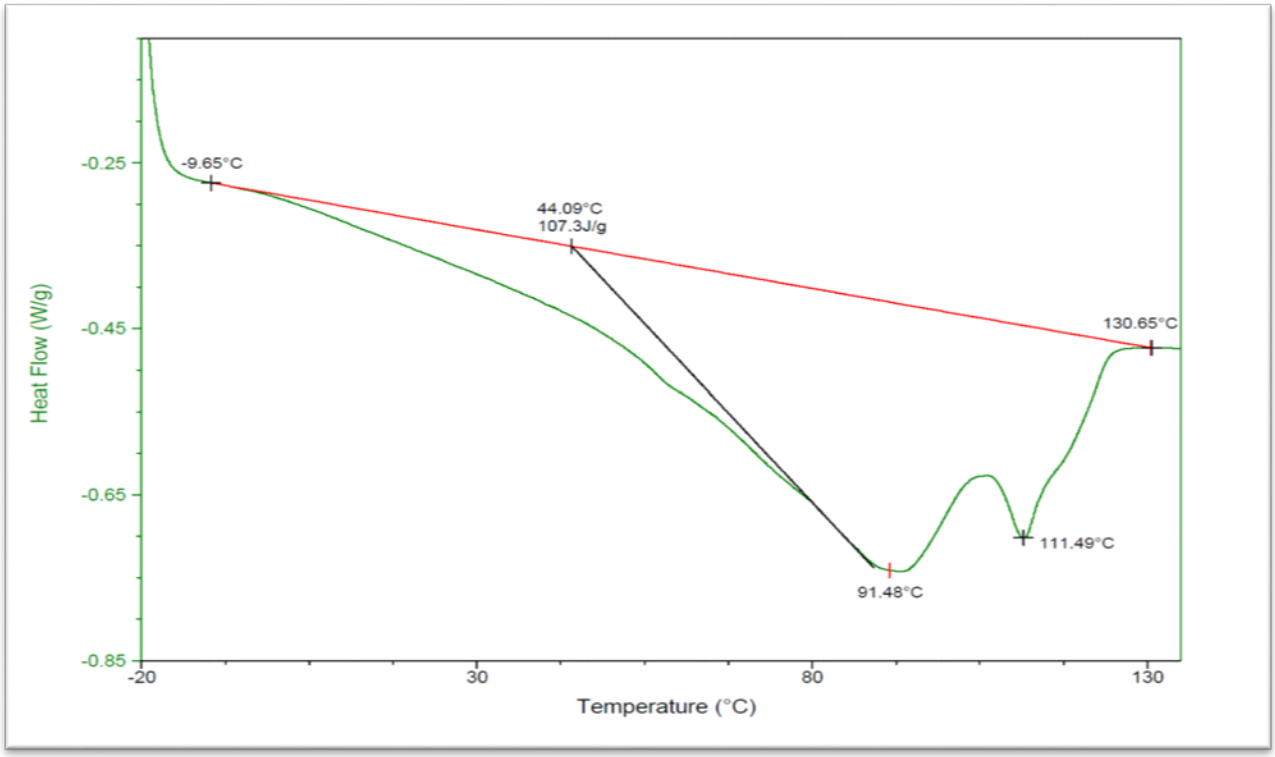

Figure B.24 – DSC plot for Second Heating Cycle of sample run 19 with Extracted Values

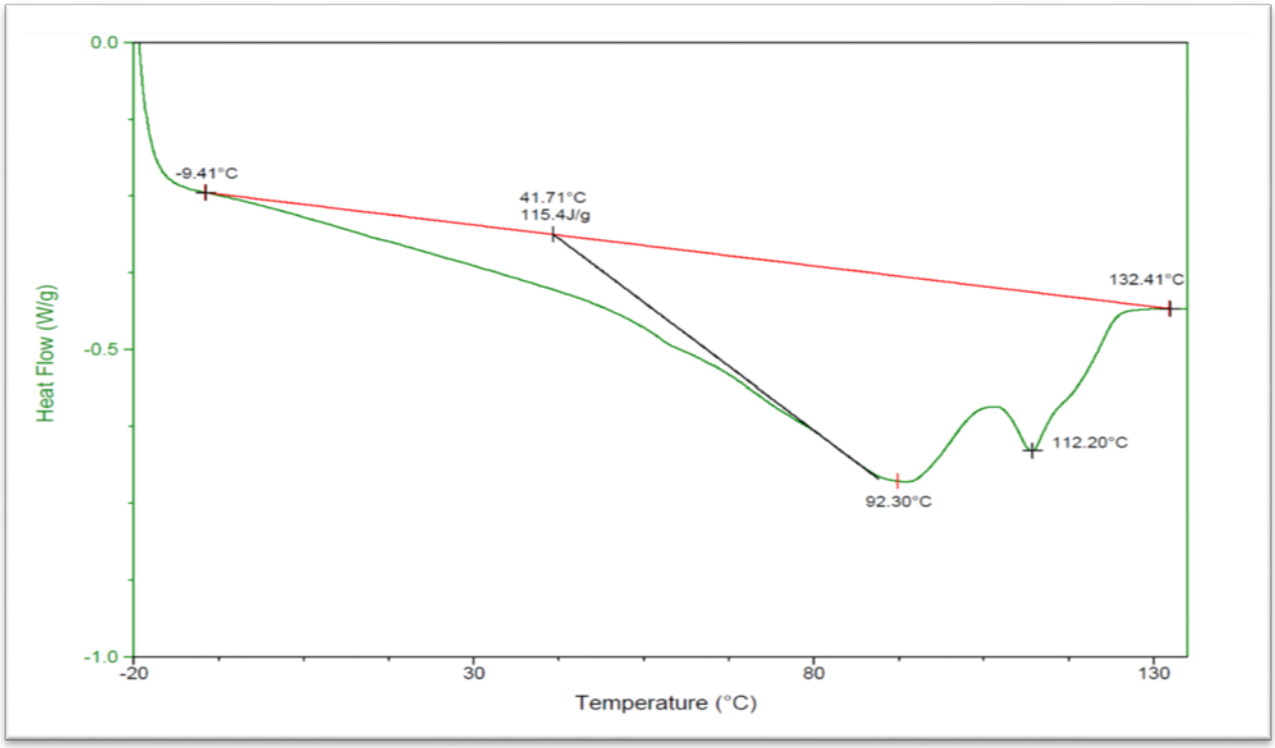

Figure B.25 – DSC plot for Second Heating Cycle of sample run 20(1) with Extracted Values

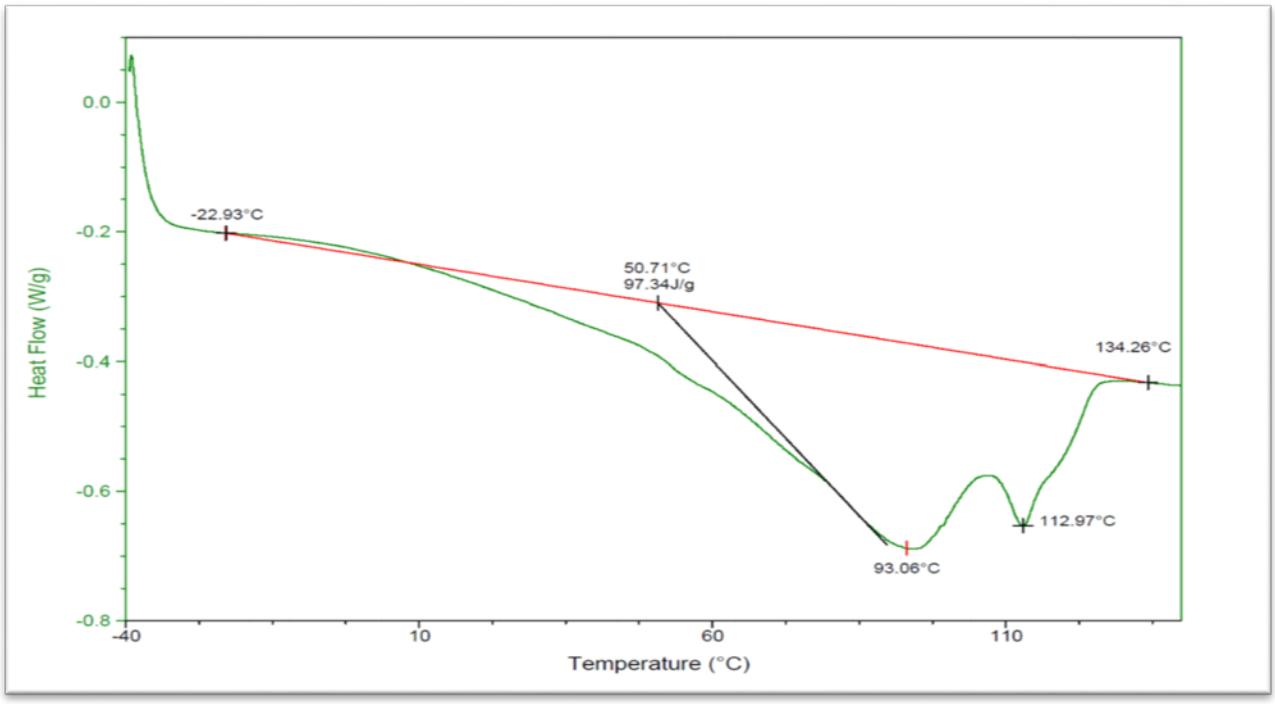

Figure B.26 – DSC plot for Second Heating Cycle of sample run 20(2) with Extracted Values

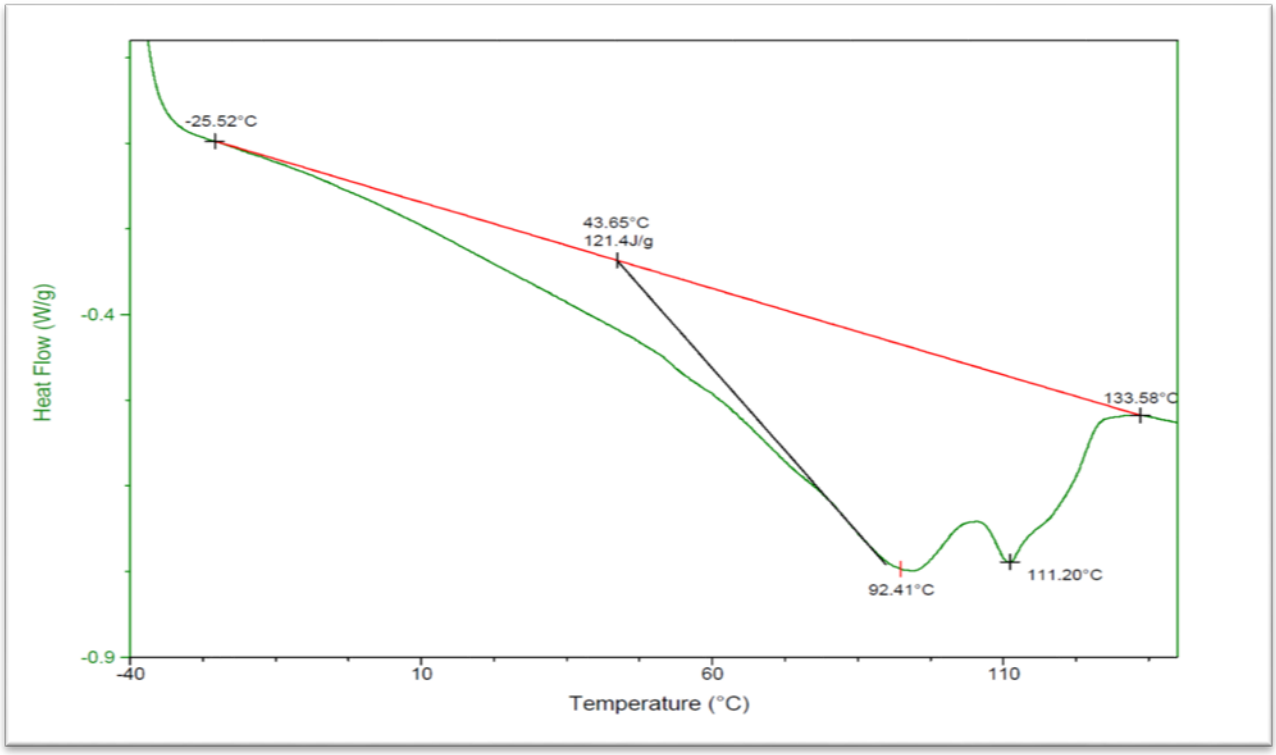

Figure B.27 – DSC plot for Second Heating Cycle of Virgin Material with Extracted Values